AUBURN UNIVERSITY

SAMUEL GINN
COLLEGE OF ENGINEERING

Final Report
Project Number 930-862

CULVERT WING TAB DESIGN LOADS

Submitted to

The Alabama Department of Transportation

Prepared by

J. Brian Anderson, Ph.D., P.E.
Robert W. Barnes, Ph.D., P.E.
Pavel Voitenko, Ph.D.
Lester Lee, M.S.

SEPTEMBER 2021

1. Report No. 930-862	**2. Government Accession No.**	**3. Recipient Catalog No.**
4 Title and Subtitle CULVERT WING TAB DESIGN LOADS		**5 Report Date** September 2021
		6 Performing Organization Code
7. Author(s) J. Brian Anderson, Ph.D., P.E., Robert W. Barnes, Ph.D., P.E., Pavel Voitenko, Ph.D., Lester Lee, M.S.		**8 Performing Organization Report No.** **ALDOT 930-862**
9 Performing Organization Name and Address Highway Research Center Department of Civil and Environmental Engineering 238 Harbert Engineering Center Auburn, AL 36849		**10 Work Unit No. (TRAIS)**
		11 Contract or Grant No. 930-962
12 Sponsoring Agency Name and Address Alabama Department of Transportation 1409 Coliseum Boulevard Montgomery, AL 36130-3050		**13 Type of Report and Period Covered**
		14 **Sponsoring Agency Code**

15 **Supplementary Notes**

16 Abstract

The Alabama DOT has proposed the use of a disconnected or jointed interface between the culvert and wing wall to mitigate cracking during and post construction. This research project determined the magnitude forces acting on a culvert wing tab and developed an LRFD design guideline for the wing tab.

Three culverts with the tabbed wing wall-to-culvert connection were constructed and earth pressure cells were installed in each tab to monitor the compression stresses imposed on the wing tab by the wing walls. The wing walls were also instrumented to monitor movement relative to the culvert.

Numerical models were used to simulate the three field tested culverts and other similar culverts under the same field conditions and extreme events. Stage analysis was used to replicate the construction process and model scour progression. The distribution of stresses normal to the contraction joint surface and movement of the wing wall were studied. These results were used to predict the maximum forces acting on the tab overlapping surface. These field and numerical results were used together to develop a simple equation for determining the force on a culvert wing tab based on the wing wall geometry and at-rest earth pressure.

A design procedure for a culvert wing tab was developed and a narrative example is presented. The procedure is based primarily on adapting AASHTO LRFD (2020) beam ledge design philosophy and provisions to the loads and geometry of the tab. The structural concrete design steps begin with the determination of tab length and thickness, followed by the verification of adequate size, spacing, and configuration of reinforcing steel. A process and example for the design of the wing wall tab using the strut-and-tie method is also described.

17 Key Words culvert, cast-in-place, tab, wing wall, design, LRFD, load testing, finite element		**18 Distribution Statement** No restrictions.	
19 **Security Classification (of this report)** Unclassified	20 **Security Classification (of this page)** Unclassified	**21 No. of pages** 168	**22 Price** None

Final Report 930-862

CULVERT WING TAB DESIGN LOADS

Submitted to

The Alabama Department of Transportation

Prepared by

J. Brian Anderson, Ph.D., P.E.
Robert W. Barnes, Ph.D., P.E.
Pavel Voitenko, Ph.D.
Lester Lee, M.S.

SEPTEMBER 2021

DISCLAIMERS

The contents of this report reflect the views of the authors, who are responsible for the facts and the accuracy of the data presented herein. The contents do not necessarily reflect the official views or policies of the Alabama Department of Transportation or the Auburn University Highway Research Center. This report does not constitute a standard, specification, or regulation. Comments contained in this paper related to specific testing equipment and materials should not be considered an endorsement of any commercial product or service; no such endorsement is intended or implied.

NOT INTENDED FOR CONSTRUCTION, BIDDING, OR PERMIT PURPOSES

J. Brian Anderson, Ph.D., P.E.
Robert W. Barnes, Ph.D., P.E.
Research Supervisors

Acknowledgements

This project was sponsored by the Alabama Department of Transportation (ALDOT). Material contained herein was obtained in connection with a research project "Culvert Wing Tab Design Loads," ALDOT Project 930-862, conducted by the Auburn University Highway Research Center. The funding, cooperation, and assistance of many individuals from each of these organizations are gratefully acknowledged. The researchers acknowledge the Chambers, Lee, and Coosa County Engineers for providing access to their culvert projects for instrumentation. The researchers are grateful for the patience of ALDOT Bridge Bureau personnel, specifically Paul Froede, Ramy Abdalla, Buddy Black, and Tim Colquitt.

Table of Contents

List of Tables

List of Figures

Abstract

Culverts are critical hydraulic and transportation structures. They are often subjected to complex load conditions such as geostatic pressure, hydrostatic pressure, backfill earth pressure, and live load forces. Compressibility of soils beneath the culverts may results in total and differential soil settlement. And due to their nature, culverts are often subject to loads induced by aggradation and degradation scour. Any of these may lead to distress or damage, usually in the form of cracking, sometimes immediately after construction. One way to mitigate this problem is to alter the wing wall-to-culvert connection. ALDOT has proposed the use of a disconnected or jointed interface between the culvert and wing wall to mitigate damage. This research project determined the magnitude forces acting on a culvert wing tab and developed an LRFD design guideline for the wing tab.

Three culverts with the tabbed wing wall-to-culvert connection were constructed in Alabama. During the construction, earth pressure cells were installed in each tab to monitor the compression stresses imposed on the wing tab by the wing walls. The wing walls were also instrumented to monitor movement relative to the culvert.

Numerical models were used to simulate the three field tested culverts and other similar culverts under the same field conditions and extreme events. Stage analysis was used to replicate the construction process and model scour progression. The distribution of stresses normal to the contraction joint surface and movement of the wing wall were studied. These results were used to predict the maximum forces acting on the tab overlapping surface. These field and numerical results were used together to develop a simple equation for determining the force on a culvert wing tab based on the wing wall geometry and at-rest earth pressure.

A design procedure for a culvert wing tab was developed and a narrative example is presented. The procedure is based primarily on adapting AASHTO LRFD (2020) beam ledge design philosophy and provisions to the loads and geometry of the tab. The structural concrete design steps begin with the determination of tab length and thickness, followed by the verification of adequate size, spacing, and configuration of reinforcing steel. A process and example for the design of the wing wall tab using the strut-and-tie method is also described.

Chapter 1. Introduction

Traditionally, cast-in-place reinforced concrete box culverts are built integrally with their wing walls resulting in a monolithic structure. While this design is expedient due to being less formwork intensive, it results in a concentration of stress where the wing wall joins the culvert. As the structure settles or rotates, the difference in weight as well as bearing area of the two components leads to differential settlement between the culvert barrels and the wing walls. This differential settlement, which can be exacerbated by scour, poor construction, and the out-of-plane flexibility of the wall, causes a moment to occur at the location of the concentration of stress. To explain this, the wing wall is considered to be a cantilevered beam which transfers moment to the body of the culvert. The flexure which results from the differential movement creates tensile stresses in the extreme fibers which, in turn, lead to cracking. Depending on which element displaces more, this distress can occur at either the bottom or top of the junction and proliferate from there. This cracking reduces the effective cover of the reinforcement and can lead to a host of issues, such as corrosion, spalling, and in extreme cases, failure of the wing wall.

1.1 Problem Statement

Cracking along the vertical wing joint in newly built culverts was recently reported in Alabama (ALDOT 2012a). The culvert, located on AL49 near Dadeville, has cracked along the wing-to-tab joint shortly after construction (Figure 1-1). A second culvert, near Centerville, cracked after the formwork was removed and before backfill was placed (Figure 1-2).

Figure 1-1. Culvert distress on AL 49 near Dadeville, AL

Figure 1-2. Culvert distress near Centerville, AL

Considering these distresses at the joint between headwall and wing wall, a new design was proposed by the Alabama Department of Transportation, show in figure 1-3, to disconnect the members to eliminate the stress transfer between them.

1.2 Objectives

The proposed solution to the problem of cracking along the wing-to-culvert involves casting the wing wall separate from the culvert box. Theoretically, the wing wall bears against a tab on the culvert. The wing walls are then designed as standalone retaining walls. The new wing wall can translate independently of the barrel, as a cantilever retaining wall with a pinned support along one side.

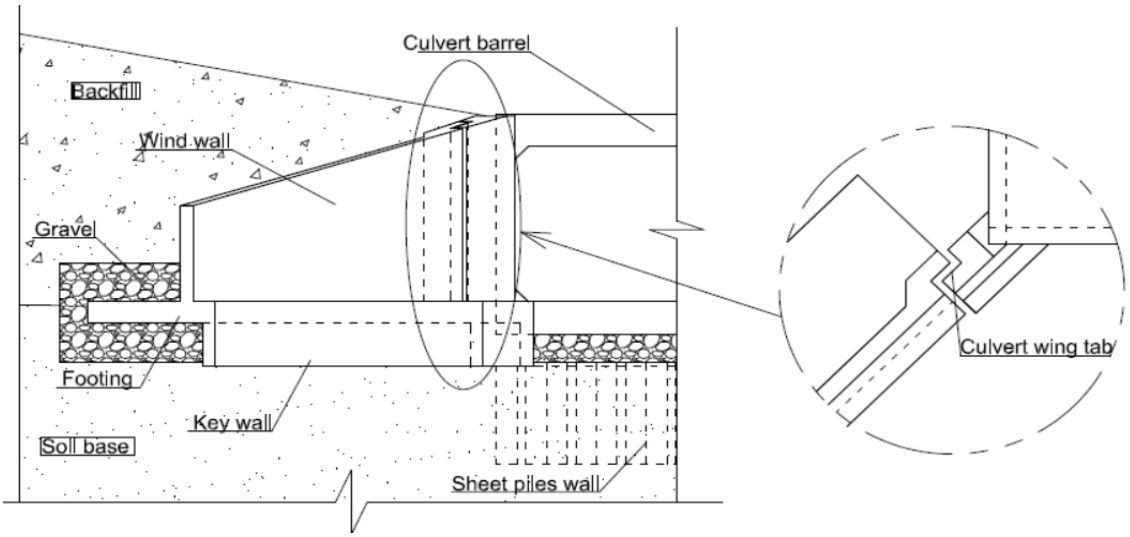

Figure 1-3. Front and plan view of the wing wall-to-culvert joint

The objectives of this study were to:

1. Determine the force on the culvert wing tab using a combination of field measurements and finite element modeling and develop a method to estimate the load in the tab.
2. Develop an LRFD design procedure for the culvert wing tab to determine dimensions and reinforcing steel details.

1.3 Scope of Work

The research objectives were accomplished by the following scope of work:

1. A detailed literature review was conducted.
2. A field study was conducted to determine the stresses on the culvert tab at full scale under real conditions.
3. Three dimensional finite element analysis was used to simulate culvert construction of the field-tested culverts and additional extreme event situations (high backfill and scour)
4. The results of tasks 1-3 were used to develop a simple equation for determining the force on a culvert wing tab based on the wing wall geometry and at-rest earth pressure.

5. An LRFD design procedure for culvert wing tab was developed considering the tab to function as a beam ledge as described in AASHTO LRFD 5.8.4.3

Chapter 2. Background and Literature Review

2.1 Overview

Structural behavior of culverts under various loads depends on the category of the culvert. Culverts are categorized as arch, box, circular and masonry (Scanlon 2012). Culverts may be divided into five main groups (ALDOT 2008; ConnDOT 2000):

- Circular Pipe – most commonly used culvert type, and highest hydraulic efficiency.
- Pipe-Arch –structural shape used mostly for limited backfill depth and cover height.
- Arch – bottomless, arch-shaped structures with natural stream bottom.
- Box Section – rectangular or square (CIP or precast concrete) cross section can be adjusted to any site conditions. Because of angular corners, box cross-section is not hydraulically efficient in comparison with a circular.
- Multiple Barrel – common shape for wide waterways or low embankment. The walls between openings may cause clogging by catching debris.

Culverts are typically made of reinforced concrete (ConnDOT 2000). However, steel, and more recently, polyethylene, and reinforced plastic are used. In accordance with Coghlan, B. K. (1916) wooden, cast-iron, vitrified clay pipe and stone box culverts were used in construction. Concrete culverts, either cast-in-place (CIP) or precast, are preferable over other materials due to relatively high resistance to applied loads, resistance to environmental hazards (such as corrosion or temperature changes during freeze-thaw periods) and low maintenance costs (FDOT 2011).

Depending on the complexity of the design, concrete culverts can be constructed with precast members or cast-in-place. While precast sections are standardized regarding their shape and the size, cast-in-place concrete construction can be specially designed to meet the in-situ

requirements. Unlike precast, which are produced for several specific strength classes, CIP box culverts can be manufactured for various load and environmental conditions. In the case of CIP construction, box culverts are usually built on site using ready-mixed concrete. Thus, the structure can be constructed without joints that reduce the risk of corrosion (ConnDOT 2000; KYTC 2011). Since CIP culverts are designed for specific load conditions, additional reinforcement can be placed in high stress locations.

A number of cases of early cracking of the structural components of culverts were reported, as well as techniques to analyze the behavior of the damaged structure. Some culverts were instrumented and rehabilitated recently (Ahmed, B. et al. 2003; Hurd 1991; IODOT 2013; Musser 1995). Finite element modeling was used along with laboratory tests to investigate the behavior of these culverts. To understand the reasons that lead to structural distress numerical analysis was repeated multiple times for different material properties and load combinations.

2.2 Background

2.2.1 Earth Pressure Theory

The main contributing and most rationally estimated forces on culverts are due to earth pressure. Thus, to properly design and construct culverts and wing walls, the lateral earth pressure acting on the retaining structures from the soil must be predicted. The lateral earth pressure estimate is based on the state of plastic equilibrium as defined by the Rankine (Rankine 1857), and the assumption that the active pressure develops in the soil on the heel side of the wall and the passive pressure on the toe side. The passive and active pressure develop with sufficient wall movement so that the full shear strength of the backfill soil occurs (Huntington 1957). The third type of soil pressure acting on the buried structures is At-Rest earth pressure which requires no wall movement.

The lateral earth pressures can be expressed as:

$$\sigma_h = K_h \cdot \sigma_v \tag{2-1}$$

where:

σ_v – effective normal stress on the base: $\sigma_v = \gamma \cdot H$

γ – unit weight of soil

H – depth below the surface of earth

K_h – coefficient of lateral earth pressure

The coefficient of lateral earth pressure expresses the ratio of the effective horizontal stresses to the effective vertical stress. After natural or artificial compaction of backfill, the value of K_h takes the form of K_o, the coefficient of earth pressure at rest. With the horizontal expansion of the soil, the value of K_h decreases until it becomes equal to K_A, the active earth pressure coefficient. If structure pushes on soil, the horizontal compression of the soil mass increases the value of K until it becomes equal to the passive earth pressure coefficient K_P (Terzaghi et al. 1996).

2.2.1.1 At-Rest Earth Pressure Coefficient (K_0)

At-Rest earth pressure (Figure 2-1) is lateral pressure acting on a rigid body, represented by a horizontal earth pressure coefficient, K_0. For cohesionless soils, its value can be approximated using Equation 2-2. In cohesive soils, the lateral earth pressure will not be developed till some depth, so the K_0 can be calculated using elastic theory through Poisson's Ratio (Equation 2-3).

For cohesionless soils (Jaky 1948):

$$K_0 = 1 - \sin\phi \tag{2-2}$$

For cohesive soils (Tschebotarioff 1973):

$$K_0 = \frac{\nu}{1-\nu} \tag{2-3}$$

where:

ϕ – effective friction angle of soil

ν – Poisons ratio

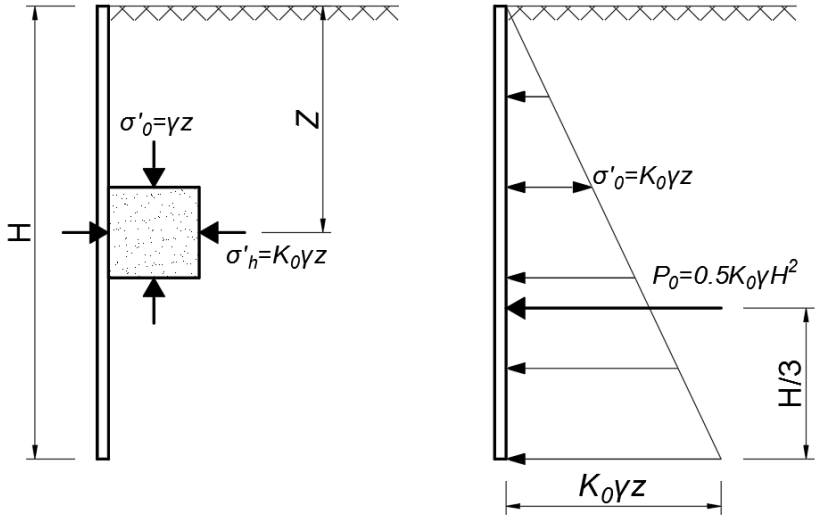

Figure 2-1. Distribution of lateral earth pressures at rest

For overconsolidated soils Mayne and Kulhawy (1982) suggest modifying the Jaky equation (2-4) using the over consolidation ratio:

$$K_0(OC) = K_0 \cdot OCR^{\sin\varphi} \tag{2-4}$$

Where

OCR – overconsolidation ratio

Kezdi (1972) provides a version of the Jaky equation ((2-5) that accounts for sloping backfills:

$$K_{0\beta} = (1-\sin\phi)(1+\sin\beta) \tag{2-5}$$

Where

β – backfill slope angle from the horizontal

2.2.1.2 Active and passive pressure (Rankine, Coulomb)

Active is an earth pressure on the retaining system that develops when the retaining structure tends to move away from the soil fill to the excavation. Unlike active, passive pressure is caused by the movement of structure elements toward the soil. Approximate ratios of these required movements relative to wall height are given in Table 2-1 of the AASHTO LRFD (2014).

Table 2-1. Approximate values of relative movements required to reach active or passive pressure conditions (*AASHTO LRFD* 2014)

Type of Backfill	Values of Δ/H	
	Active	Passive
Dense sand	0.001	0.01
Medium dense sand	0.002	0.02
Loose sand	0.004	0.04
Compacted silt	0.002	0.02
Compacted lean clay	0.010	0.05
Compacted fat clay	0.010	0.05

Coulomb (1776) and Rankine (1857) theories are most commonly used to determine active and passive earth coefficients. In Coulomb theory, derived from force equilibrium, the active state of stress develops behind the wall and the soil within the failure wedge is in the state of plastic equilibrium (Figure 2-2). The values of K_A and K_P are obtained assuming plane strain conditions, uniform shear resistance along the rupture surface, inclined wall geometry and friction develops between the wall and the soil.

The Coulomb equation for the coefficients of active and passive earth pressure are:

$$K_A = \frac{\sin^2(\theta+\phi)}{\sin^2\theta\cdot\sin(\theta-\delta)\cdot\left[1+\sqrt{\frac{\sin(\phi+\delta)\cdot\sin(\phi-\beta)}{\sin(\theta-\delta)\cdot\sin(\theta+\beta)}}\right]^2} \quad (2\text{-}6)$$

$$K_P = \frac{\sin^2(\theta+\phi)}{\sin^2\theta\cdot\sin(\theta+\delta)\cdot\left[1-\sqrt{\frac{\sin(\phi+\delta)\cdot\sin(\phi-\beta)}{\sin(\theta+\delta)\cdot\sin(\theta+\beta)}}\right]^2} \quad (2\text{-}7)$$

where:

ϕ - friction angle of soil

δ - friction angle between fill and wall

β - the angle of fill to the horizontal

θ - the angle of the back face of the wall to horizontal

The distribution of active (Figure 2-2) and passive pressure is linear with the resultant force acting at the distance of one-third of the wall height above its base.

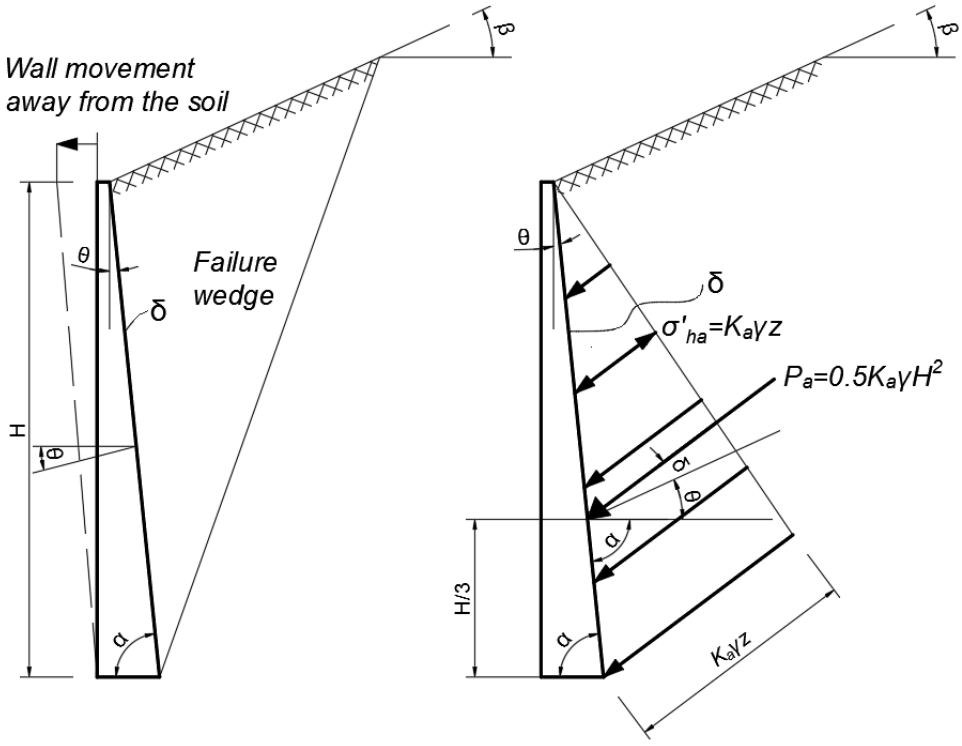

Figure 2-2. Failure wedge and distribution of lateral active Coulomb earth pressures

Rankine's theory was developed based on Mohr Coulomb theory. Wall friction is only considered for the case of sloping backfill. The failure happens when one of the principal stresses reaches the maximum compression stress (Bruner et al. 1983). The limitation of this theory for the structures with substantial wall friction, (i.e. soil on rough concrete); (Rankine 1857).

A graphical depiction of the Rankine relationships is shown in Figure 2-3. The equations for the coefficients of active and passive earth pressure with inclined backfill are included as equations (2-8) and (2-9). The Rankine pressure distribution is included as Figure 2-4.

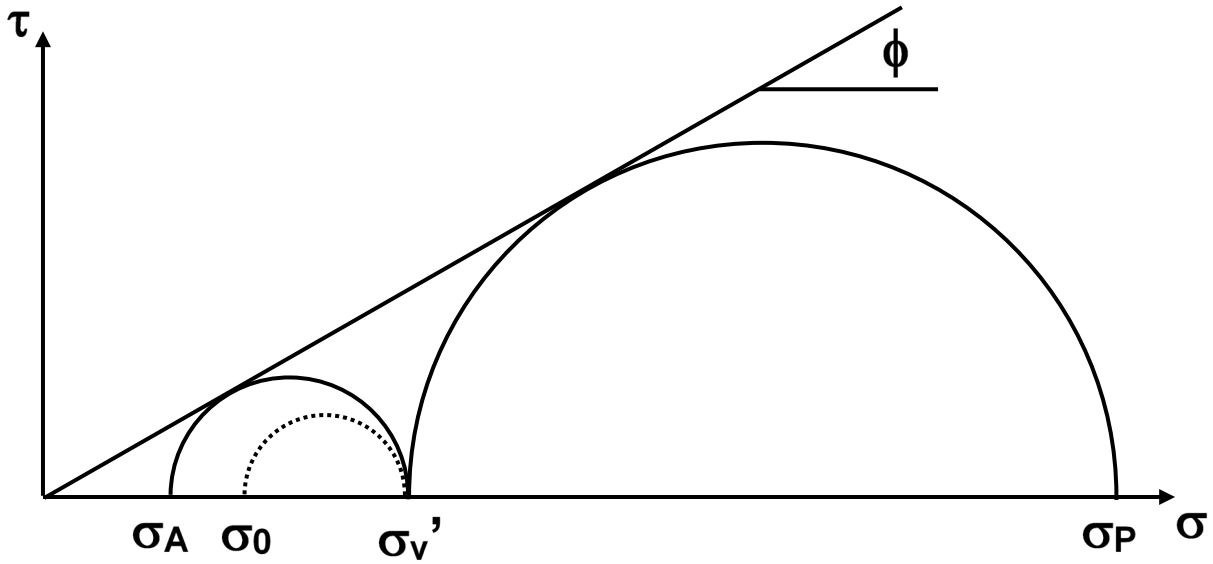

Figure 2-3. Rankine earth pressures in relation to vertical effective stress and at rest pressure.

$$K_A = \cos\beta \cdot \left[\frac{\cos\beta - \sqrt{(\cos^2\beta - \cos^2\phi)}}{\cos\beta + \sqrt{(\cos^2\beta - \cos^2\phi)}} \right] \quad (2\text{-}8)$$

$$K_P = \cos\beta \cdot \left[\frac{\cos\beta + \sqrt{(\cos^2\beta - \cos^2\phi)}}{\cos\beta - \sqrt{(\cos^2\beta - \cos^2\phi)}} \right] \quad (2\text{-}9)$$

where:

ϕ - friction angle of soil;

β - the angle of fill to the horizontal

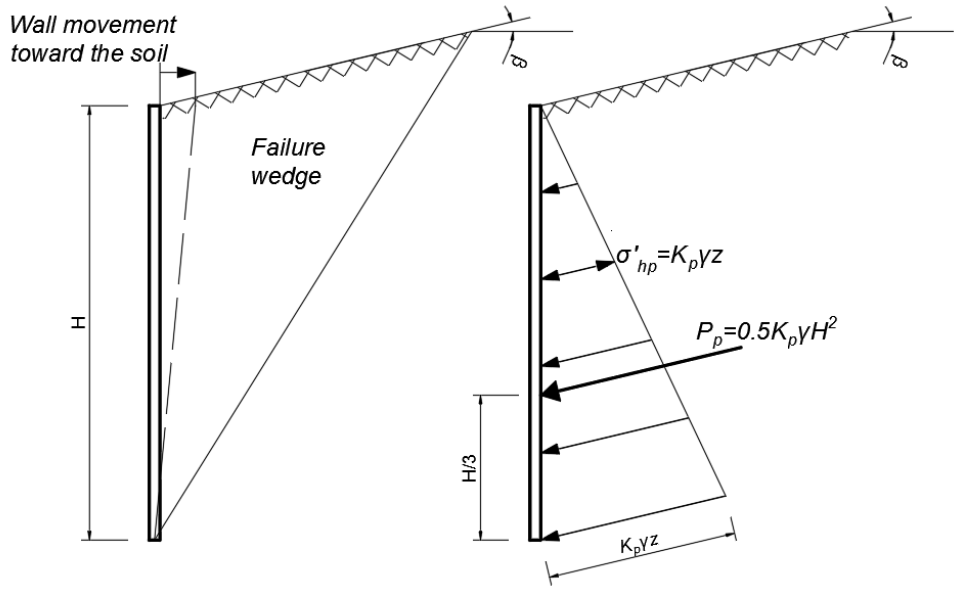

Figure 2-4. Failure wedge and distribution of lateral passive Rankine earth pressures

AASHTO LRFD (2014) allows either Coulomb theory or Rankine theory be used to calculate the value of lateral earth pressure coefficient. It is recommended to neglect any contribution from passive earth pressure in stability calculations as its development requires up to ten times larger movement then for active pressure. Exceptions may be made for the cases when the structure is deeper than the theoretical depth of the soil that could be weakened or removed due to scour, erosion, freeze-thaw, or any other means. In the calculations, only the effective embedment depth, the depth below the disturbed soil, shall be considered (*AASHTO LRFD* 2014).

2.2.1.3 Hydrostatic Pressure

Retaining structures are typically designed to prevent the buildup of hydrostatic pressure using drains (*AASHTO LRFD*, 2014). However, in case the groundwater level increases due to flooding, heavy rain or any other event, the hydrostatic pressure can develop behind an undrained wall (Figure 2-5). Since water does not change volume under the applied load, it generates equal

stresses in all directions, which can be significantly larger than the resultant at rest or active soil forces. Thus, the water pressure develops linearly with increasing the depth (Bowles 1988).

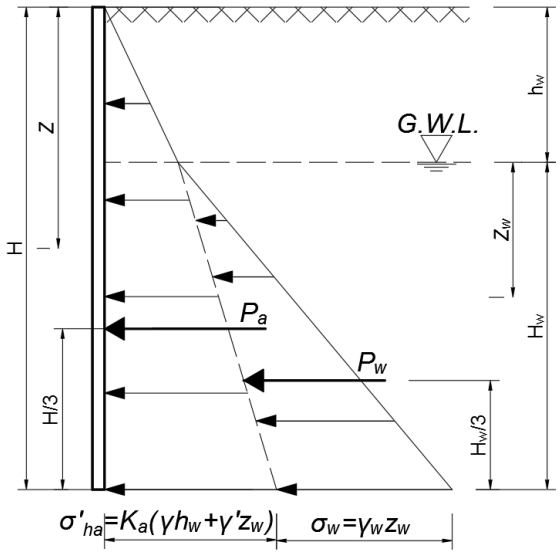

Figure 2-5. Lateral pressure from groundwater table

2.2.2 Design of Retaining Structures

The traditional design of a cast in place box culvert considers the culvert and wing wall integral as one system (*AASHTO LRFD* 2014; IODOT 2013; NYSDOT 2012). The connection between the culvert and wing walls may be designed with or without an expansion joint. However, while culvert barrels are designed similar to bridges (*AASHTO LRFD* 2014), wing walls are usually designed as cantilevered retaining walls to resist out-of-plane backfill pressures (FHWA 1983).

Wing walls, as cantilever retaining walls, are designed for the strength and extreme event limit states (*AASHTO LRFD* 2014). The strength limit state includes calculation of structural failure, bearing capacity and settlement failure, lateral sliding, and loss of base contact due to eccentric loading. At the extreme event limit state, the structure shall be investigated for overall or global stability failure.

Overturning stability analysis is accomplished by comparing the moments produced by the force that tends to overturn the wall and the moments of the resisting forces. As it is specified in Section 11.6.3.3 of AASHTO (2014), the resultant eccentricity of the loads acting on the structure determines the overturning resistance of the structure. The allowable eccentricity *e* is limited to 1/6 of the footing width *B* on either side of the center of footing.

The loads considered in wing wall design (Figure 2-6), are the following:

- self weight, dead load of structural components (DC)
- self weight of future wearing surface (DW)
- vertical earth pressure (EV)
- horizontal earth pressure (EH)
- earth surcharge load (ES)
- water pressure (WA)
- live load (LL)

Load factors for considered load combinations are outlined in Section 3.4.1 of AASHTO LRFD (2014) and summarized in Table 2-2. Load factors for Strength I and Extreme II load combinations are applicable for sliding and eccentricity limit states analysis. The notations “a” and “b” refer to minimum and the maximum values of load factors, respectively. The minimum load factors were applied to the vertical loads representing resistance while maximum load factors, to the horizontal loads, which represent load component in the design formula. For the bearing limit state, maximum load factors for both vertical and horizontal loads applied depending on Strength Ib, Extreme IV, and Extreme IIb load combinations (*AASHTO LRFD* 2014).

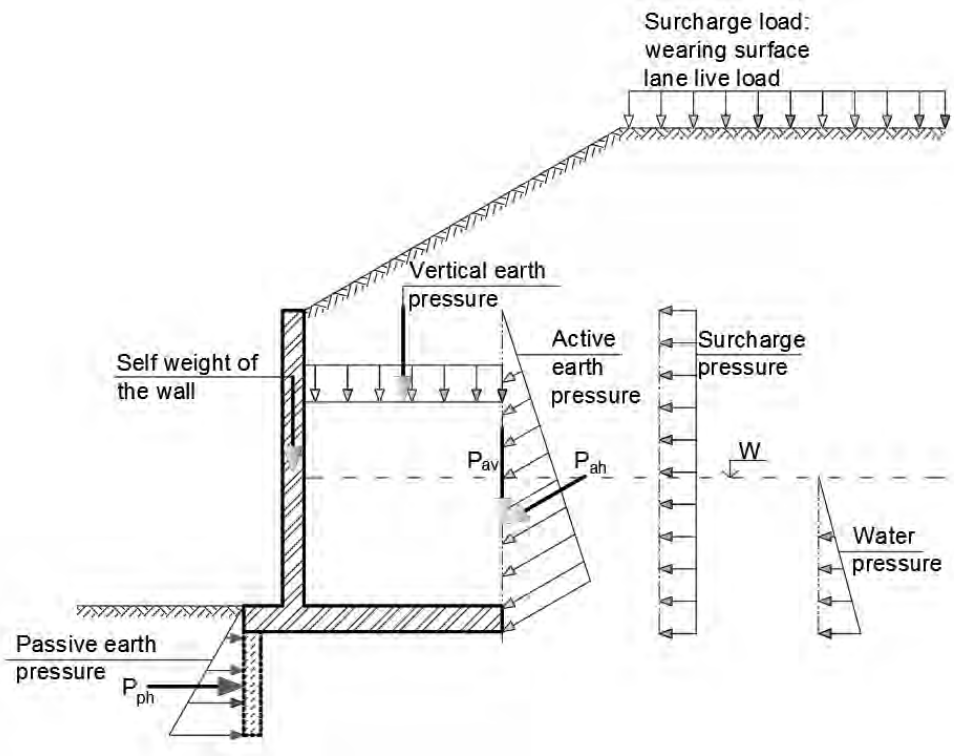

Figure 2-6. Considered load components

Table 2-2. Load factors

Load Combination Limit State	Load factors					Application
	DC, γ_{DC}	EV, γ_{EV}	LL_V, γ_{LL_V}	LL_H, γ_{LL_H}	EH, γ_{EH}	
Strength Ia	0.90	1.00	-	1.75	1.50	Sliding, Eccentricity
Strength Ib	1.25	1.35	-	1.75	1.50	Bearing, Strength, Design
Strength IV	1.50	1.35	-	-	1.50	Bearing, Strength, Design
Extreme IIa	0.50	1.00	-	-	-	Sliding, Eccentricity
Extreme IIb	1.25	1.35	-	-	-	Bearing

Geotechnical resistance factors for shallow foundations specified in Section 10.5.5.2.2. of AASHTO LRFD (2014) depend on soil type and type of concrete wall. Applicable factors for bearing and sliding limit states are summarized in Table 2-3.

Table 2-3. Resistance factors for geotechnical resistance (*AASHTO LRFD*, 2014)

Method/Soil/Condition			Resistance Factor
Bearing Resistance	ϕ_b	Theoretical method (Munkafakh et al., 2001), in clay	0.5
		Theoretical method (Munkafakh et al., 2001), in sand, using CPT	0.5
		Theoretical method (Munkafakh et al., 2001), in sand, using SPT	0.45
		Semi-empirical method (Meyerhof, 1957), all soils	0.45
		Footing on rock	0.45
		Plate Load Test	0.55
Sliding Resistance	ϕ_τ	Cast-in-Place Concrete on sand	0.8
		Cast-in-Place Concrete on clay	0.85
	ϕ_{ep}	Passive earth pressure component of sliding resistance	0.5

2.2.3 Design of Corbels and Beam Ledges

Because the culvert tab length is relatively short relative to its thickness (Figure 2-7), it is unreasonable to assume that plane sections remain plane in this reinforced concrete element. Therefore, the tab should be classified as a discontinuity region (D-region) and designed as such. AASHTO LRFD (2020) requires that D-regions be designed in accordance with the provisions of Article 5.8.2 (the strut-and-tie method) in general or with the provisions in Article 5.8.4 that apply to specific types of components. Article 5.8.4 contains design provisions for two types of discontinuity regions that behave similarly to the culvert tab: a) corbels (and brackets) and b) beam ledges.

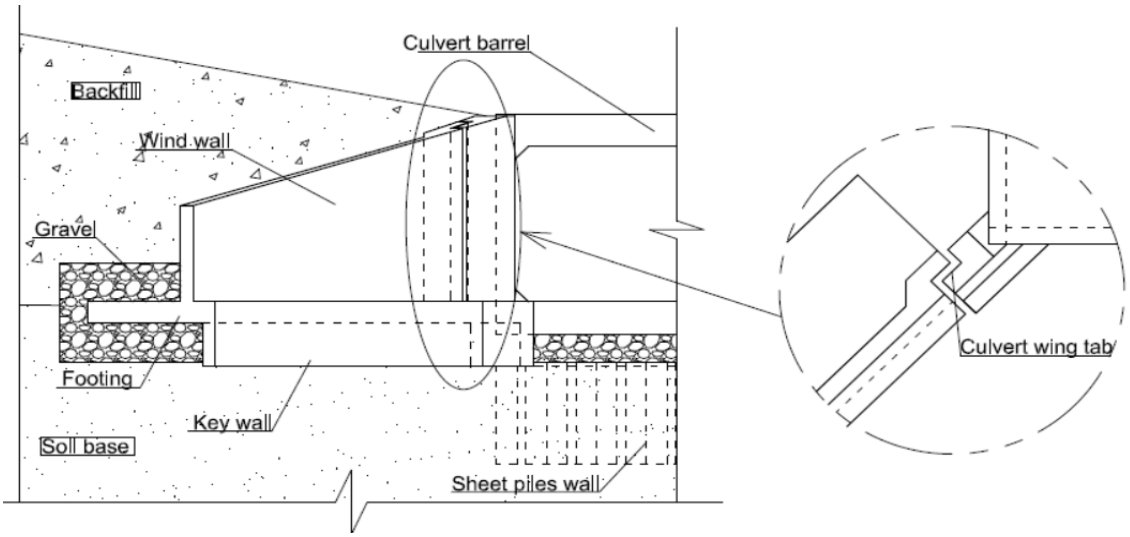

Figure 2-7. Wing wall-to-culvert joint

A corbel (Figure 2-8) is a short cantilever reinforced concrete member, cast monolithically with the column or wall element, used to support concentrated loads or beam reactions. The potential failure modes of a corbel are (Mattock 1976; Powell and Foster 1996):

- yielding of a tensile tie due to a combination of the flexural and axial load
- shear interface failure of the contact surface with the supporting member
- flexural failure leading to the diagonal splitting of the concrete
- splitting of the end anchorage of the tensile tie

In accordance with design provisions summarized in Article 5.8.4.2 of AASHTO LRFD (2020), the potential failure modes of corbels include the loss of flexural or shear capacity, crushing or splitting of the compression strut, and failure of the end anchorage of the primary tension (tie) reinforcement (A_s in Figure 2-8). Failure modes of corbels are shown in Figure 2-9.

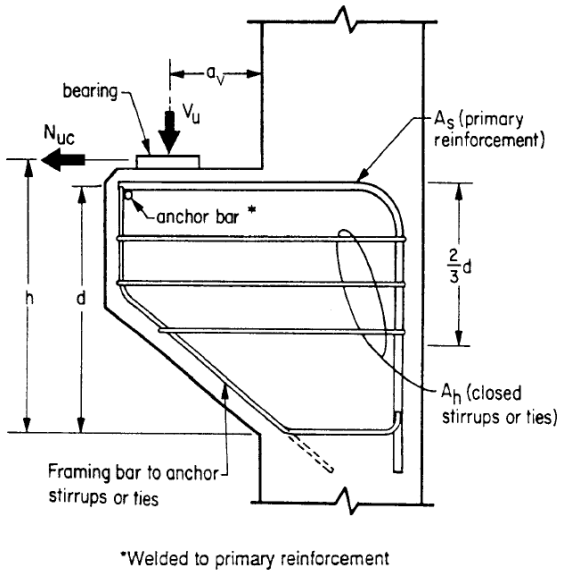

Figure 2-8. Corbel with typical reinforcement (AASHTO 2020)

A shear crack occurs near the point of application of the concentrated force and propagates to the bottom corner of the corbel interface (Figure 2-9a). It can also start at the upper corner of the tab and proceed vertically to the bottom fiber (Figure 2-9b). Failure due to the splitting of concrete around the tensile reinforcement may occur if the anchorage length is insufficient (Figure 2-9c). Inadequate proportions of the tab can result in failure due crushing of the concrete under concentrated load (Figure 2-9d) (Ashari 2014; Mattock 1976).

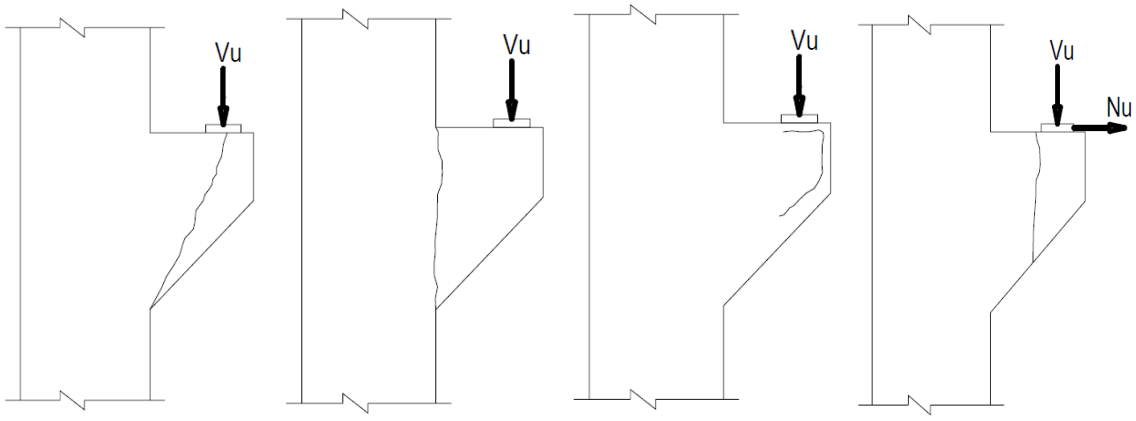

Figure 2-9. Modes of failure of corbel (Ashari 2014)

General provisions for Article 5.8.4 corbel design are laid out by AASHTO (2020) as follows:

- The resultant force of the applied load (V_u in Figure 2-8) on the corbel should be located no further from the support than a distance equal to the effective depth d of the corbel section. Otherwise, it should be designed as a cantilever beam.
- The corbel section at the face of support shall be designed to simultaneously resist a factored shear force V_u, a factored bending moment M_u, and a concurrent tension force N_{uc} acting parallel to the loaded surface. The reinforcement provided to resist these load effects shall satisfy the requirements of Article 5.8.4.2.2.
- The shear-friction reinforcement provided to resist V_u shall satisfy the shear-friction design requirements of Article 5.7.4 with the additional limitations of Article 5.8.4.2.2.
- N_{uc} shall be treated as a live load and shall not be taken less than $0.2V_u$.
- The amount of primary tension reinforcement at the face of the support (A_s in Figure 2-8) shall be at least $0.04(f_c'/f_y)bd$.
- The area of closed ties A_h shall be no less than 50 percent of the area of the primary tension reinforcement, A_s. These ties shall be uniformly distributed adjacent to the primary tension reinforcement: within a distance equal to two thirds of the effective depth.
- At the front face of the corbel, the primary tension reinforcement shall be anchored to develop the specified yield strength. This may be achieved by bending the bars to form a continuous loop.

Although some key concepts from corbel design apply, the culvert wing tab more closely matches the loading, configuration, and behavior of a beam ledge, which is addressed in Article 5.8.4.3 of AASHTO LRFD (2020) and depicted in Figure 2-10. Both the dapped beam and the

supporting ledge itself are designed as “beam ledges” in accordance with Article 5.8.4.3. Based on loading and support configuration, the wall tab and culvert wing tab may be considered beam ledges rotated 90 degrees about a horizontal axis.

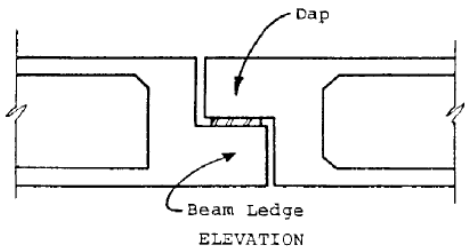

Figure 2-10. Dapped beam and beam ledge (AASHTO 2020)

Figure 2-11 depicts cracking and potential failure mechanisms for beam ledges. Crack locations 1, 3, and 4 are like behavior found in corbels; however, crack location 2 was not a critical design consideration for corbels because of the more complex load path in a beam ledge. This crack is resisted by “hanger” reinforcement, the vertically oriented bar shown in the figure, which takes the load applied to the ledge and “hangs” it back up into the larger supporting beam. Adequately proportioning and developing this hanger reinforcement, which is horizontal in the culvert wing tab, is critical to detailing the tab reinforcement to provide good structural performance. Crack locations 1 and 2 are somewhat idealized for capacity-checking purposes. In reality, diagonal cracks oriented between these orthogonal are more likely—reflecting the shear-influenced diagonal tension that results from this biaxial state of tension stresses.

Beam ledges may be designed using the strut-and-tie method or by the provisions of Article 5.8.4.3. However, the Article 5.8.4.3 provisions can be reduced in complexity for the culvert wing tab because the tab loading is distributed along the tab height, rather than concentrated at discrete locations as is often the case with ledges supporting beams or girders.

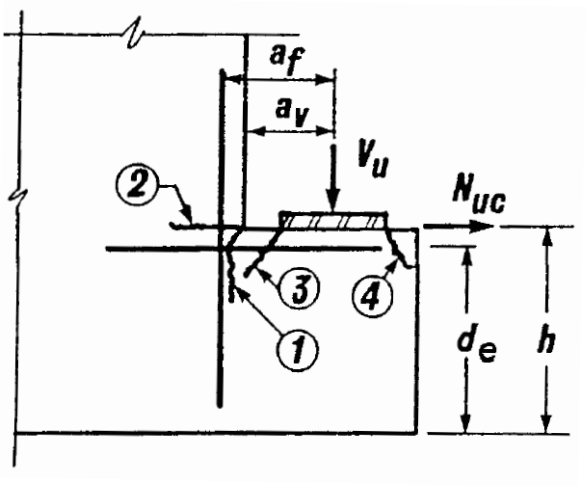

Figure 2-11. Potential crack locations for ledge beams (AASHTO 2020)

Therefore, punching shear will not dictate the critical shear demand on the tab, and there is no need to determine an “effective width” that resists the shear due to concentrated loads.

Chapter 3. Tabbed Wing Wall to Culvert Connection

3.1 Introduction

As it was mentioned in previous chapters, a new design that disconnects the culvert wing walls from the box was proposed by ALDOT in response to the observed cracking of the newly built cast-in-place culverts. The details of the newly developed design and its deployment are presented and discussed in this chapter.

3.2 Tabbed Wing Wall-to-Culvert Connection Design

A high stress concentration zone exists in the monolithic connection between wing walls and culvert barrels (Voitenko, 2018). The new culvert design proposed by ALDOT allows the wing wall and concrete barrel to move independently in the vertical direction. The plan view of the culvert constructed according to the new design is shown in Figure 3-1 and Figure 3-2. In particular, the changes made to the wing wall design are listed below:

- The width of the footing was increased.
- A key wall was included to provide additional sliding stability in case of scour.
- Overlapping culvert and wing wall tab extensions were added.

Since the wing wall was disconnected from the culvert barrel, it was further re-designed as a free-standing cantilever retaining wall. To provide the overall stability of the wing wall and effectively distribute the weight to the foundation soil, the footing width was increased.

According to the AASHTO LRFD (2014), the stability of a free-standing wing wall depends not only on structural resistance but on sliding, bearing and overturning capacity of the soil-structure system. In this case, the dimensions of the footing were controlled by bearing capacity of the soil. Thus, the stronger soil allowed for narrower footing dimensions, while weaker types of soil required an increased footing width.

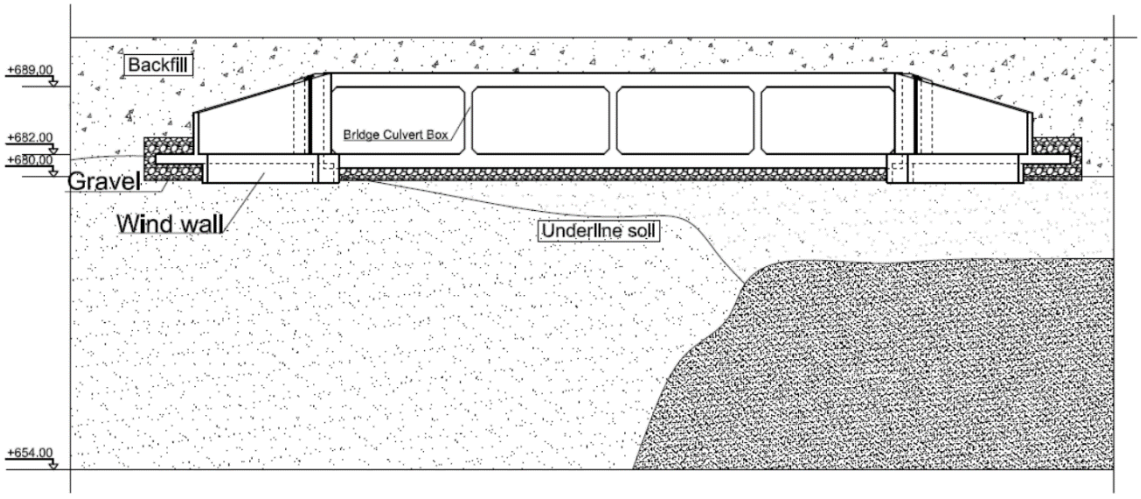

Figure 3-1. Tabbed culvert design.

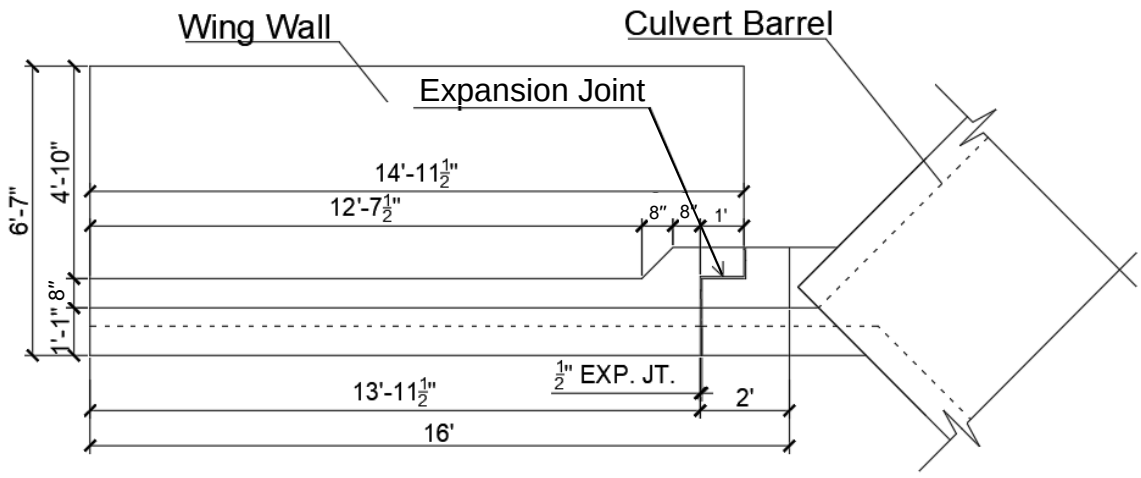

Figure 3-2. Tabbed wing wall-to-culvert connection.

As the wing wall was designed as a cantilever retaining wall, it may settle and rotate independently from the barrel. Due to this movement, some compression forces could be transferred between two overlapping tab extensions. In terms of sufficient anchorage length of horizontal reinforcement, both tabs were designed 12-in (1-ft) deep (Figure 3-2).

These improvements allow differential settlement to occur without generating large stresses at the connection zone. Thus, the probability of crack formation along the joint decreases.

3.3 Tab Extension Design

The changes to the current design, discussed in the previous chapter, were offered by ALDOT in order to solve the problem of cracking along the wing wall-to-culvert joint. By eliminating the rigid connection, the stress concentration zone was removed and both structural components were allowed to move independently. Without the rigid connection, the wing wall behaves as a short cantilever retaining wall with pin support along one side. This also decreases the excessive stresses that lead to the rapid crack formation. Thus, the durability service life of the structure is increased.

An overlapping tab extension was added to each corner of the body of the culvert to serve as a horizontal bearing support for the wing walls to ensure the two structural elements continued to perform jointly in resisting the loads associated with backfill. In this way, the wing walls still benefit from the lateral stiffness of the culvert, but restraint is removed from what was previously a concentration of stress. Also, the newly designed tabbed connection allows for the translation of loads from the wing wall to culvert barrel horizontally. The dimensioned plan view of the wing wall-to-culvert joint is shown in Figure 3-3.

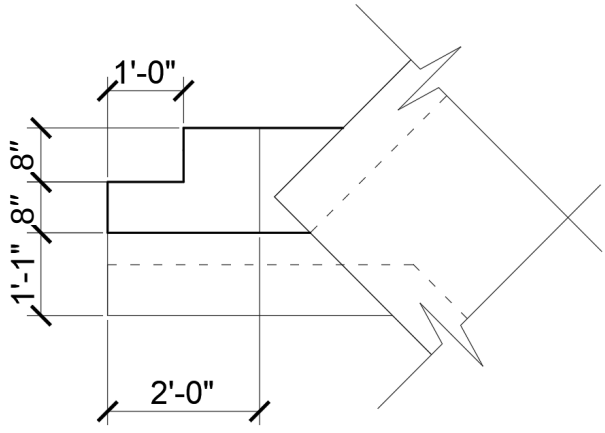

Figure 3-3. Sketch of the tab extension.

Initially, the depth of the tab extension was 8 in. based on the new experimental design. These dimensions were chosen to be sufficient for an effective transfer of stresses from the wing wall to the barrel. It was also suitable in terms of sufficient anchorage length for the horizontal reinforcement. Later, the actual wing wall-to-culvert connection was designed with 12-in (1-ft) tab extension. The ½-in gap between overlapping tab extension was filled with a layer of bituminous material in order to provide the independent movement of the structures, allow the transfer of stresses from the wing wall to the culvert, and prevent the soil ingress into the joint. For three different culverts constructed according to the new design, the thickness of the tab was the same as the wall thickness and equal to 8, 9, and 10-in respectively (Appendix A).

3.4 Constructed Culverts

ALDOT designed three new culverts in conjunction with county engineers for testing as part of this project. The culverts were located in reasonable proximity to Auburn, Alabama: Chambers County Road 258, Lee County Road 156 and Coosa County Road 68. In all three cases, the novel tab connection was implemented. Thus, the cast-in-place wing wall and barrel were constructed separately opposite to the traditional design.

3.4.1 Chambers County

The first culvert was built on Chambers County Road 258, located over Whatley Creek, in April 2016. It is shown in Figure 3-4. This culvert consists of four barrels with total outer dimensions of 44-ft by 51-ft in the directions along and transverse to the stream, respectively. The depth of the culvert barrel is 8.4-ft, which is the smallest depth of all locations. The 1.25-ft deep key wall was added to each side to prevent soil erosion under the barrel and increase the overall stability of the structure.

Figure 3-4. Location of Chambers County culvert ("Google Maps" 2017a)

Four identical free-standing wing walls were cast with an angle of 45° to the barrel. The height of the wing walls varied from 7.16-ft at the connection with the barrel to 4.5-ft at the opposite side. The total length of the wall was 15-ft with the total width of the footing (toe with a heel) of 6.5-ft. The key wall attached to the wing wall was 1.5-ft deeper than the bottom of the footing. After construction, the backfill 1.16-ft above the culvert top slab was added along with the pavement. The detailed drawings of the culvert at Chambers County are shown in Figure 3-5 and Figure A-1-4 (Appendix A).

3.4.2 Lee County

The second culvert, located in Lee County Road 156, was built in September 2016 (Figure 3-6).

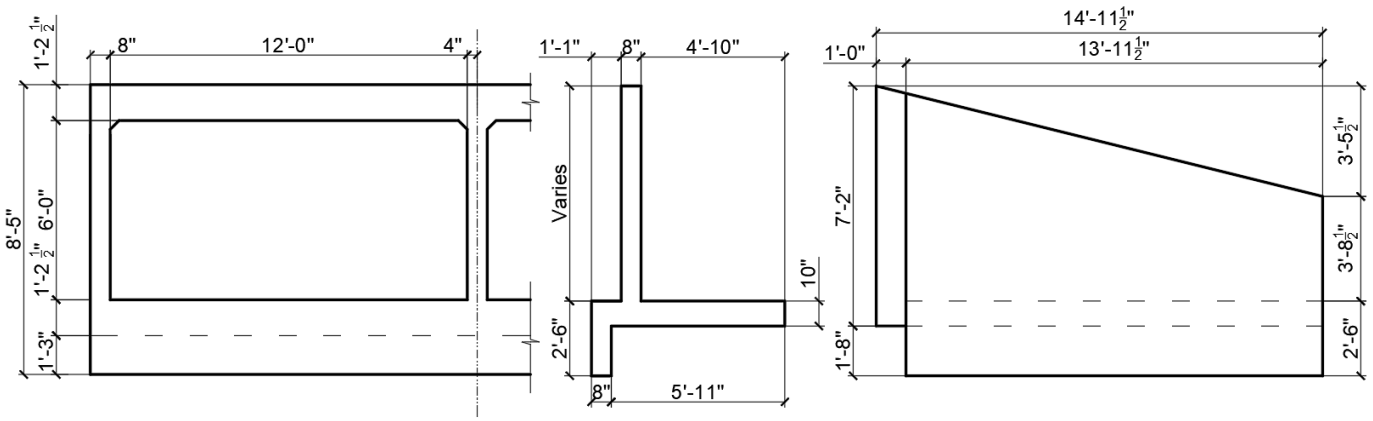

Figure 3-5. Outer dimensions of the Chambers County culvert

Figure 3-6. Location of Lee County culvert ("Google Maps" 2017b)

This structure consists of three equal size barrels with 10-ft by 8-ft waterway openings. The total length of the culvert along the stream was 44-ft, while the total width transverse to the

stream is 32.6-ft. The depth of the culvert was 10.16-ft extended with a 1.3-ft key wall. Similar to the previous case, four wing walls were constructed at an angle of 45° to the barrel which is skewed by 15°. While the heights of the wing walls were greater than those in Chambers County (9-ft), the length of the wing walls were 4-ft shorter. The height of the wing wall gradually decreased from 9.5-ft at the barrel side to 4.6-ft at the outer edge. The total width of footing (toe with a heel) was 8.25-ft. The key wall attached to the wing wall extends 1.6-ft deeper than the bottom of the footing. The backfill was 1.2-ft above the culvert top slab with the wearing surface above. The dimensioned drawings of this culvert are shown in Figure 3-7 and Appendix A.

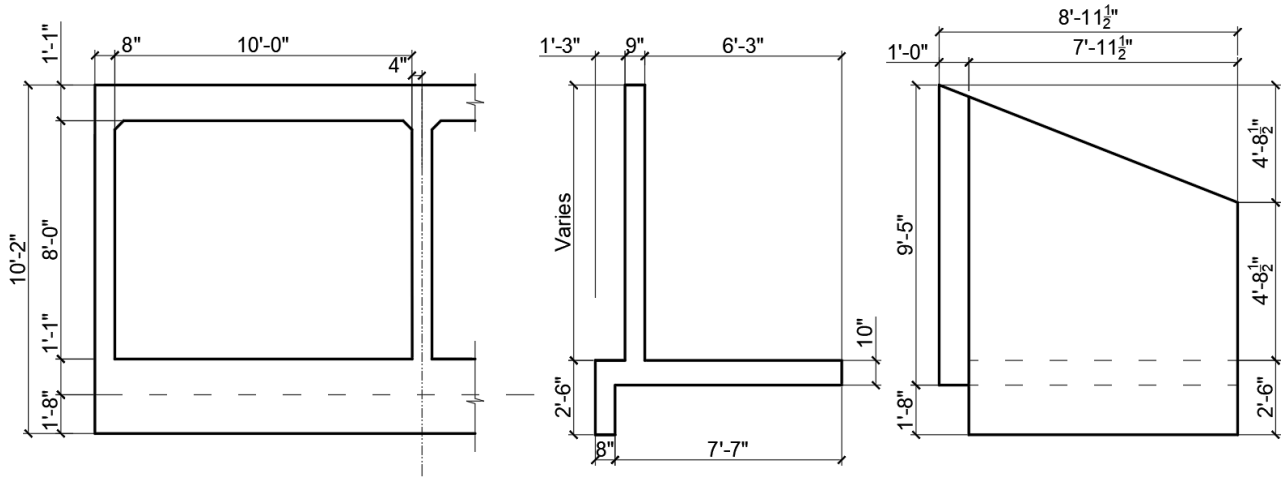

Figure 3-7. Outer dimensions of the Lee County culvert

3.4.3 Coosa County

Construction of the third culvert over Shelton Creek on Coosa County Road 68 was completed in October 2016 (Figure 3-8). This culvert was the largest considered in this study. It consisted of four CIP barrels with 14-ft by 10-ft waterway openings. The total dimensions of the culvert were 44-ft by 60-ft in the direction along and across the stream, respectively.

Figure 3-8. Location of Coosa County culvert ("Google Maps" 2017c)

The depth of this culvert was 12.25-ft extended with a 3.8-ft deep key wall. Each diagonal pair of wing walls had slightly different geometry, but all of them were constructed at an angle of 45° to the culvert barrel. The difference was only in footing width, which for the first pair was 10-ft, and for the second was 8.5-ft. The wing wall was 11-ft long. The height of the wall gradually decreased from 11.5-ft at the culvert side to 5.5-ft at the outer edge. The key wall was the same as in the barrel and 3.8-ft deeper than the footing bottom. Unlike others, this culvert had backfill only to top of the wall. Pavement placed directly on the culvert box. The detailed drawings of this culvert are shown in Figure 3-9 and in Appendix A.

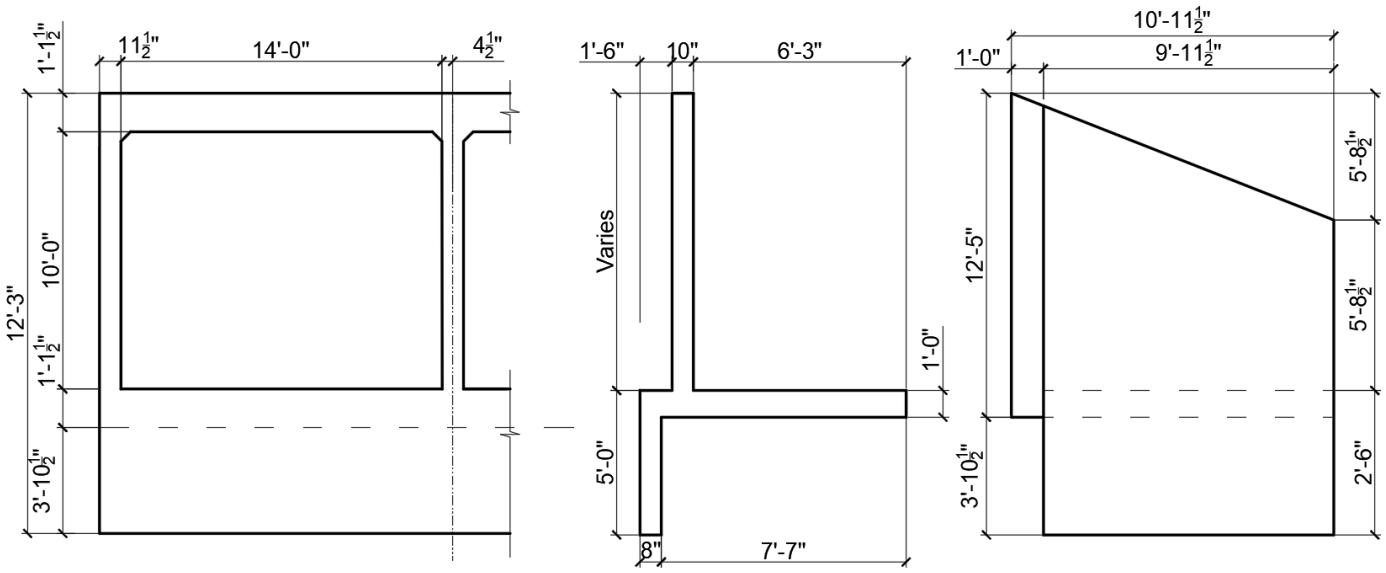

Figure 3-9. Outer dimensions of the Coosa County culvert

Chapter 4. Culvert Construction and Instrumentation

This chapter details all aspects of the instrumentation, construction and long term monitoring program.

4.1 Tab Pressure with Vibrating Wire Earth Pressure Cells

The magnitude of this pressure acting upon the tabs of the culverts was measured using Model 4810 Vibrating Wire Pressure Cells manufactured by Geokon, Inc, shown in Figure 4-1. This model was chosen because its intended use is the measuring of soil pressure on structures and because the expected values of pressures predicted by the finite element models fell within the applicable range and granularity of the sensors. Furthermore, the thin profile and 9 inch diameter of the pressure cells fit well within the necessary area of the tab and did not add much complexity to the construction process.

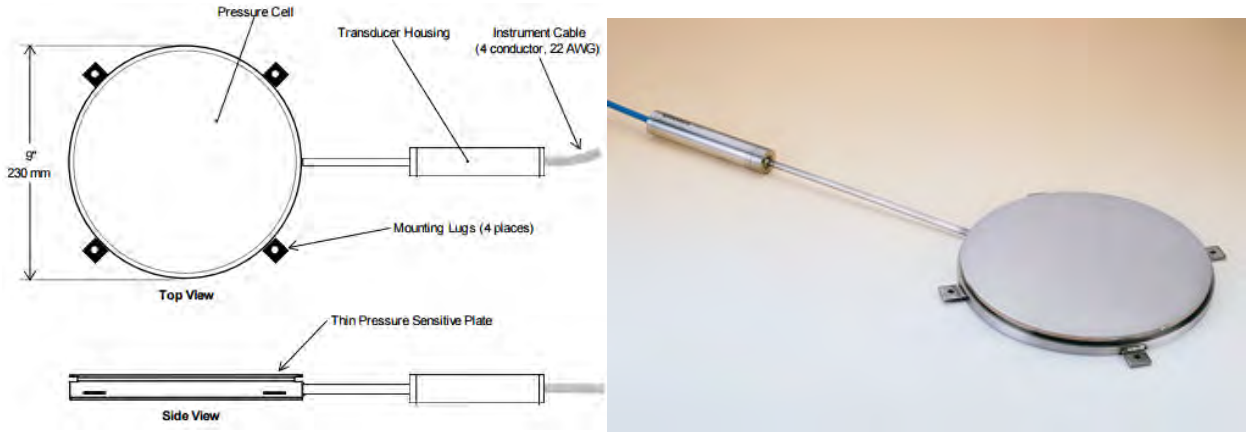

(a) (b)

Figure 4-1. Model 4810 Contact Pressure Cell (Geokon, Inc., 2011)

These pressure cells operate based on hydraulic principles. Two thin, round, flat plates were welded together along their circumference and the gap between them was filled with hydraulic fluid. The specific cell used for this research was made with one rigid plate for bearing against the structure and one flexible plate which deforms according to the applied pressure. The

flexibility of the plate exposed to the pressure functions such that the external pressure is in equilibrium with the hydraulic fluid between the plates. This fluid is connected hydraulically to a vibrating wire pressure transducer which converts the pressure into an electrical signal through the use of a plectrum that induces a corresponding vibration. This value is then transmitted through the connected wires. Also, a thermistor located within the transducer which provides a value for the temperature at the location of the cell (Geokon, Inc., 2011).

Although it is typical to install these cells with the deformable face directly exposed to soil, the aim of this project was not to measure soil pressure, but rather the pressure experienced by the tab of the culvert. The cells were installed in the gap between the tab and wing wall and therefore measured the magnitude of the pressure transferred into the tab through contact with the wing wall. Review of literature did not uncover any previous attempts at using these pressure cells in a similar manner; however, the use of a bituminous material to cover the deformable face of the pressure cells ensured that the pressure applied to the cells was distributed appropriately and therefore it was believed that this application of these cells was valid.

Each instrumented tab contained three pressure cells distributed through its height, with one placed 1 inch above the location of the cold joint at the bottom of the tab, one placed 2 inches below the lowest point of the slope of the top of the tab, and another placed centered, between the other two cells. Cables were attached to the tab surface so that they would not pass in front of the cells (Figure 4-2).

A handheld readout was connected via alligator clips to the five exposed wires of the pressure cells to take readings. The readout showed the temperature and a raw digit value, based on the vibration frequency, which was used to calculate pressure. The data was recorded by hand in a field book.

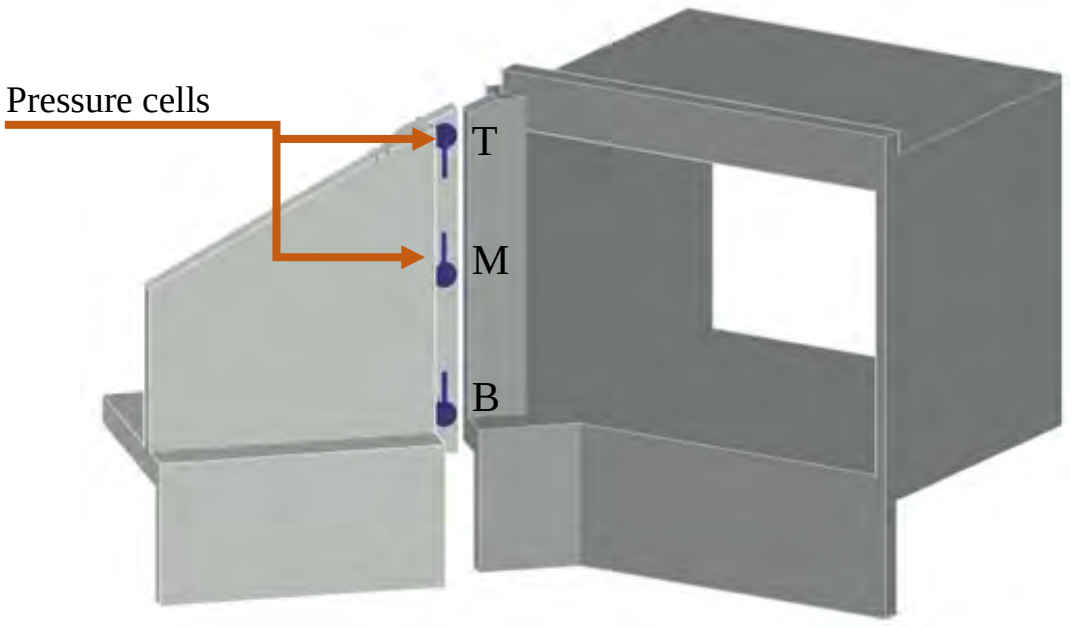

Figure 4-2. Location of the pressure cells

Prior to the construction of the first culvert, two methods of cell installation were proposed: embedded installation and post-construction installation.

4.1.1 Embedded Installation

The embedded method of installation required that the pressure cells be attached to the formwork, as shown below in Figure 4-3 (a), so that they could be completely embedded in to the concrete of the tab, as shown in Figure 4-3 (b). The cells were attached using steel wire so that the wire could be cut when it came time to remove the formwork. Plastic cable ties were used to ensure the cables would follow an appropriate path to the top of the tab.

This method proved to be labor intensive due largely to the difficulty associated with the added care necessary to place the formwork with attached pressure cells while navigating through already placed reinforcing steel. There was also an increase in the difficulty of removing said formwork.

(a) (b)

Figure 4-3. Formwork prepared for embedded installation of pressure cells and Pressure cells embedded in culvert tab

4.1.2 Post-Construction Installation

The post-construction method of pressure cell installation, shown in Figure 4-4, involved using block-outs on the formwork in order to create recesses in the hardened concrete of the tab into which the cells could be installed using concrete screws. The cables were attached to the perimeter of the cells using zip ties to ensure that the cables would not pass in front of the cells and affect pressure measurements.

The method of post-construction installation allowed for reusability of formwork and resulted in an easier construction process overall in comparison to the embedded method of installation. An added benefit of this method was that, unlike the embedded cells, the post installed cells protruded a slight amount beyond the face of the tab which increased the likelihood of contact with the wing wall registering as pressure on the cells. For these reasons, it was decided that the

post-construction installation method was the better choice; thus, it was utilized for all subsequent installations on this project.

(a)

(b)

(c)

Figure 4-4. Formwork with block-outs for post installation Recesses in tab for post installation and Post installed pressure cells

4.2 Gap Movement Measurement across Horizontal Face

The opening or closing of the gap between the wing wall and tab on the horizontal face of each was measured using a 200 mm Mayes demountable mechanical concrete strain gauge (DEMEC), shown in Figure 4-5. The DEMEC gauge has one fixed point and one movable point that are set apart at a fixed distance by a rigid bar. The movable point allows for variability in the distance between the two points and their separation is measured by the attached dial gauge.

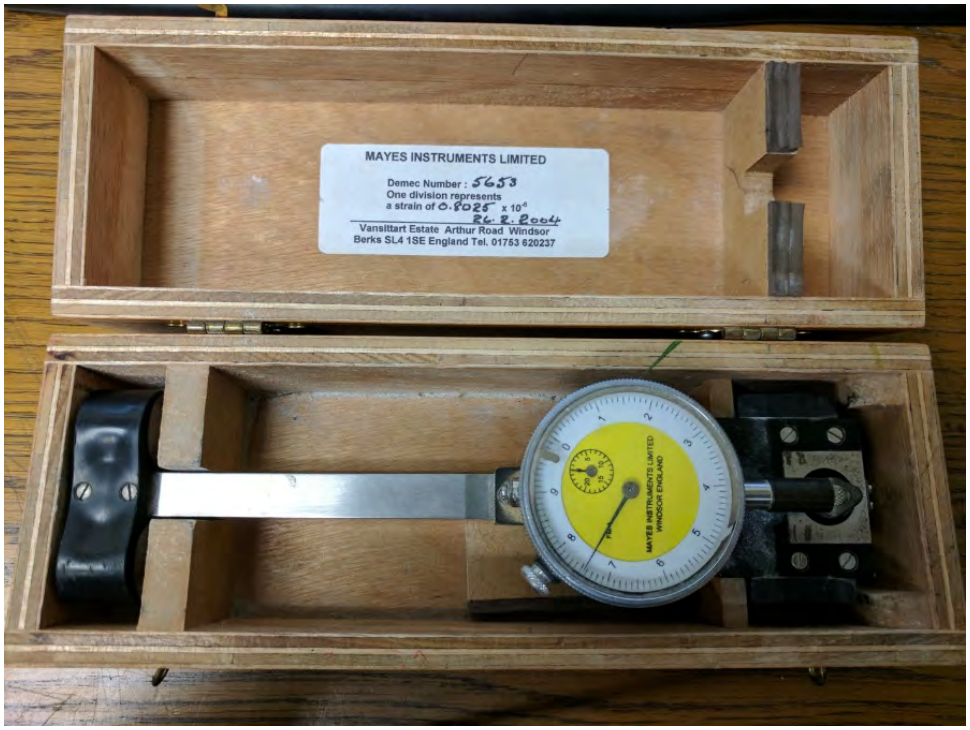

Figure 4-5. Mayes demountable mechanical concrete strain gauge (DEMEC)

To use the DEMEC, metal studs, with dimples that serve as receptacles for the two points on the DEMEC, were installed a set distance apart into the concrete, as shown in Figure 4-6. The x-marks on Figure 4-7 indicate the approximate location of the studs on the culvert.

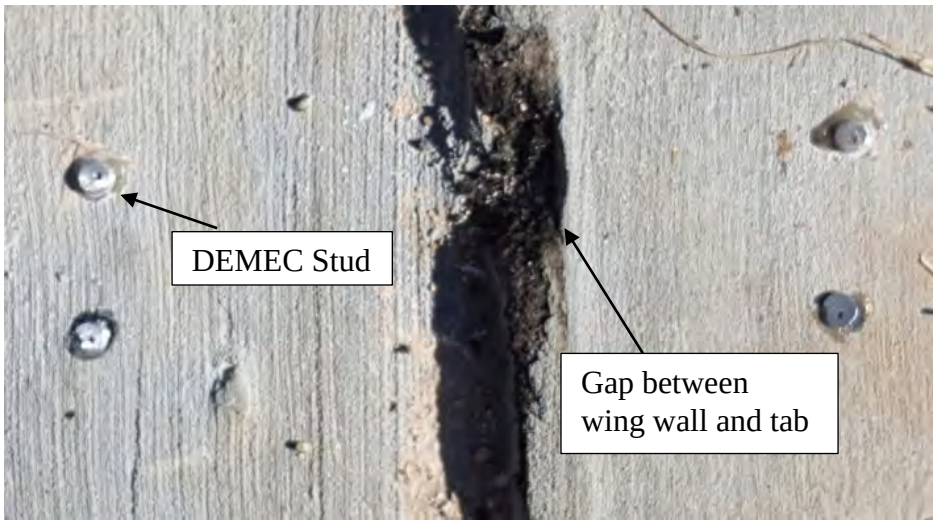

Figure 4-6. DEMEC studs

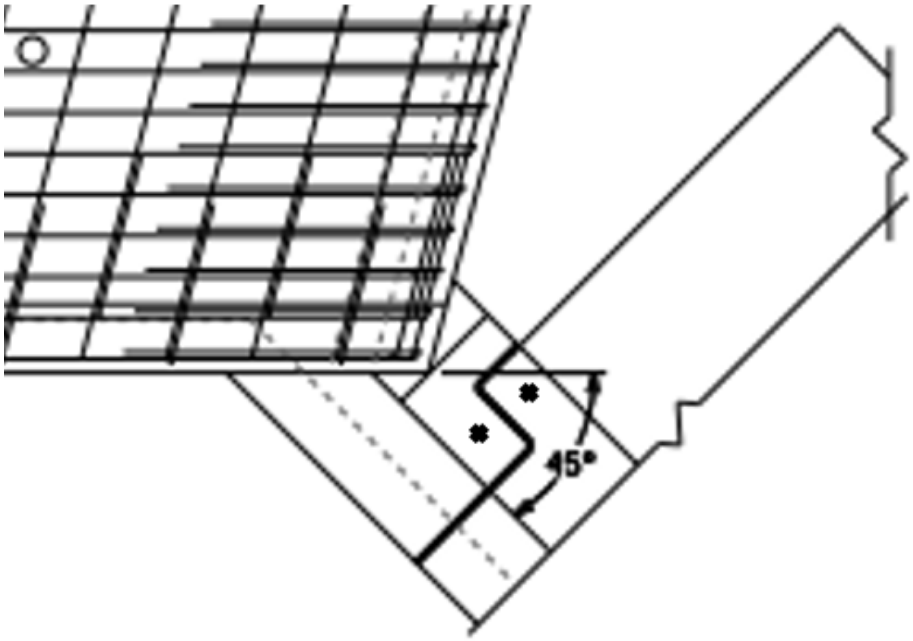

Figure 4-7. Location of DEMEC studs

4.3 Gap Movement Measurement across Vertical Face

The movement of the gap between the wing wall and tab on the vertical face was measured using Avongard tell-tales, as shown below in Figure 4-8. These were used in place of the DEMEC due to the potential for larger displacements that fall outside of the range of the DEMEC. The tell-

tales provided a visual depiction of gap movement by attaching one half of the tell-tale to either side of the gap, with the graduated half of the tell-tale overlapped by an indicator for the original location of the center. Over time, the magnitude of the movement of the gap was quantified by reading where the indicator aligned with the scale.

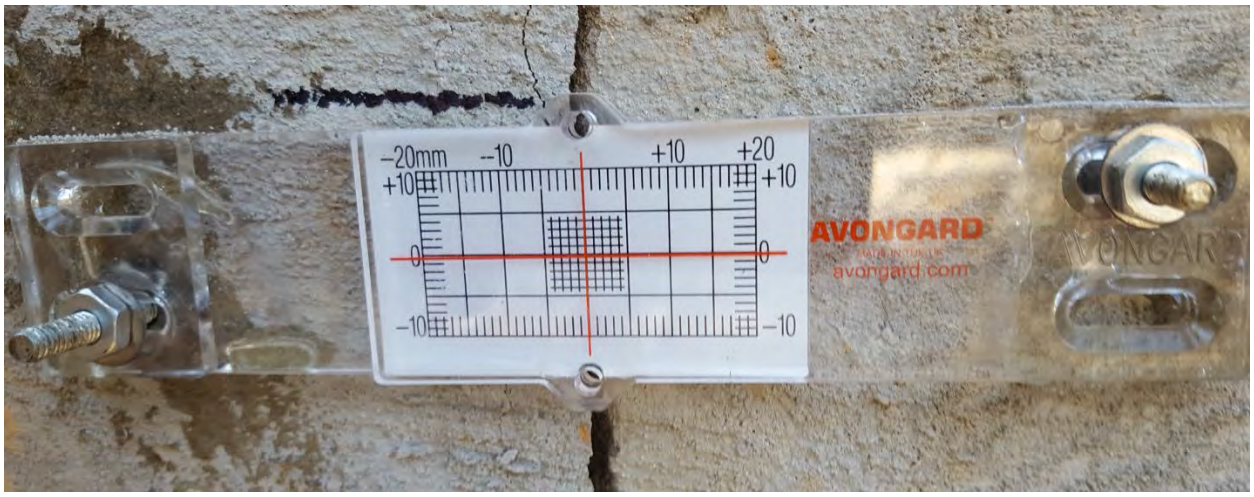

Figure 4-8. Avongard tell-tale

The tell-tales were installed by first marking the location of the tell-tale holes on the concrete with a marker, such that the center of the tell-tale aligned with the gap. Depicted in the figure, only two screws were used to install the tell-tales due to the holes in the tell-tale being too close for two holes to be drilled on one side without compromising the integrity of the concrete between the two holes. A caulk gun was then used to fill the holes with silicone adhesive and a screw was placed head first into each hole. Once the adhesive had set, the parts of the tell-tale that would make contact with the concrete were also coated in adhesive and the tell-tale was placed onto the screws and pushed flush with the concrete. Finally, a washer and nut were fixed onto the exposed threads of the screws and hand tightened. In order to track the movement of the gap, a photo of each tell-tale was taken during all site visits that followed their installation.

4.4 Culvert Construction

4.4.1 Chambers County

The culvert constructed in Chambers County crosses Whatley Creek on Chambers County Road 258. It replaced a multi span bridge supported by wood piles with additional steel piles used for repair. Figure 4-9 shows the original bridge.

Figure 4-9. Original bridge in Chambers County

Below is a list of significant dates during the construction and monitoring of the culvert in Chambers County, followed by a selection of photos, Figure 4-10 through Figure 4-13, showing the construction process.

- June 29, 2015: The southern wall of the culvert was placed with the pressure cells installed integrally in western tab.

- July 6, 2015: The pressure cells were installed in the eastern tab of the southern wall and the southern wing walls were placed.
- July 21, 2015: The southern half of the elevated mat was placed.
- August 24, 2015: The northern wall of the culvert was placed.
- August 27, 2015: Pressure cells were installed in both northern tabs and the northern wing walls were placed.
- September 9, 2015: The northern half of the elevated mat was placed.
- January 12, 2016: Significant backfill had been placed but no pavement.
- March 31, 2016: The pressure cell wires at Tab 3 were cut but still readable and a measurement recorded during significant rainfall.
- April 19, 2016: The first measurements after paving were recorded.
- September 13, 2016: A 24-hr cycle of measurements was recorded.
- November 17, 2016: All DEMEC studs and tell-tales were installed.

Figure 4-10. Workers construct formwork for southern end of culvert and formwork for embedded pressure cells

Figure 4-11. Southern wing wall formwork removed and formwork for northern half of elevated mat

Figure 4-12. All formwork removed and backfill completed

Figure 4-13. Paving completed

4.4.2 Lee County

The culvert constructed in Lee County crosses a tributary to Halawakee Creek on Lee County Road 156. The culvert replaced a single span steel truss bridge, shown in Figure 4-14.

Figure 4-14. Original bridge in Lee County

Below is a list of significant dates during the construction and monitoring of the culvert in Lee County, followed by a selection of photos, Figure 4-15 through Figure 4-18, showing the construction process.

- January 14, 2016: The first visit to the site was made. Demolition of existing structure had not yet been completed.
- February 26, 2016: The culvert barrels were placed.
- March 8, 2016: Pressure cells were installed in the eastern tabs of the culvert and both eastern wing walls were placed.
- March 22, 2016: Pressure cells were installed in the western tabs of the culvert and both western walls were placed.

- August 29, 2016: Researchers were alerted that backfill was underway. Measurements were recorded periodically, as well as with an approximately 40 ton truck located near each tab location.
- September 28, 2016: Backfill had been completed and a tack coat was placed in preparation for the placement of a bearing surface.
- September 29, 2016: Measurements were recorded after each lane of the bearing surface was placed.
- October 13, 2016: Initial DEMEC studs were installed.
- November 4, 2016: Improved DEMEC studs were installed along with all 4 tell-tales.

Figure 4-15. Water flow redirected and on-site water retention

Figure 4-16. Water flow redirected to construct western wing walls and completed culvert

Figure 4-17. 40 ton truck placed near tab and culvert in process of being paved

Figure 4-18. Paving competed

4.4.3 Coosa County

The culvert constructed in Coosa County crosses Shelton Creek on Coosa County Road 68. The culvert replaced a short single span bridge. Figure 4-19 is a photograph of the bridge.

Figure 4-19. Original bridge in Coosa County

Below is a list of significant dates during the construction and monitoring of the culvert in Coosa County. Figure 4-20 through Figure 4-22 show the construction process.

- March 29, 2016: The first visit to the site was made. Formwork for both culvert walls was already being erected and the necessary block out locations were explained.
- April 7, 2016: The western wall of the culvert was placed.
- April 14, 2016: The elevated mat of the culvert was placed.
- May 4, 2016: The northern wing walls were placed without pressure cells placed due to an error by the contractor regarding the placement of block-outs. The southern tabs were chiseled away to make space for the pressure cells to be placed appropriately.
- May 5, 2016: Pressure cells were installed in both of the southern tabs.
- May 9, 2016: The southern wing walls were placed.
- October 8, 2016: The first measurements post paving were recorded.

Figure 4-20. Workers construct formwork for barrels

Figure 4-21. Workers install pressure cells in corrected block outs

Figure 4-22. Completed culvert

4.5 Field Measurements

The instrumentation was monitored from the day sensors were installed until the last month of monitoring, which was March 2018. The data was recorded on a approximately monthly basis for the three constructed culverts. The monitoring of the Chambers County culvert started on July 6, 2015. The Lee County culvert was finished on March 3, 2016. In the case of the Coosa County culvert, the monitoring of this culvert started on May 5, 2016. Readings were limited due to travel distance.

The readings from pressure cells and displacement sensors are presented in this section. The distribution of recorded pressure in the tabs from all three culverts shows the same trend. After backfill was placed, pressure increased almost to its maximum value and over time gradually reduced to almost zero. However, fluctuations of pressure occurred within the monitoring period due to environmental factors - predominantly rain. The maximum observed pressure typically

occurred at the bottom of the tab. Observed displacements were on the order of hundredths of an inch.

4.5.1 Chambers County

The normal pressure in all tabs was less than 1-psi after construction was finished and until the backfill was placed. The pressure was not recorded immediately after the backfilling due to miscommunication with the construction crew. The maximum recorded pressure in the tab after the backfilling observed in tab #1 was 2.9-psi (Figure 4-23). Also, pressure peaks up to 5.7-psi were recorded in tab #1 due to significant rain. These peaks gradually reduced to 2-psi at the bottom and zero at the middle and top sensors. Stresses recorded at tab #2 (Figure 4-24) after backfilling were 0.7-psi and 0.8-psi following rain. During the remainder of the monitoring period, they oscillate around zero. In tabs #3 and #4 maximum recorded pressure of 6.7-psi was during culvert construction (Figure 4-25 and Figure 4-26). During the remaining monitoring, pressures in these tabs oscillated between 0 and 1-psi. Figure 4-27 and Figure 4-28 show these stresses also plotted with depth for each data collection. Displacement measurements are included for each tab in Figure 4-29 through Figure 4-31.

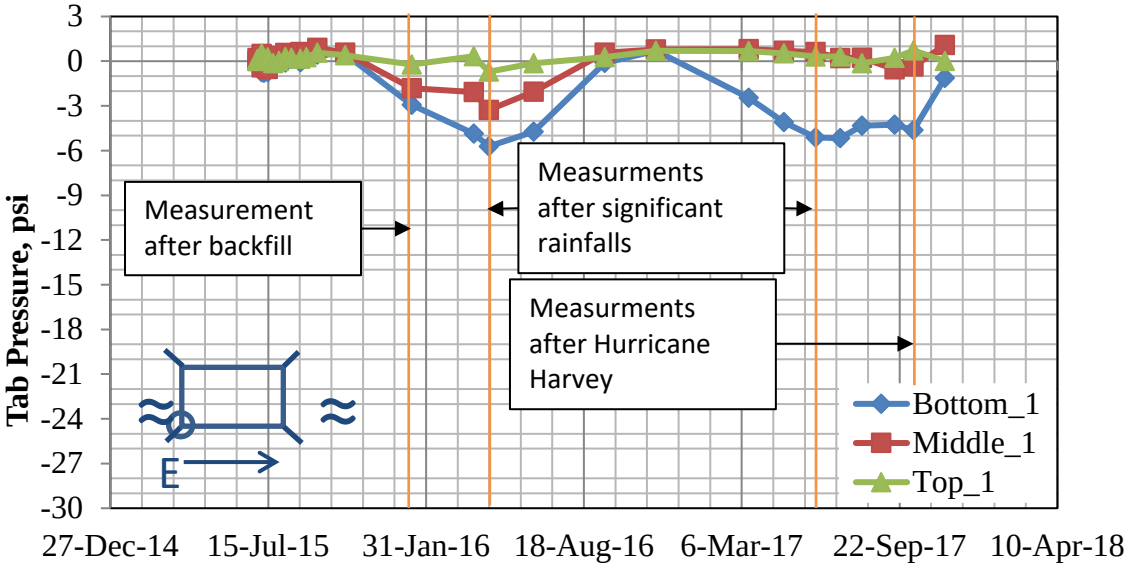

Figure 4-23. Chambers County stresses tab #1

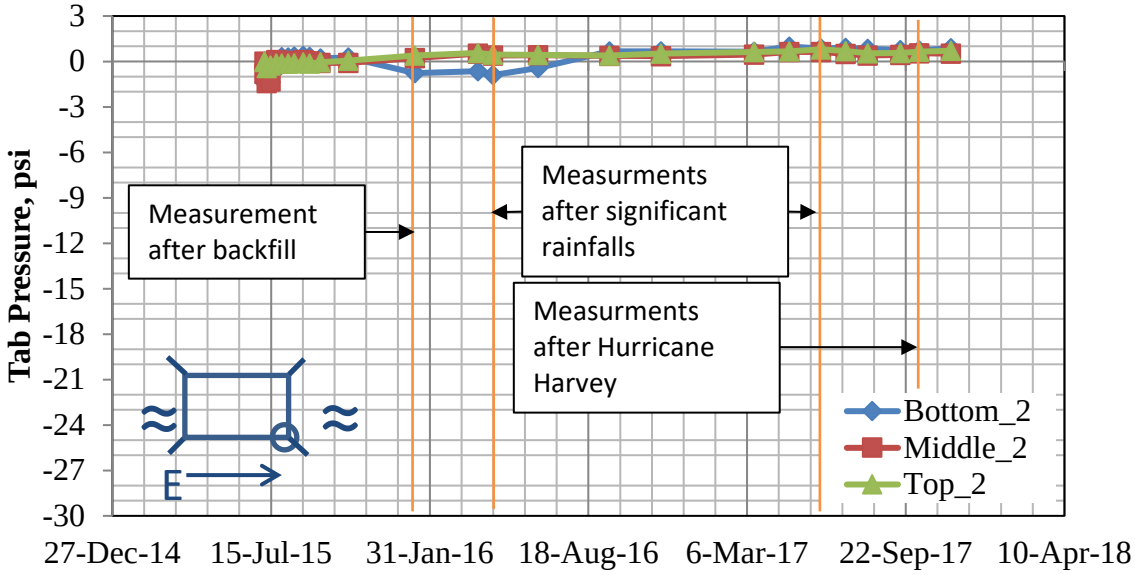

Figure 4-24. Chambers County stresses tab #2

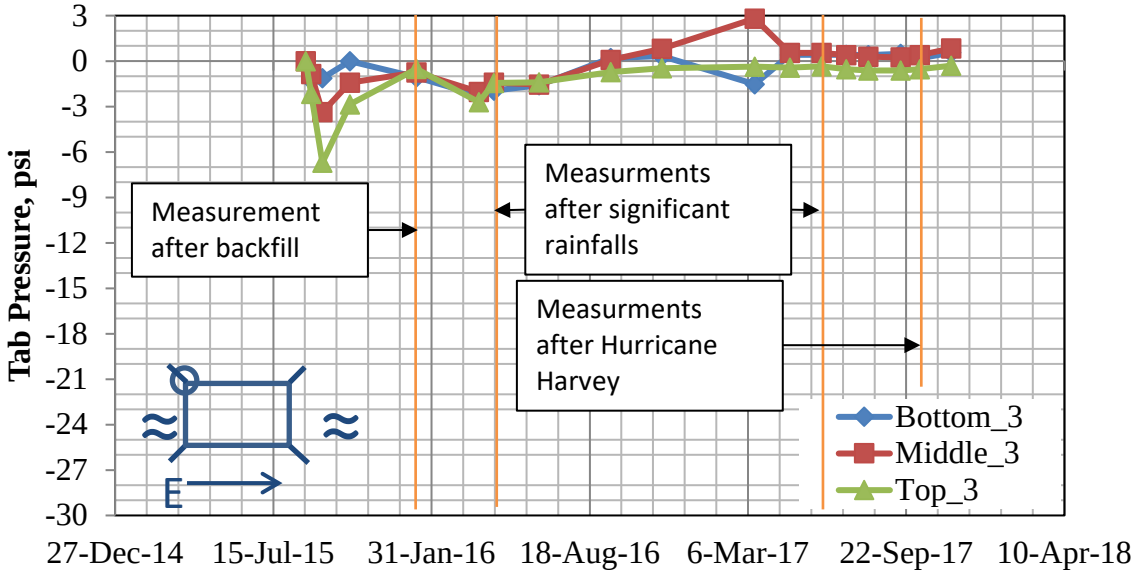

Figure 4-25. Chambers County stresses tab #3

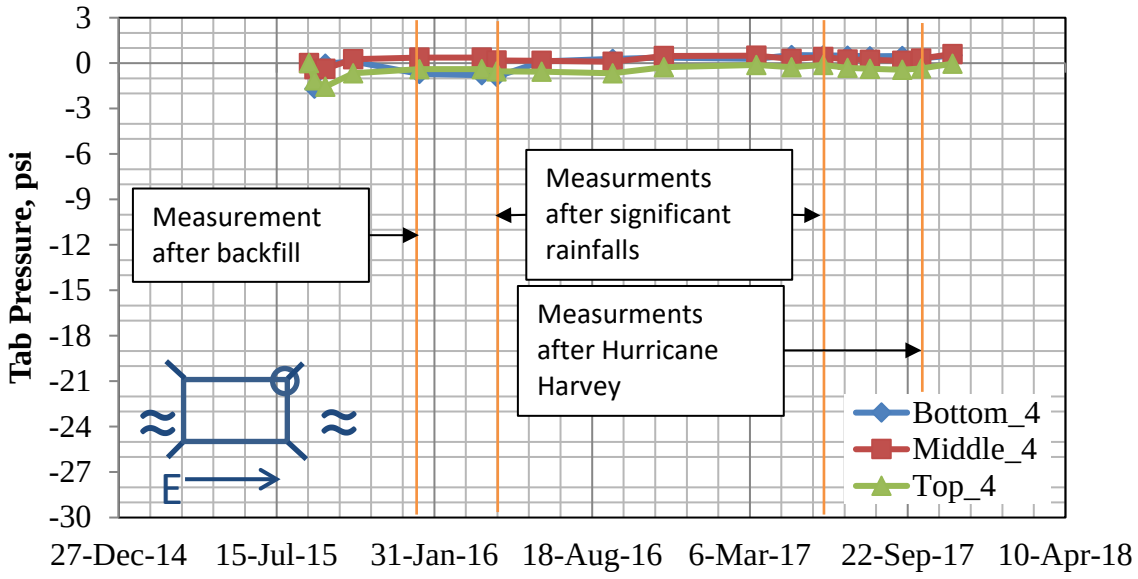

Figure 4-26. Chambers County stresses tab #4

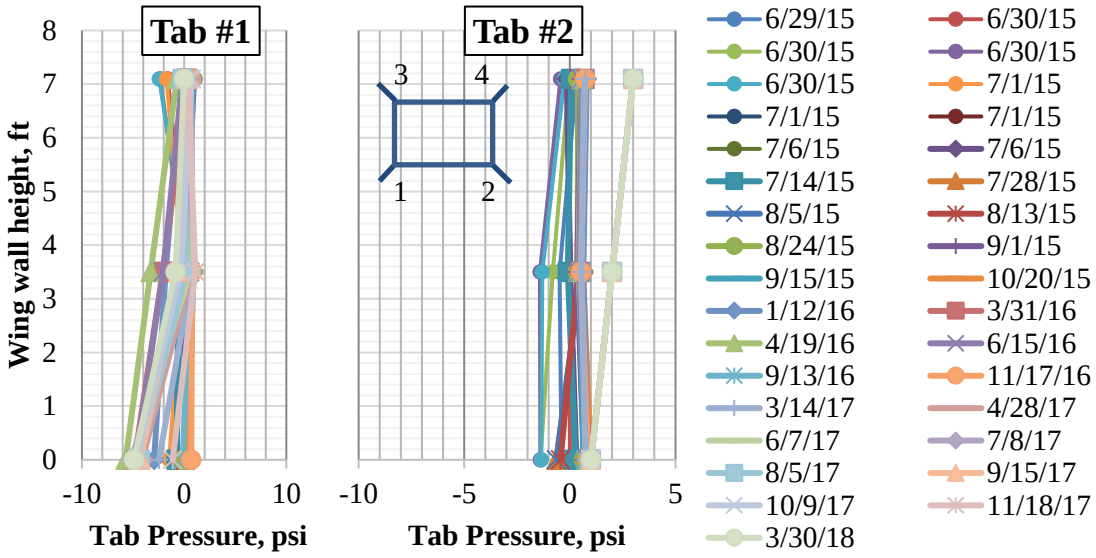

Figure 4-27. Comparison of recorded stresses along the wing wall height for the Chambers County culvert Tabs 1 and 2.

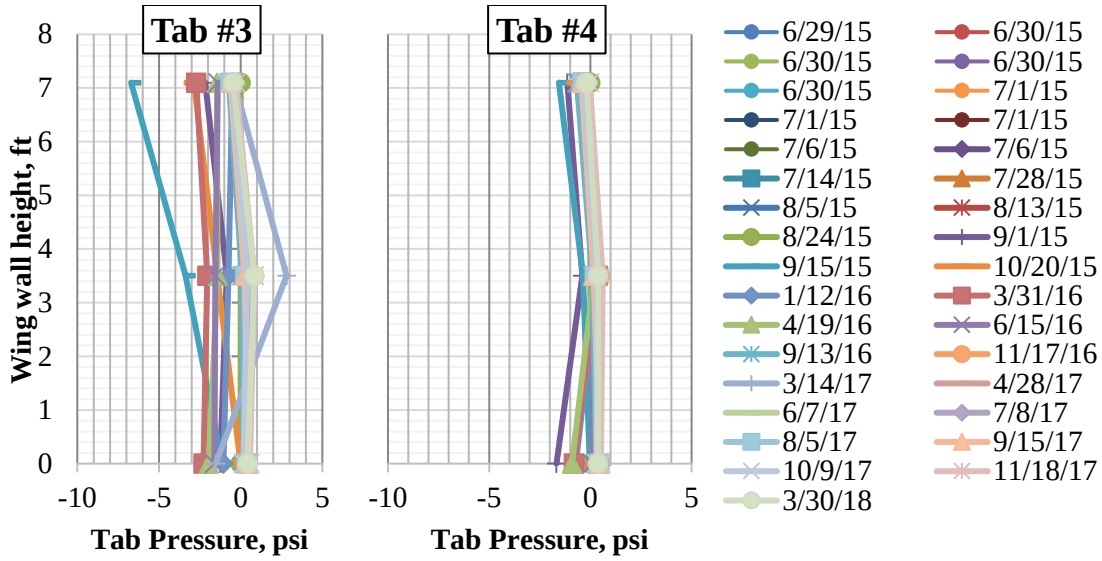

Figure 4-28. Comparison of recorded stresses along the wing wall height for the Chambers County culvert Tabs 3 and 4.

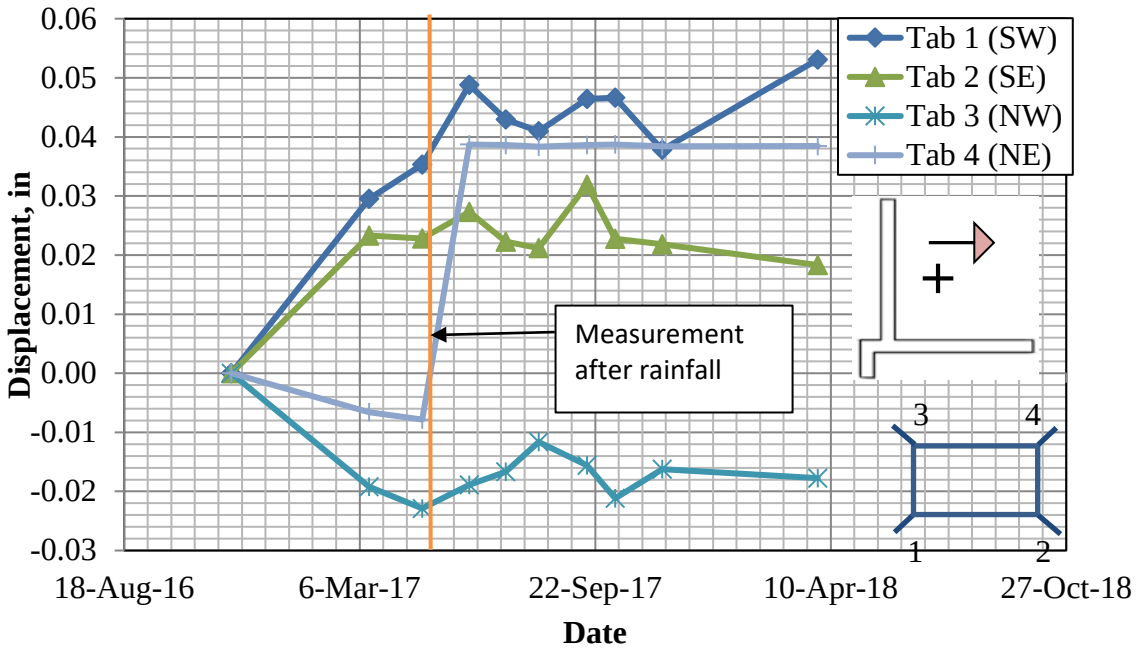

Figure 4-29. Out of plane movements of the Chambers County culvert wing walls based on strain gage measurements.

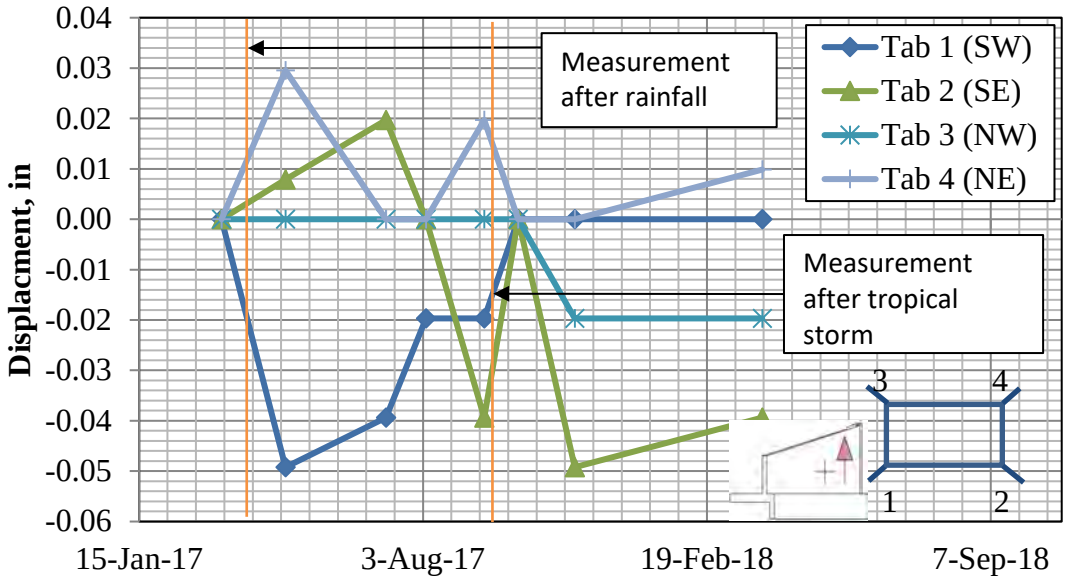

Figure 4-30. Vertical movements of the Chambers County culvert wing walls based on tell-tale measurements.

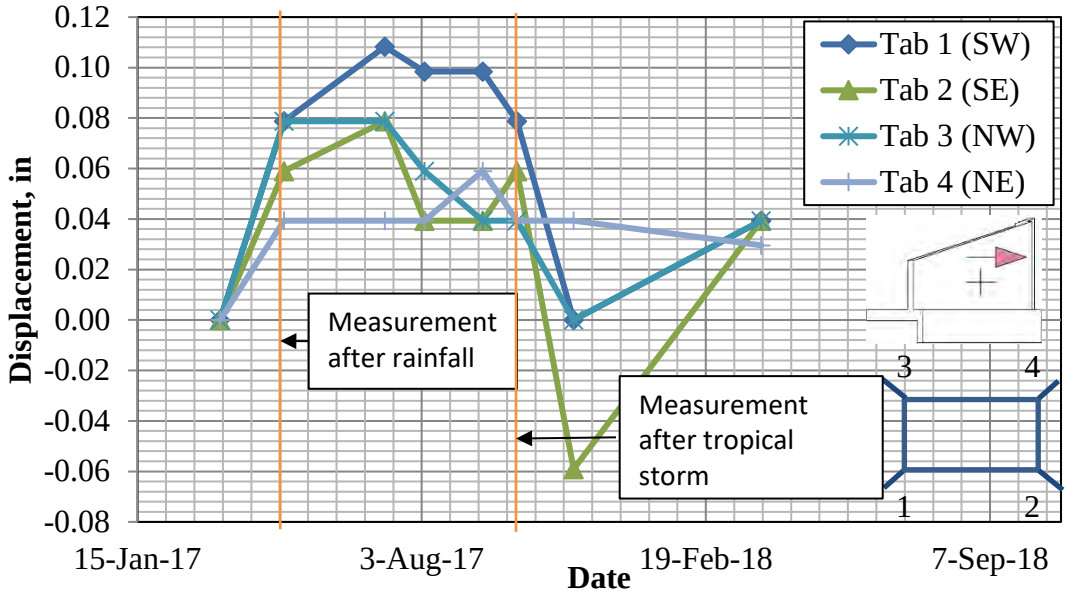

Figure 4-31. Horizontal movements of the Chambers County culvert wing walls based on tell-tale measurements.

4.5.2 Lee County

Unlike the Chambers County culvert, the maximum pressure in Lee County culvert was recorded on August 29, 2016, immediately after the backfill was placed and compacted. In addition to backfill, these measurements include the effect of an approximately 80-kip truck parked as close to each tab as possible. The maximum pressure in tab #1 after the backfill was 26.6-psi at the

bottom, 3.6-psi in the middle and zero at the top sensors. Within a short period of time, the pressure magnitude decreased to 14.6-psi at the bottom and 1.8-psi in the middle (Figure 4-32). Also, the stresses in tab #1 were the maximum observed among all instrumented tabs. The pressure in tab #2 after the backfilling was 17.6-psi, 11.7-psi, and 4.5-psi at the bottom, middle and top sensors, respectively (Figure 4-33). Similar to tab #1, the pressure magnitude decreased to 9.3-psi at the bottom, 5.5-psi in the middle, and 1-psi at the top, which remains the same for the recorded period. Pressure recorded in sensors installed in tab #3 remained constant during the monitoring period. The average pressure 2-psi was recorded by the bottom sensor, 0.3-psi by the middle and zero by the top (Figure 4-34). Unlike other tabs, the pressures detected by sensors in tab #4 did not decrease with time after placing backfill. The average value at the bottom was 10-psi during the monitoring period and around 1-psi at the middle and top sensors (Figure 4-35). Figure 4-36 and Figure 4-37 show these stresses also plotted with depth for each data collection. Displacement measurements are included for each tab in Figure 4-38 through Figure 4-40.

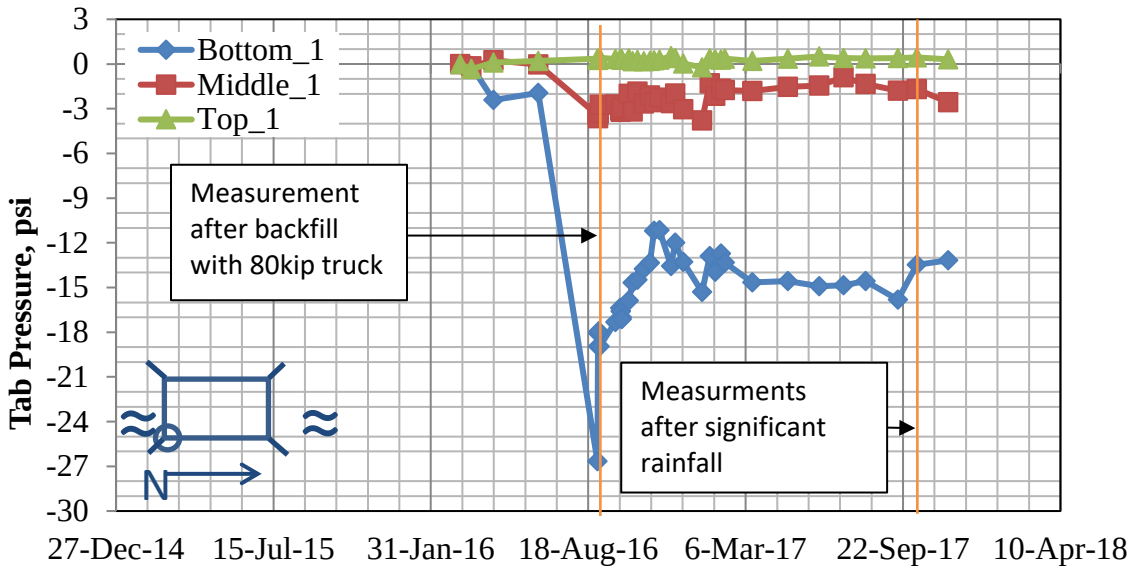

Figure 4-32. Lee County stresses tab #1

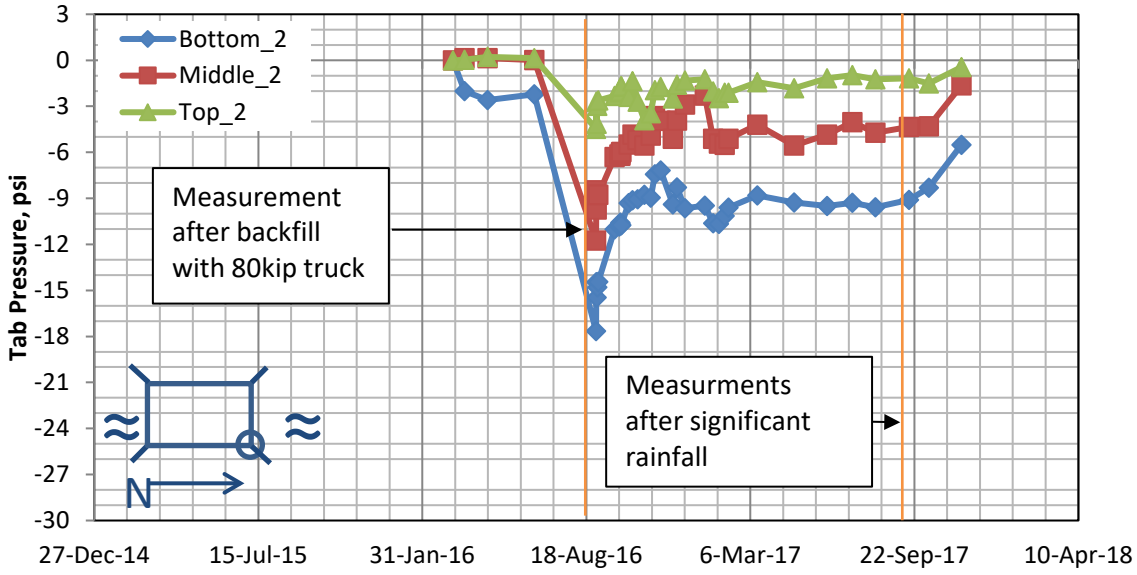

Figure 4-33. Lee County stresses tab #2

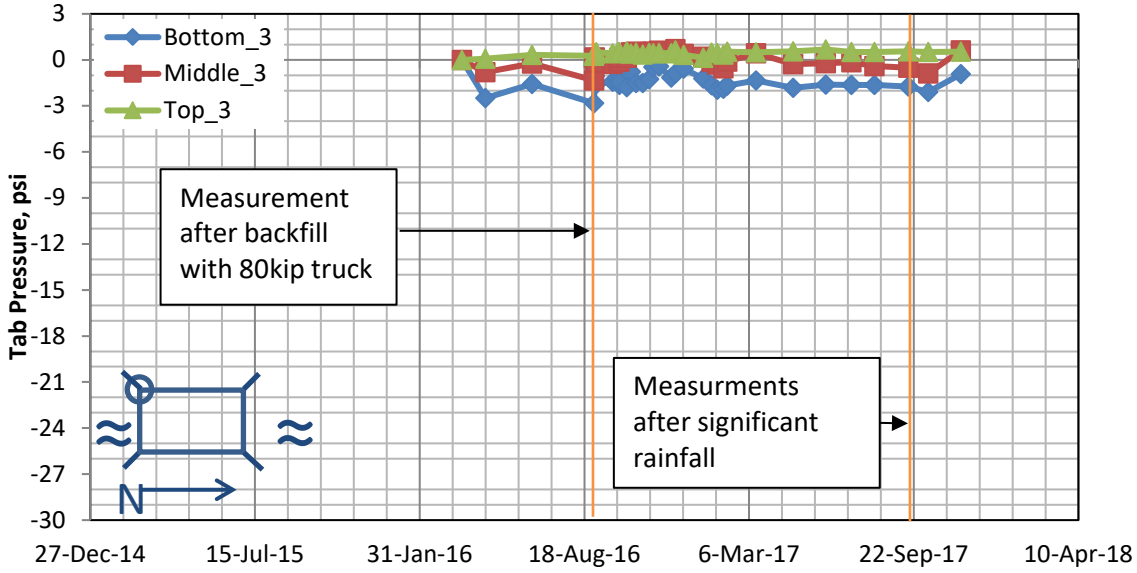

Figure 4-34. Lee County stresses tab #3

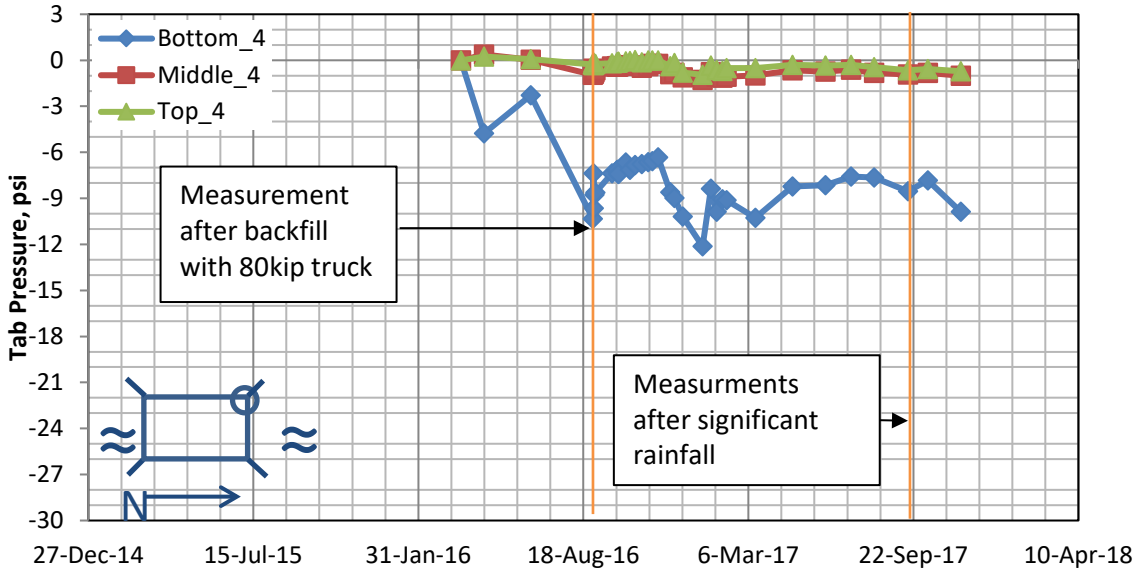

Figure 4-35. Lee County stresses tab #4

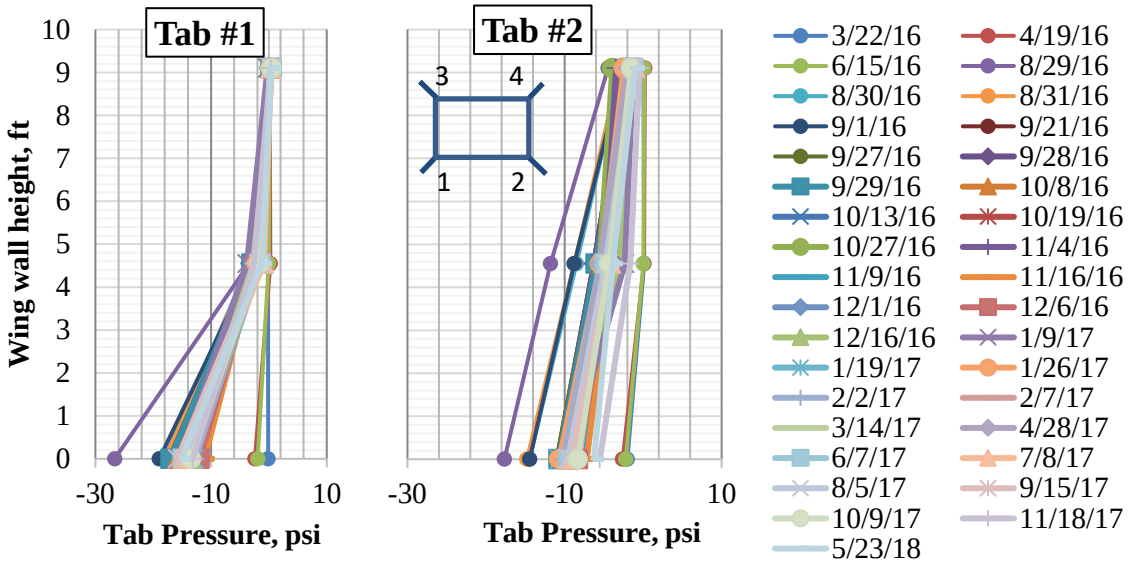

Figure 4-36. Comparison of recorded stresses along the wing wall height for the Lee County culvert Tabs 1 and 2.

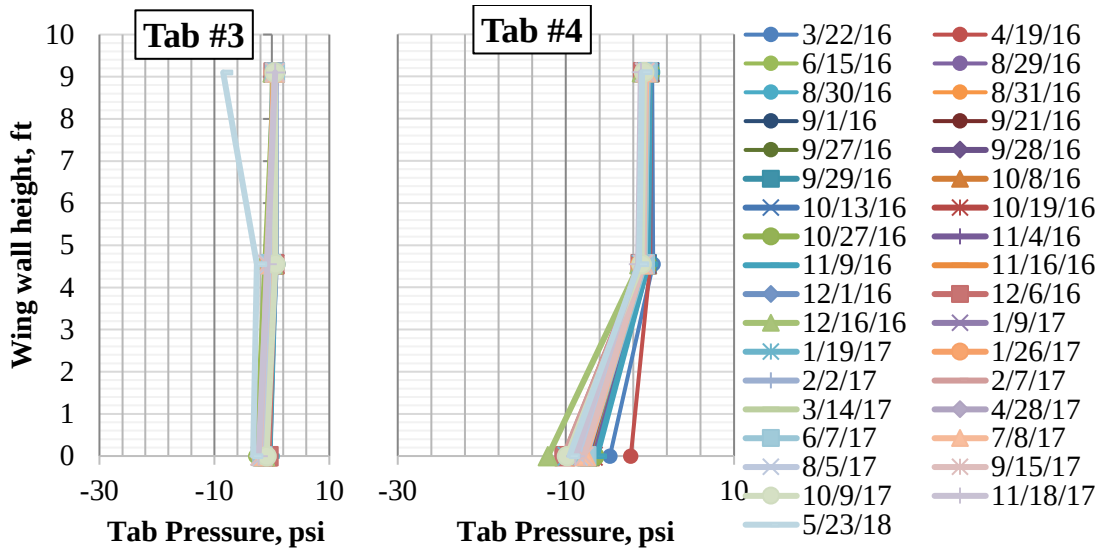

Figure 4-37. Comparison of recorded stresses along the wing wall height for the Lee County culvert Tabs 3 and 4.

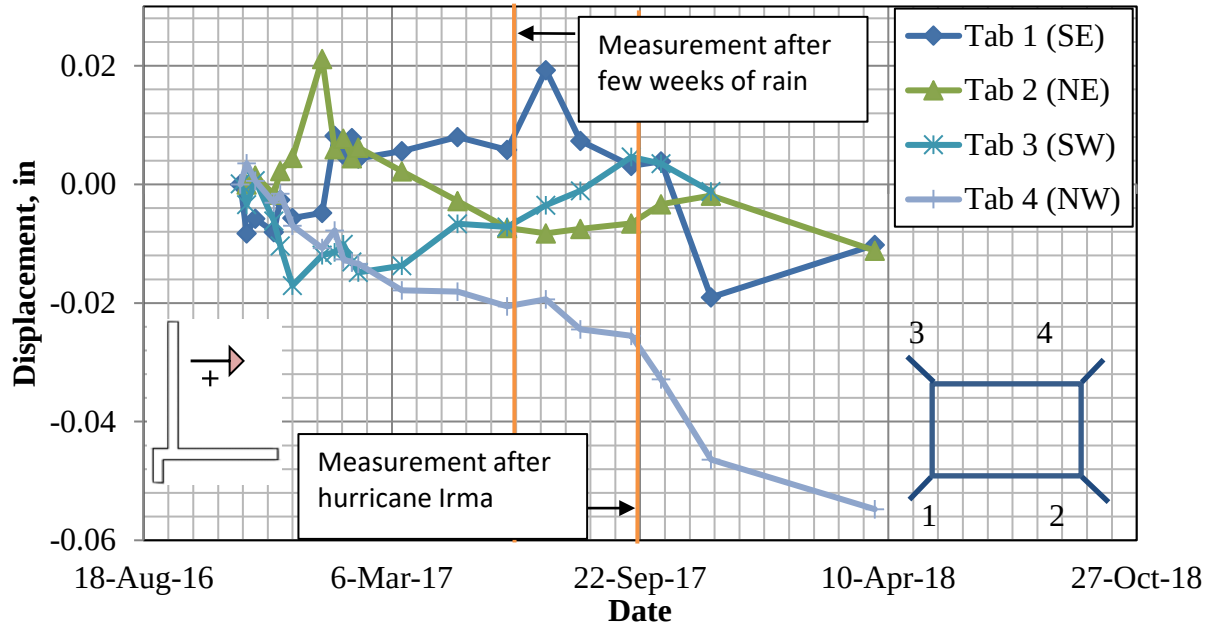

Figure 4-38. Out of plane movements of the Lee County culvert wing walls based on strain gage measurements.

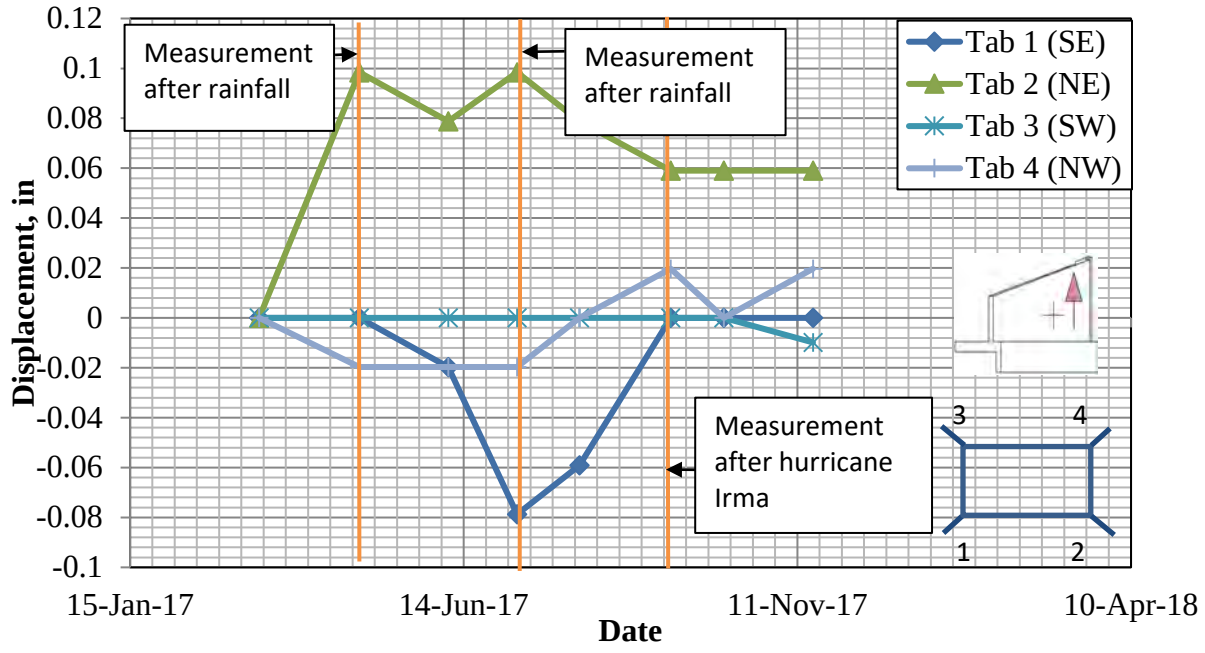

Figure 4-39. Vertical movements of the Lee County culvert wing walls based on tell-tale measurements.

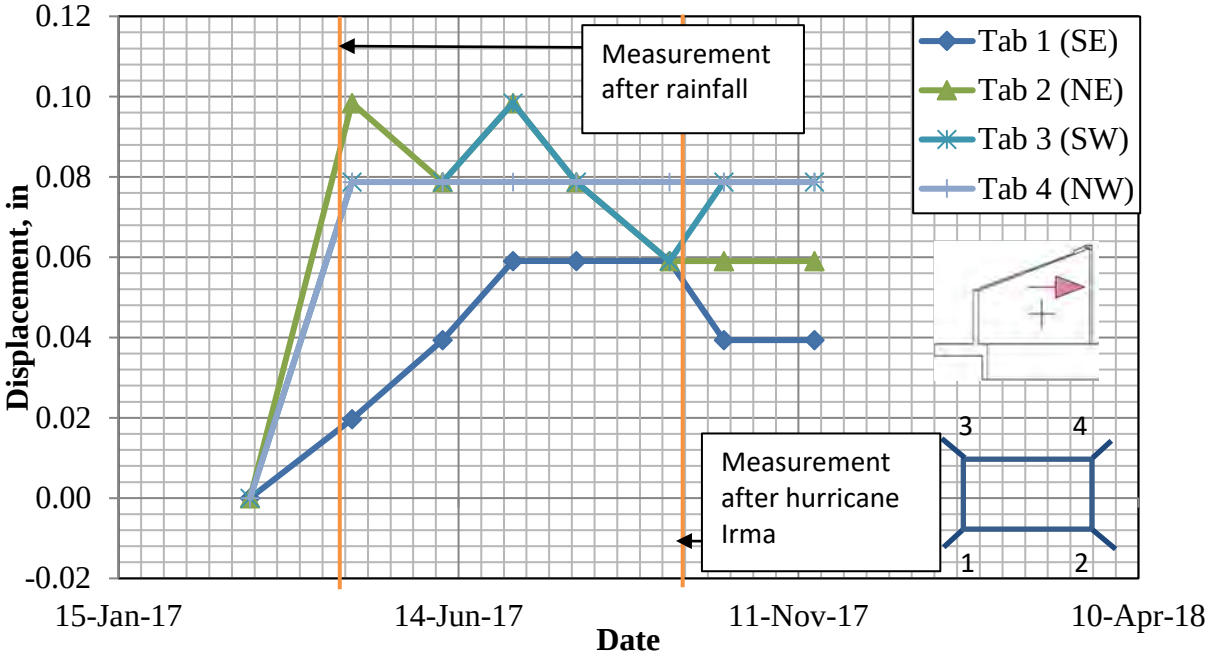

Figure 4-40. Horizontal movements of the Lee County culvert wing walls based on tell-tale measurements.

4.5.3 Coosa County

The pressure recorded in tab #1 at the Coosa County culvert had a uniform distribution with highest recorded pressure of 6.8-psi at the top. The pressures in the middle and at the bottom were 2.4 and 3.0-psi, respectively. This suggested simultaneous rotation of the wing wall and sliding of the wing wall away from the backfill (Figure 4-41). The pressure distribution in tab #2 showed an unforeseen type of behavior for the wing wall. Due to possible bending of the wall, the center cells recorded the highest compression pressure of 2.1-psi while pressure at the bottom was 1-psi (Figure 4-42). The top cell did not record any pressure during the monitoring period. Figure 4-43 shows these stresses also plotted with depth for each data collection.

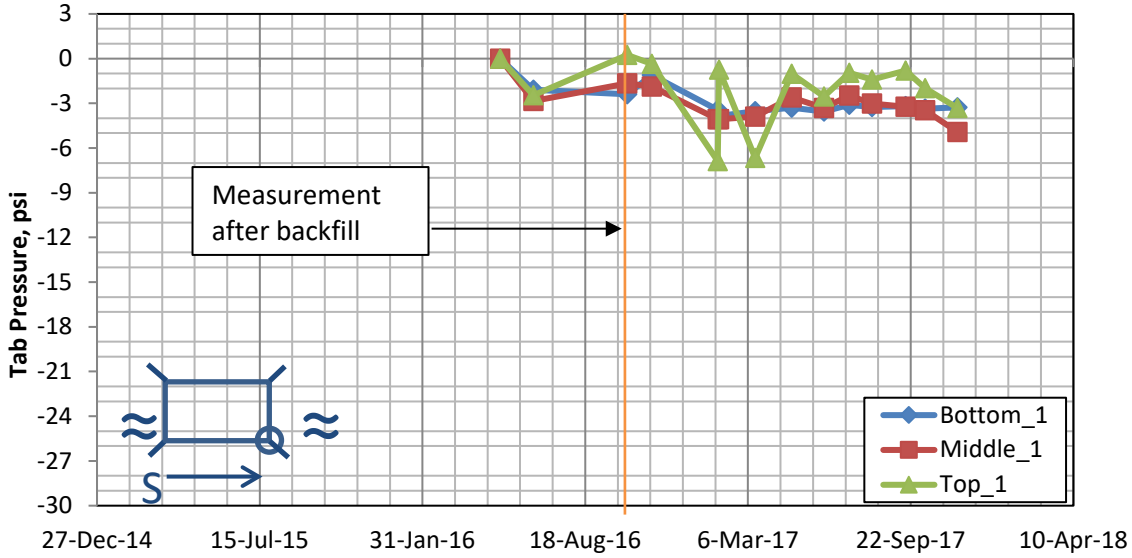

Figure 4-41. Coosa County stresses tab #1

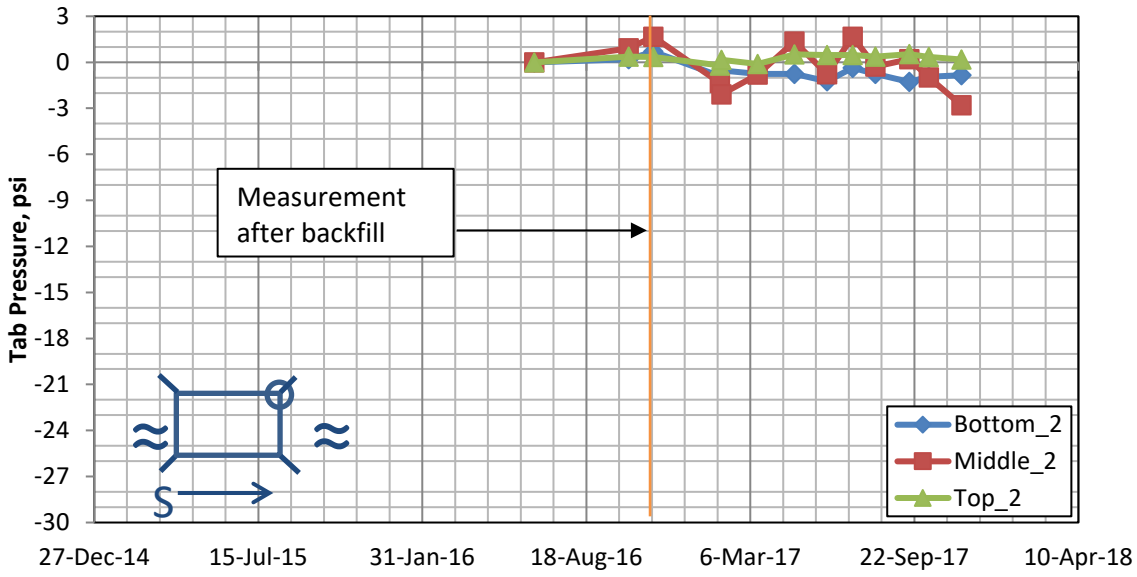

Figure 4-42. Coosa County stresses tab #2

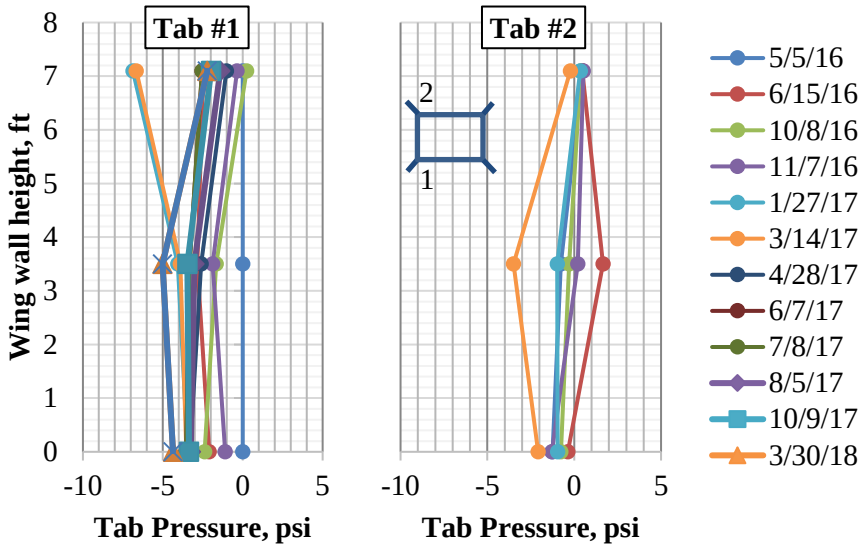

Figure 4-43. Comparison of recorded stressed along the wing wall height for the Coosa County culvert.

4.6 24-Hour Cycle Pressure Measurements

The charts in this section depict the pressure measurements recorded hourly over the course of a 24-Hour period at the Chambers County Culvert. Rather than depict the actual magnitude of

the pressure observed, these charts display the variation in the pressure in relation to the initial measurement. The charts for each tab (Figure 4-44 through Figure 4-47) are scaled to accommodate the largest variation observed at a location and the data is presented both in tab groupings and in cell location groupings.

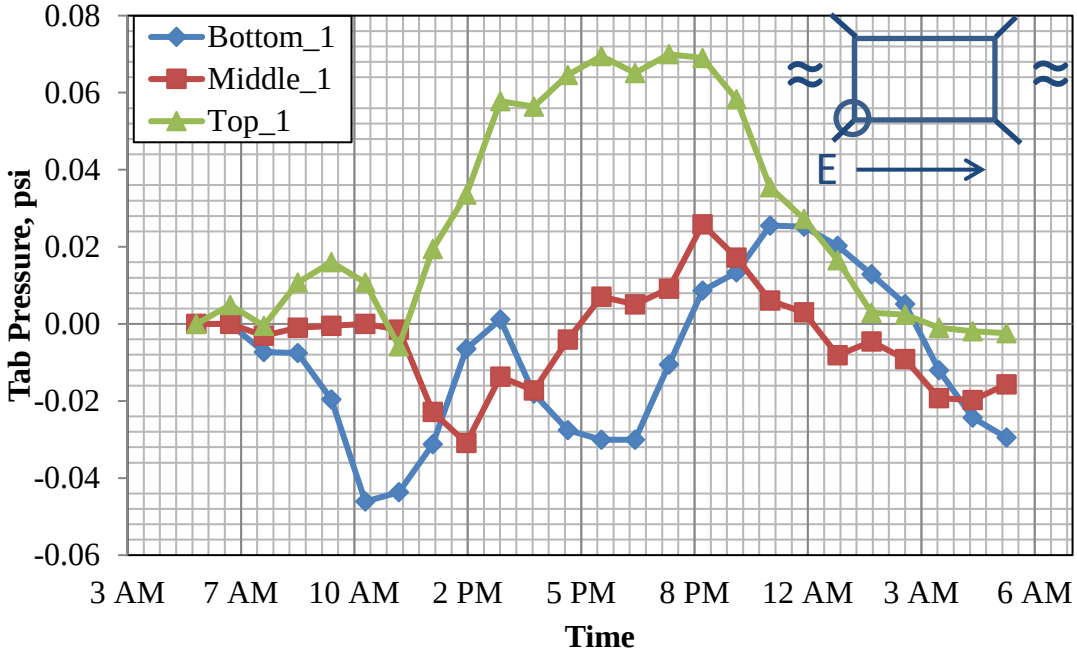

Figure 4-44. Chambers County stresses tab 1, 24-Hour Cycle

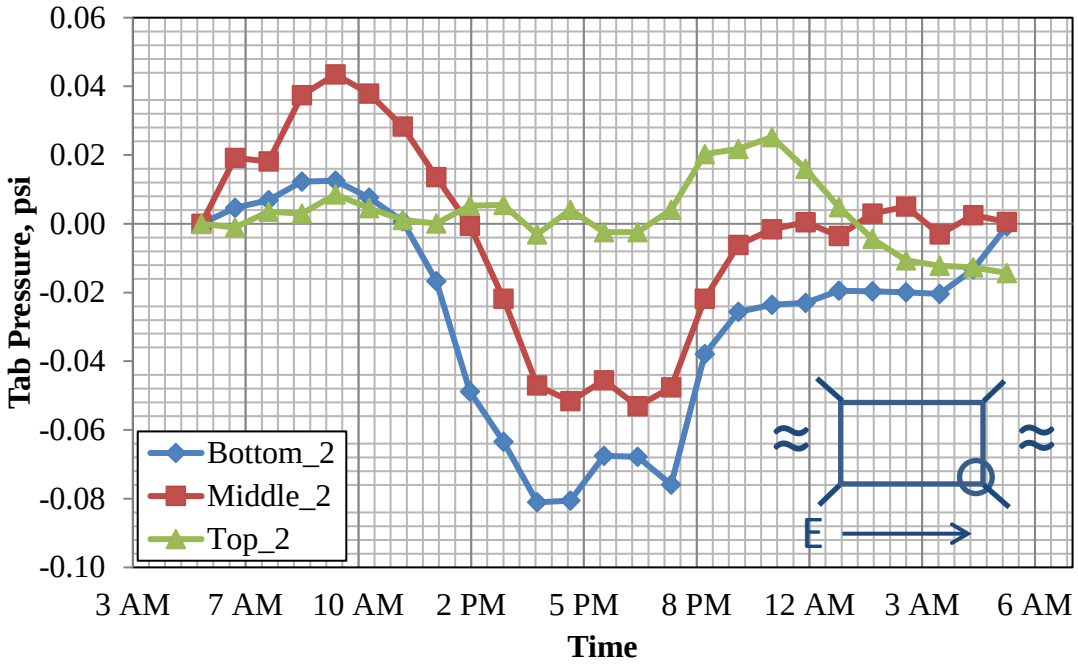

Figure 4-45. Chambers County stresses tab 2, 24-Hour Cycle

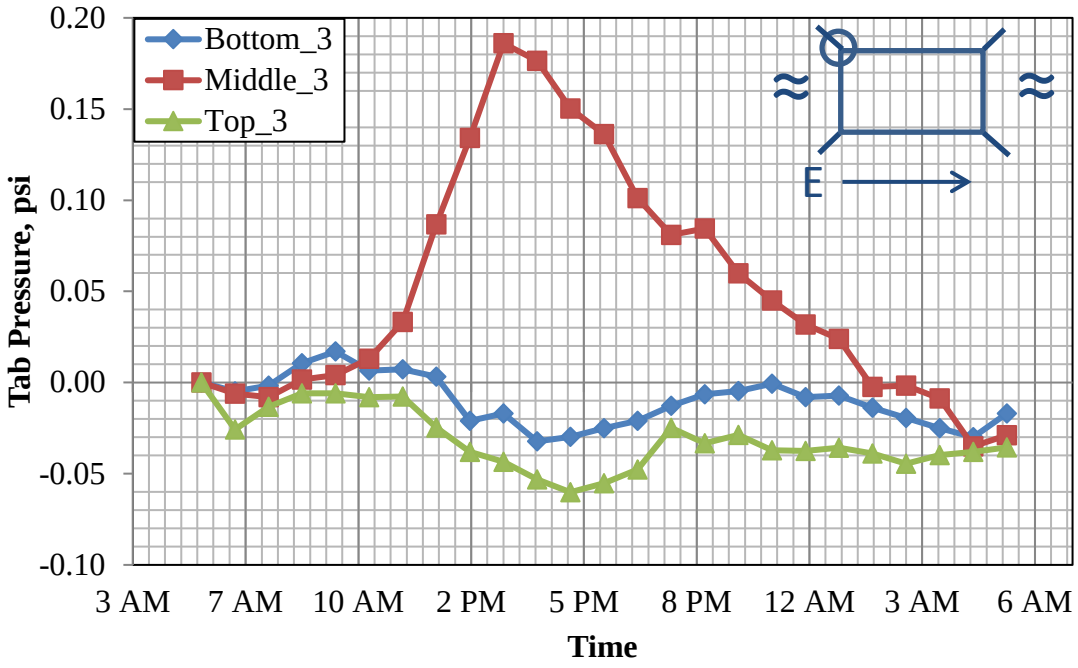

Figure 4-46. Chambers County stresses tab 3, 24-Hour Cycle

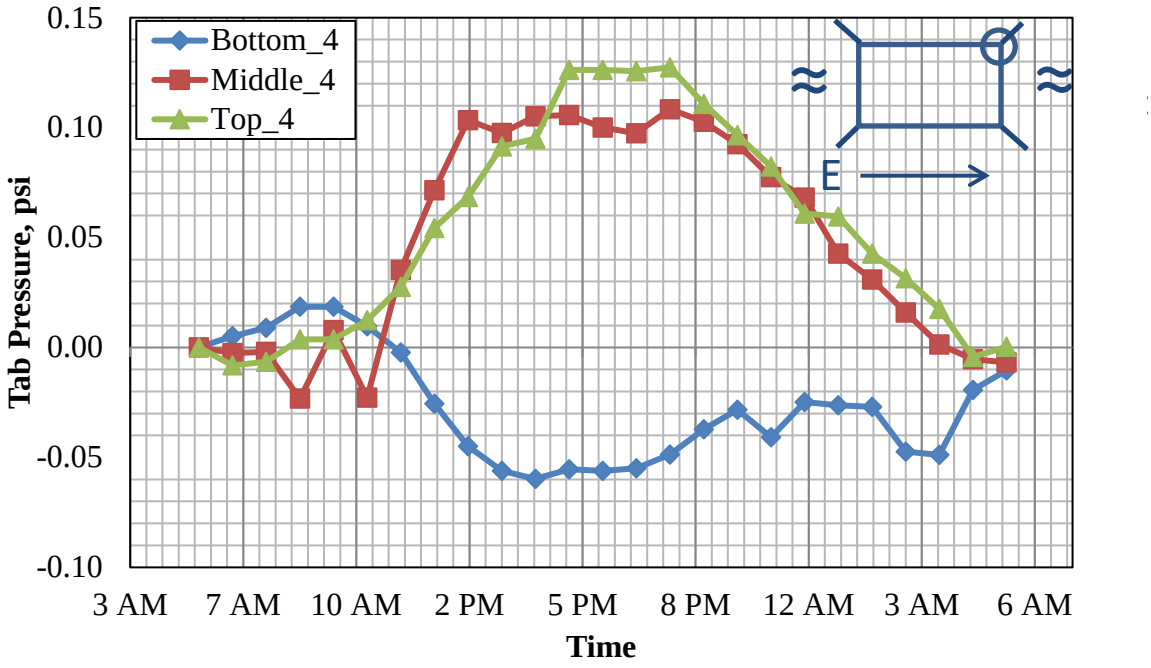

Figure 4-47. Chambers County stresses tab 4, 24-Hour Cycle

4.7 Summary

The broad lessons that can be learned from the information provided in the above charts are as follows:

- The greatest pressure in the culvert tab is likely to occur at the bottom of the tab
- The greatest pressure in the culvert tab is likely to occur during the process of backfill. The maximum observed tab stress was of 26 psi.
- Over time, the pressure on the culvert tab trends toward zero
- Daily variations in tab pressure are minimal but occur most predominantly in the upper portions of the tab
- Displacements of the culvert tab relative to the culvert box were minimal.

Chapter 5. Finite Element Simulation

5.1 Introduction

Plaxis 3D was selected for this study, as it is one of the most commonly used numerical programs for geotechnical engineering. Plaxis3D is equipped with abilities to calculate static elastic-plastic deformations, stability analysis, safety-analysis, consolidation, and steady-state groundwater flow. Also, it is suited to efficiently and properly model soil-structure interaction for complex geotechnical structures. With the ability to divide analysis process into a number of separate modeling phases, it is capable of modeling the actual construction process.

In this study, finite element (FE) models were created for the three constructed culverts and for additional theoretical cases with deeper culverts. All aspects of the system including the culvert barrel, wing walls, filling material, and surrounding soil were modeled using three dimensional (3D) block elements. The interfaces between different materials were modeled using 3D shell elements. The applied surcharge and traffic loads were distributed through corresponding areas. The construction stages included building the culvert, backfilling, high backfill, traffic load, and erosion due to scour. The reader is directed to the dissertation by Voitenko (2018) for a more in depth discussion of the FE modeling.

5.2 Material Properties

Three types of materials were considered in this study: soil, concrete, and fiberboard filling material. The subgrade and backfill soil was modeled using the Mohr-Coulomb material model with the properties correlated to the results of standard penetration tests (SPT). Concrete was modeled using a linear elastic material model, which required only the modulus of elasticity and Poisson's ratio. The filling material (Bitumen Impregnated Fiberboard) modeled with the

Hardening Soil model that was dependent on three different elastic moduli to capture the most realistic behavior of the material. These properties are summarized in Table 5-1.

Table 5-1. Material parameters

Layers	Unit weight unsat/sat (lb/in^3)	Modulus of elasticity, (ksi)				Poison ratio, ν		Friction angle, ϕ (°)	Dilatacy angle, ψ (°)	Cohesion, c (psi)
		E	E_{50}^{ref}	E_{oed}^{ref}	E_{ur}^{ref}	ν	ν_{ur}			
Mohr-Coulomb										
Backfill	0.070	10.0	-	-	-	0.3	-	30	0	1
1st layer (0-5 ft)	0.062/ 0.074	2.9	-	-	-	0.3	-	34	4	1
2nd layer (5-15 ft)	0.062/ 0.074	5.9	-	-	-	0.3	-	34	4	1
3rd layer (15-25 ft)	0.062/ 0.074	8.1	-	-	-	0.3	-	34	4	1
Hardening Soil										
Fiberboard Filling material, Saturated	-	-	0.03	0.056	0.24	-	-	34	-	-
Filling material, unsaturated	-	-	0.23	0.21	0.65	-	-	34	-	-
Linear-elastic										
Concrete	0.08842	3307	-	-	-	0.2	-	-	-	-

5.2.1 Development of Soil Properties Used in the Models

Of the three built culverts, the only provided subsurface data was for County Road 258 in Chambers County, where SPT borings were investigated up to 30-ft depth. The raw data for three boring logs are contained in Appendix B.

The measured *N* values from SPTs were corrected to N_{60} (Equation 4-7) following (Skempton 1986) procedure. Based on the calculated value of N_{60}, the soil was divided into three layers (Figure 5-1):

1. Very soft, dark grey, fine sandy CLAY.

2. Medium dense, light grey, fine to coarse SAND.

3. Very dense, tan and light grey, fine to coarse SAND.

The required soil parameters for the analysis were determined based on recommendations from Meyerhof (1956) and Kulhawy et al. (1985). The properties of the compacted backfill were adapted from reasonable values associated with cohesionless compacted soil.

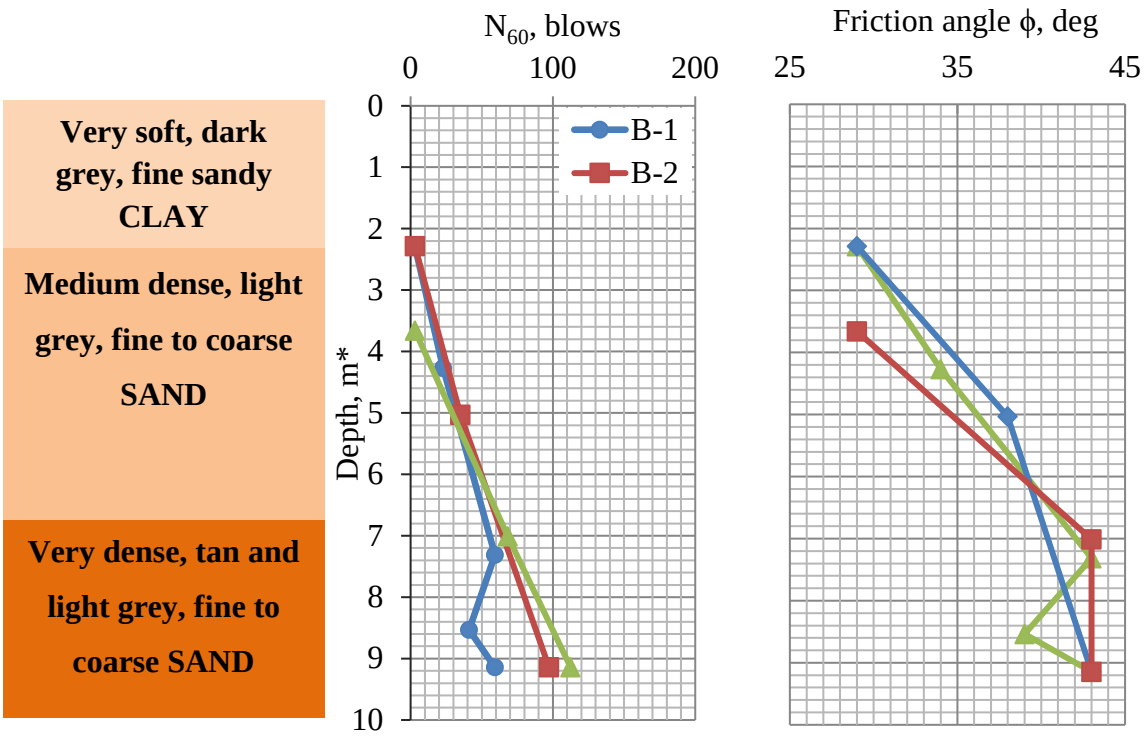

Figure 5-1. Friction angle for Chambers County borings.

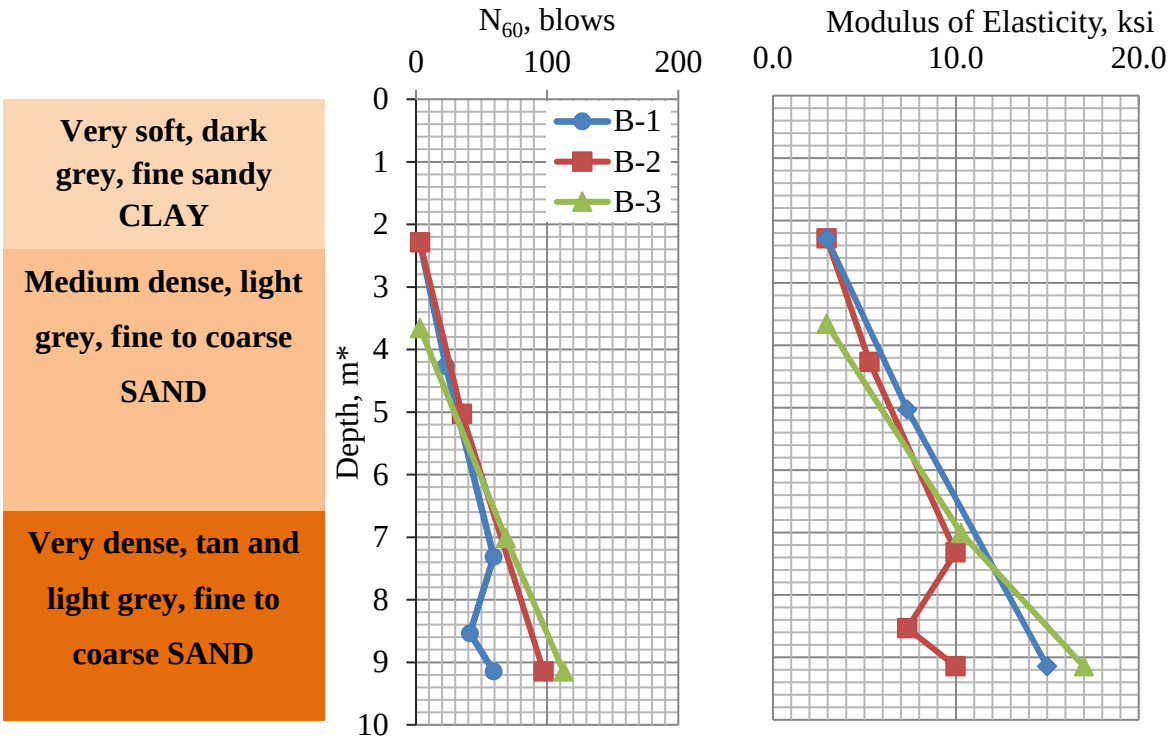

Figure 5-2. Modulus of Elasticity for Chambers County borings.

5.2.2 Fiberboard Filling Material

The joint between the culvert tab and the wing wall was filled with a 1/2-in thick Southern Pine Asphalt Impregnated Fiberboard. Since the data on this material was limited, one-dimensional compression tests were conducted to obtain the stress-strain relationship.

The actual installed conditions of the fiberboard filling material were not well defined. Therefore, the cases of saturated and unsaturated along with confined and unconfined boundary conditions. Saturated specimens were less stiff and more compressible. Thus, in the FE model, this fiberboard filling material causes more deflection. However, when the material is considered unsaturated, it is less compressible but transfers more stresses. The confined specimens were trimmed to fit the confining ring with a diameter of 2½-in. The unconfined tests were performed

on specimens that were 0.1-in smaller than the ring. The results of compression tests simulated in Plaxis3D for saturated and unsaturated conditions are shown in Figure 5-3.

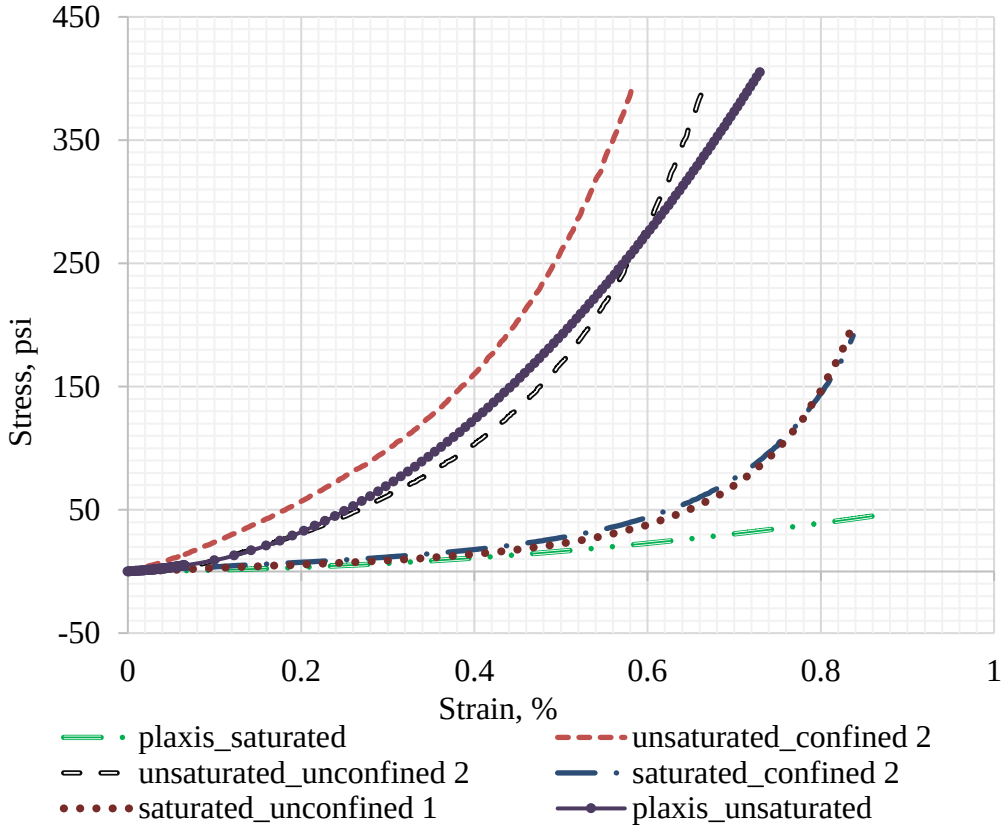

Figure 5-3. Stress-strain diagram of bitumen impregnated board

5.2.3 Concrete

Properties of the concrete were determined by testing concrete cylinders, formed during construction in accordance with (*ASTM C31/C31M* 2015) and (*ASTM C39 / C39M* 2017). Altogether, 14 samples were tested for the Chambers County culvert, six for the Lee County culvert, and eight for the Coosa County culvert. A summary of the average modulus and strength values is included in Table 5-2. Culvert Concrete Averages.

Table 5-2. Culvert Concrete Averages

	28 Day Averages	
	Ec (ksi)	f'c(psi)
Chambers County	3400	4280
Lee County	5900	5260
Coosa County	4950	5290

5.3 Development of the Model

Because the culverts were symmetric about two axes, a quarter of the culvert was simulated in Plaxis3D for computational efficiency. This allowed for focus on a wing wall and tab, which would have been identical across the symmetric axes. A view of the culvert structure without soil elements is shown in Figure 5-4

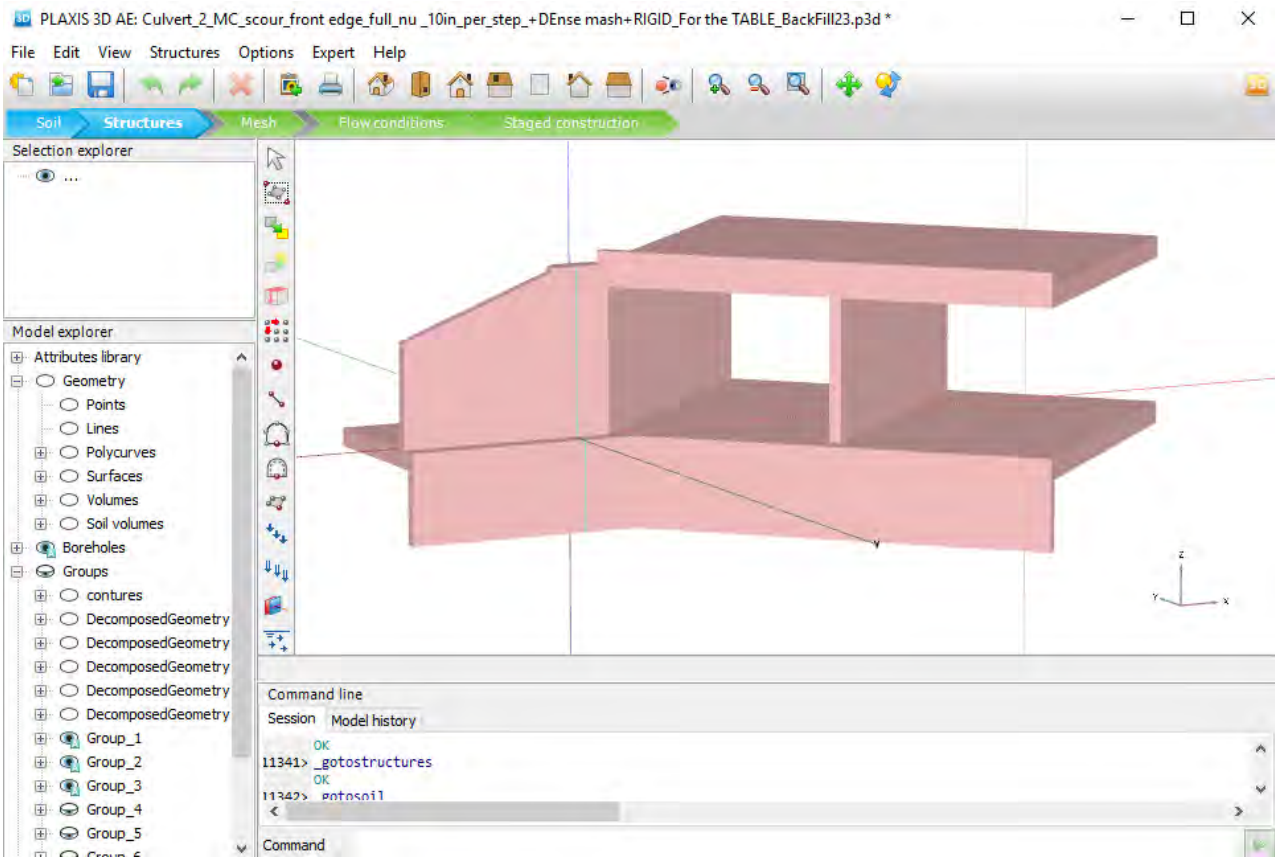

Figure 5-4. View of Plaxis3D structural input interface

5.3.1 Modeling of Loads

The primary source of loading on the wing wall was the backfill soil. In the FE models, it was distributed automatically during the simulation of fill. Other loads, such as surcharge and traffic, were applied as distributed surface loads. The surcharge load included the 3-in paving layer that was applied over the one-foot soil layer on top of the culvert (Figure 5-5). Based on the unit density of the asphalt wearing surface of 0.140-kcf, the applied redistributed load was 0.035-ksf (0.000243-ksi). The traffic load was applied according to AASHTO (2014). Two load components were considered simultaneously: lane load and HL-93 tandem load. AASHTO LRFD (2014) specified the value of lane load is equal to 0.64-klf. As the analysis is performed in 3D space, the lane load was redistributed over the area of the road width. In accordance with Section 3.6.1.2.4 of AASHTO LRFD (2014), lane load was assumed to be uniformly distributed over a 10-ft width, equal to 0.064-ksf (0.000444-ksi).

Since the maximum truck load effect on the wing wall was considered, the design tandem load was chosen as governing one of the design live load combinations. This load was applied in the closest possible position to the wing wall, where the truck can be located. It was estimated to be 3-ft away from the headwall and 1-ft from the barrel wall (Figure 5-5). The axle load was applied as uniformly distributed over the wheel area 20-in x10-in (Figure 5-6) with the magnitude of 4.52-ksf (0.03125-ksi).

5.3.2 Mesh Generation

With geometric boundaries established, Plaxis3D can generate a mesh of pyramidal 3D finite elements. The sizes of the elements were coarser near the boundaries. The space between the culvert tabs was a limiting factor in order that the behavior of the joint with the fiberboard filling

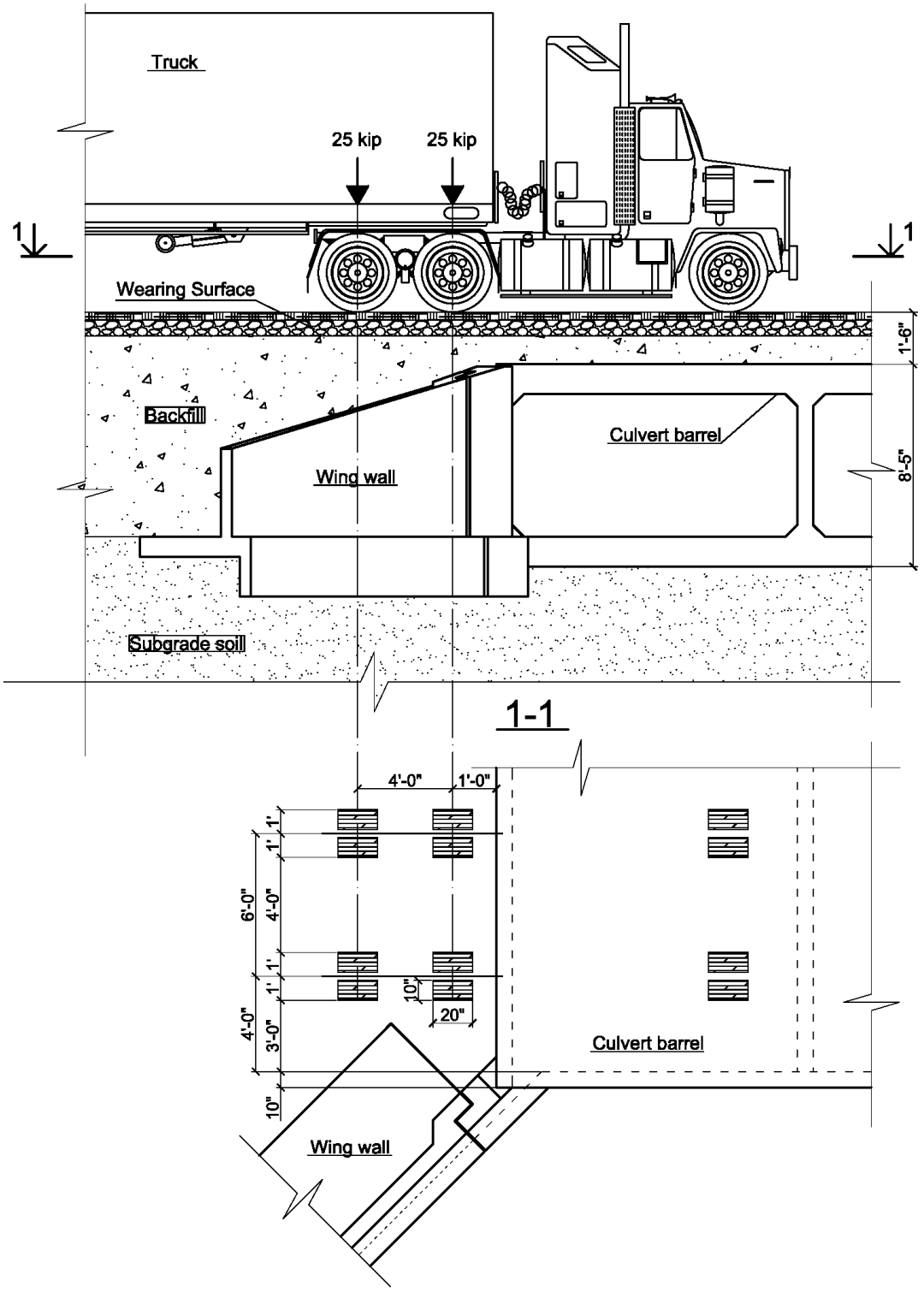

Figure 5-5. Design tandem load

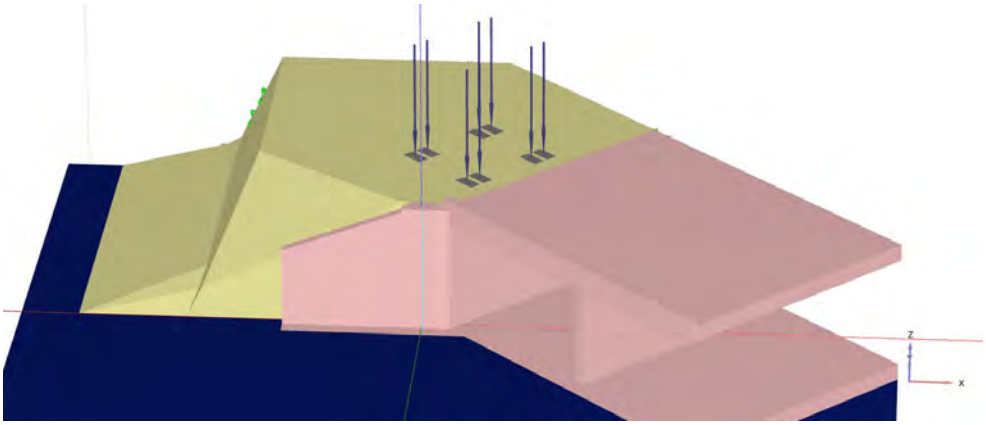

Figure 5-6. Tandem load in Plaxis 3D

material was modeled without losing element functionality. Figure 5-7 and Figure 5-8 display the mesh.

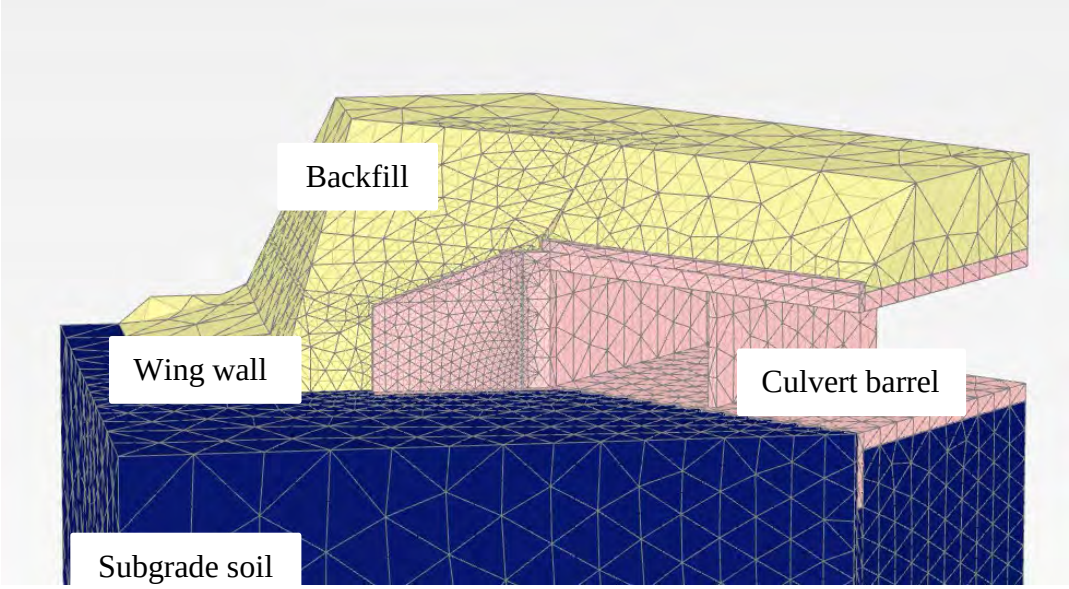

Figure 5-7. Finite element mesh of the culvert.

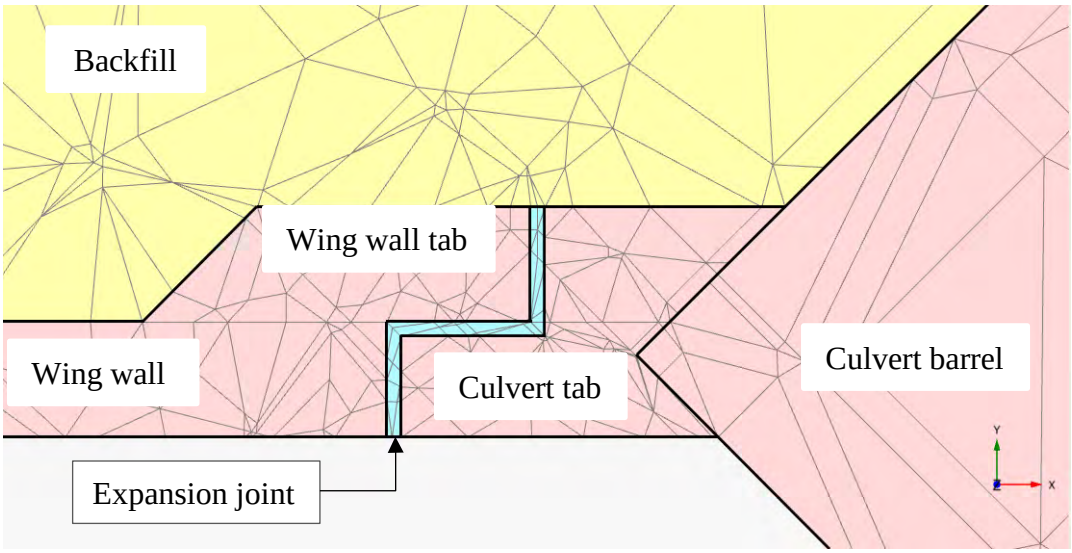

Figure 5-8. Mesh of the joint cross section

5.3.3 Calculation Phases and Analysis

The construction process was modeled using several sequential "stages." Typically for retaining structures, the stages are as follows: excavation of soil, erection of the structure, and backfilling. Each stage is characterized by the development of specific stresses and displacement. Except for design conditions, the structures can also experience erosion processes and other extreme events. Thus, to analyze the actual behavior of the structure, different stages of construction along with different load scenarios were included in the analysis.

For the culverts considered in this study, excavation, construction, and backfilling were modeled in six primary phases. Scour was modeled using 15 to 20 secondary phases.

The stages were:

0. Initial stage or K_0 procedure. The soil is a stress-dependent material, so the stress conditions of the undisturbed soil mass must be determined. At this stage, the model represents the site conditions before the construction (Figure 5-9). As the stream bed level

was not defined, the initial phase represents the condition before construction. The excavation phase was not considered.

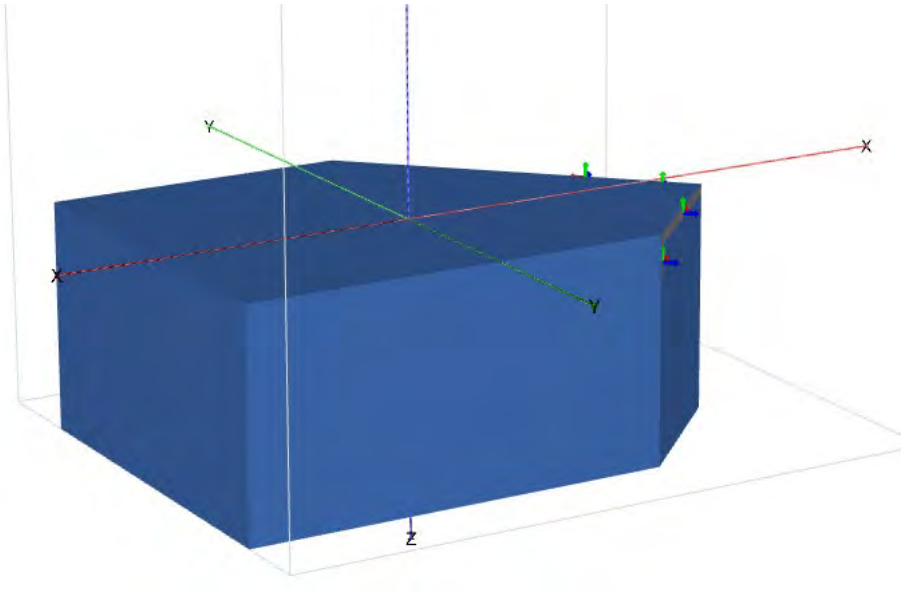

Figure 5-9. The initial stage of the analysis.

1. Placement of the culvert along with the wing wall (Figure 5-10). During this phase, the culvert barrel with the wing wall were activated/erected. No additional load except the self-weight of the structure was considered. The whole culvert was simulated instantly, excluding concrete pouring. The relative movement of both components along with interaction between them was recorded separately due to their independent settlement.

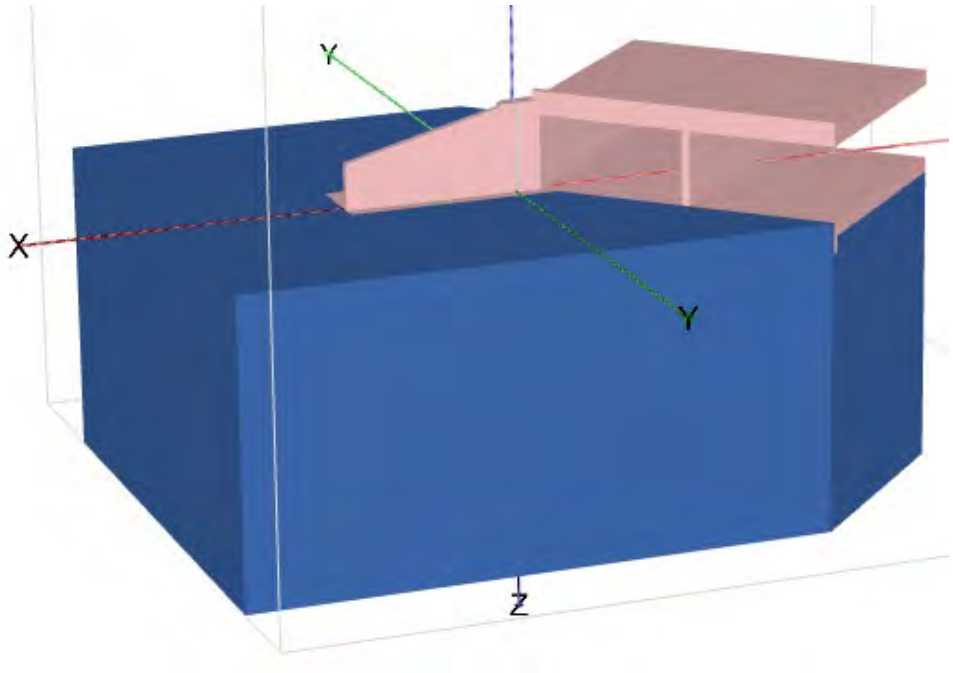

Figure 5-10. Placing the culvert with a wing wall

2. Backfilling to the level of the culvert (Figure 5-11). As it was observed on the field, the backfill was placed and compacted within one day to the same level with the culvert barrel. Thus, it was simulated within one phase for the culverts up to 10-ft deep. For deeper culverts, this stage was divided into two steps: filling backfill to the mid-height of the culvert, and then from the mid-level to the top. The dynamic effect of compaction was not considered. The obtained stresses and displacements of the wall and the tab recorded during this stage will be further compared with the field test results.

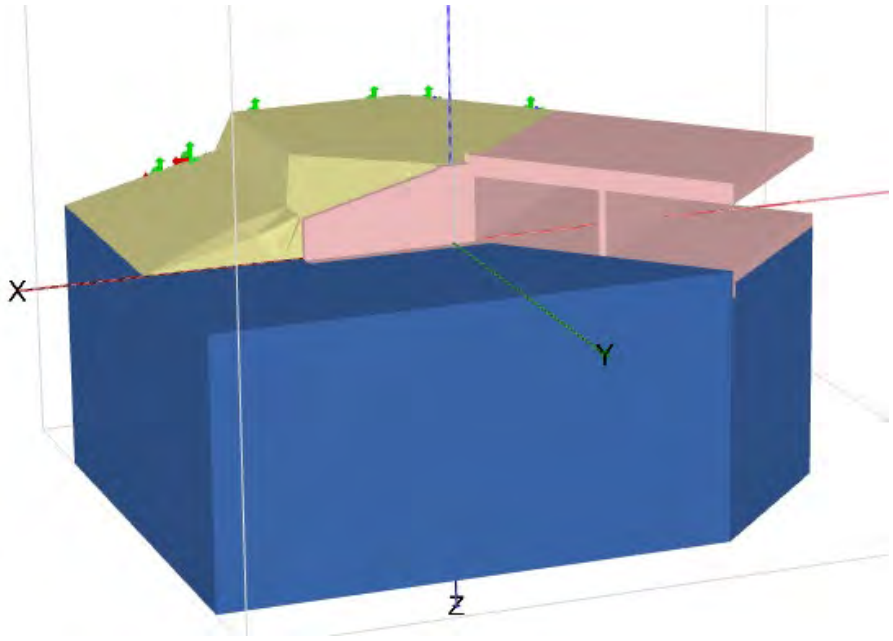

Figure 5-11. Backfill to the level of the culvert

3, 4, and 5. Backfilling gradually raised up to 23-ft (Figure 5-12). During these stages, the effect of deep backfill on the development of stress along the tab surface was studied, as well as the behavior of the wing wall.

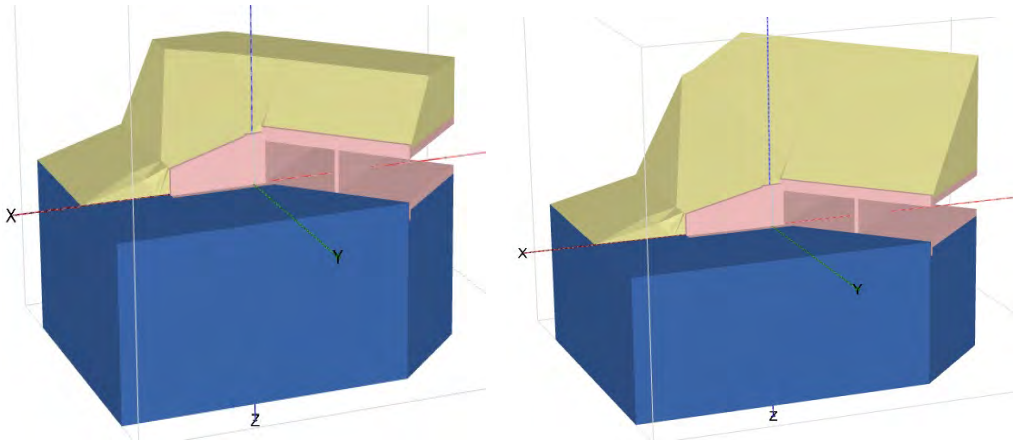

Figure 5-12. Backfilling 6-ft above the culvert (left picture), and 23-ft above (right picture)

6. The traffic load was modeled with a 1-ft soil layer at the top of the culvert similar to the constructed culverts. This phase was divided into two stages. First, the surcharge load was modeled only with the lane load. The second case included a combination of lane and tandem loads applied in the position described in Section 4.6.3 (Figure 5-13).

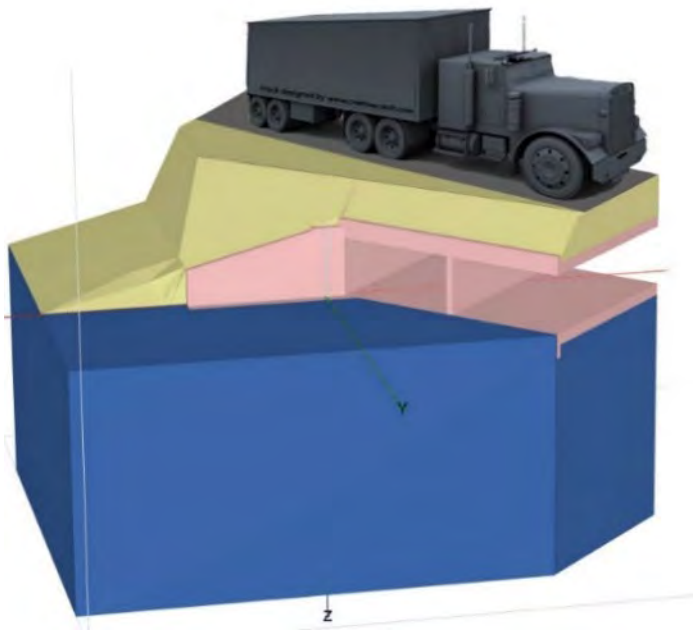

Figure 5-13. Visualization of traffic load

7. Scour. The series of phases between 15 and 20 were developed to consider the effect of an extreme event, such as scour, on the wing wall behavior. Erosion due to scour was model by removing 5-10-in of soil per stage as shown in Figure 5-14.

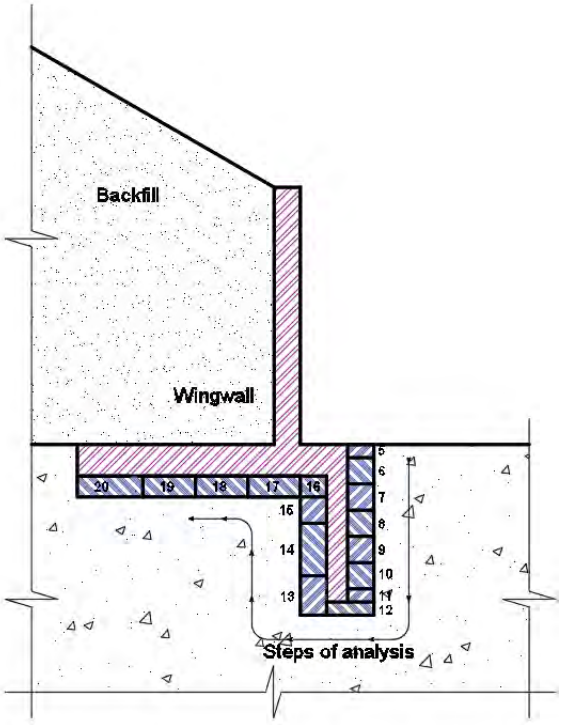

Figure 5-14. Development of the scour in the analysis

5.3.4 Orientation of Results and Sign Convention

A cross section was cut through the finite element mesh along the face of the tab. The displacements presented from the models are expressed as displacements deviating from the (vertical) plane of the tab. Stresses reported were normal stresses along the tab face.

For convenience, the directions of displacements and compression stresses normal to the joint surface were set the same for all models (Figure 5-15). Unlike typical geotechnical convention, Plaxis 3D has the following sign convention:

Compression stresses –”-“.

Tensile stresses – “+“.

Displacement in axes direction – “+”.

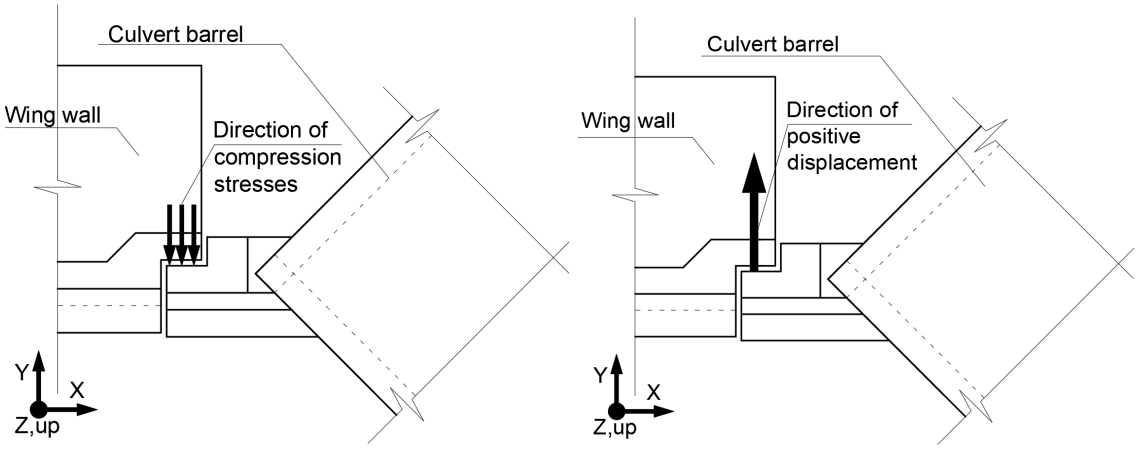

Figure 5-15. Directions of compression stresses (left picture) and positive displacement (right picture)

Chapter 6. Numerical Modeling Results

6.1 Introduction

In order to analyze the behavior of the newly designed and constructed culverts under a set of expected loads, three finite element model sets were developed as described in Chapter 5. The applied geometry was based on the new designs in Chambers, Lee, and Coosa Counties described Chapter 3. Two different load scenarios were applied to each simulated structure: design load, including backfilling and traffic load, and an extreme event, such as scour.

6.2 Displacement

Upon the applied load, the movement trends of a free standing wing wall and barrel are the same for each set of models. The maximum/dominating displacement occurs in the vertical direction under both sets of loads, while the values of horizontal displacement are much smaller. However, the horizontal translation is of interest in this study, since the transfer of stresses in a tabbed connection occurs in this direction.

When the design loads were applied, the top of the wing wall tended to rotate towards the backfill, regardless of the culvert depth. At the same time, the bottom slid away from the backfill. The displacement of the other end of the wall followed the same with a higher magnitude. The uneven translation and rotation of the wall depended on the footing width, wall geometry and restraint at the tab connection.

With scour development (Figure 5-14), the direction of the free-standing wing wall displacement reversed. While soil erosion progressed in front of the key wall, the wing wall changed the direction of rotation and starts moving towards the barrel. The magnitude was relatively small and linearly increased through all stages of scour propagation along the key wall. While scour gradually grew under the footing, the horizontal displacement increased significantly

at every stage. The soil erosion under the footing caused vertical settlement of the wing wall to fill the formed cavity.

For all three culverts, the trends of displacement were similar. For simplicity, the horizontal displacements for each of culverts from the FE results are in Figure 6-1(Chambers), Figure 6-2 (Lee), and Figure 6-3 (Coosa).

6.3 Stresses

Similar to displacements discussed in the previous section, stresses from the FE models were calculated at the same location where the actual sensors were installed – along the vertical centerline of the tab. The compression stresses acting along the tab surface (Figure 5-15) were determined for each constructed culvert and load. The stress distribution correlates with the displacement of the tab surface presented in the previous chapter.

Under the design loads (backfill and traffic), the maximum compression stresses occurred at the bottom of the tab and gradually decreased toward the top. The magnitude of these stresses was relatively small (up to 20-psi). The height of the wall and backfill depth were the most sensitive factors.

As with the displacements, the stresses on the tabs of all three culverts followed similar trends under construction, fill, traffic, and scour simulations. The computed stress distrubitions along the tab surfaces are shown in Figure 6-4 (Chambers), Figure 6-5 (Lee), and Figure 6-6 (Coosa).

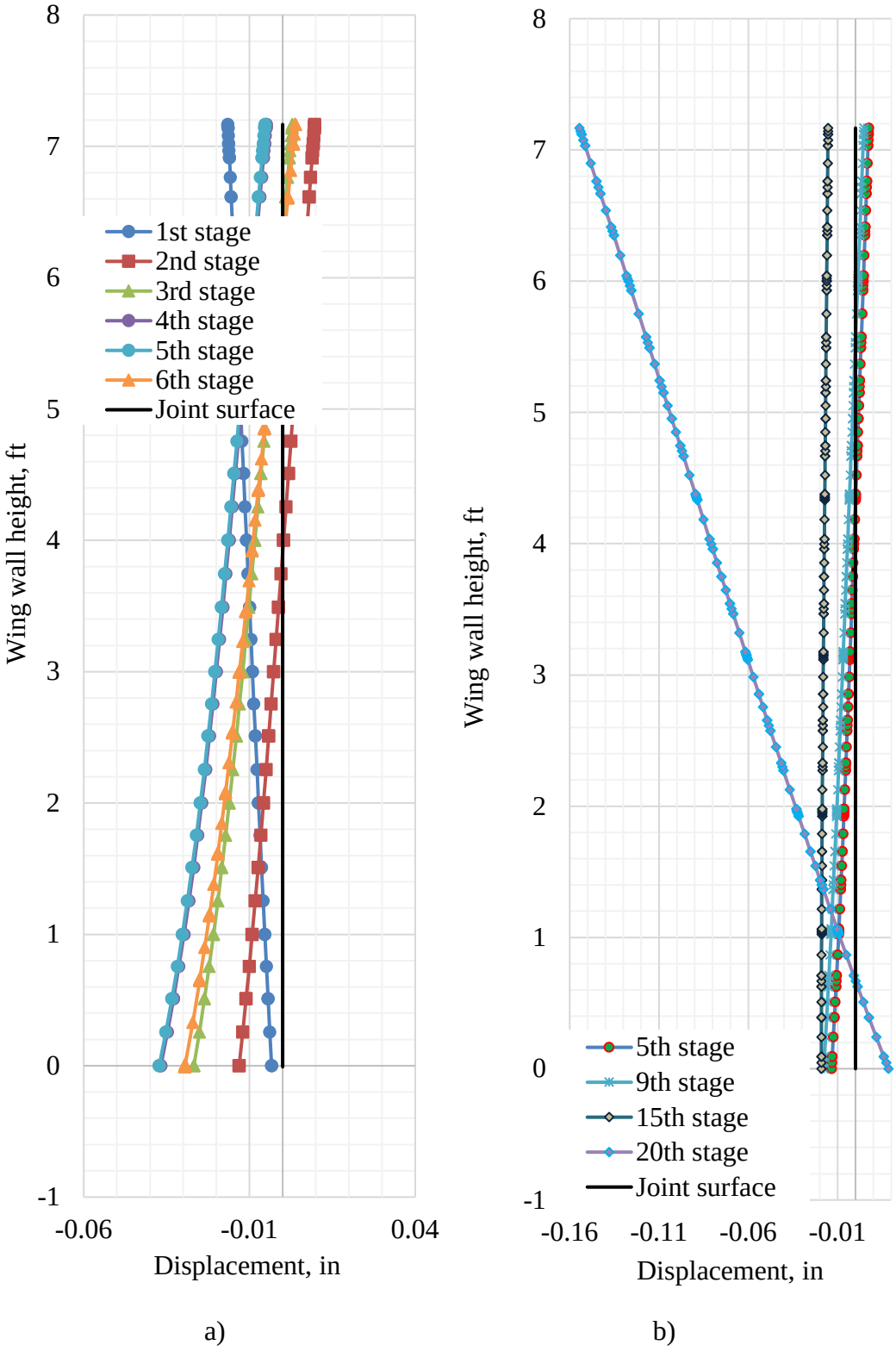

Figure 6-1. Summarized displacement of the wing wall along the tab extension a) under design loads and b) with scour development in Chambers County culvert

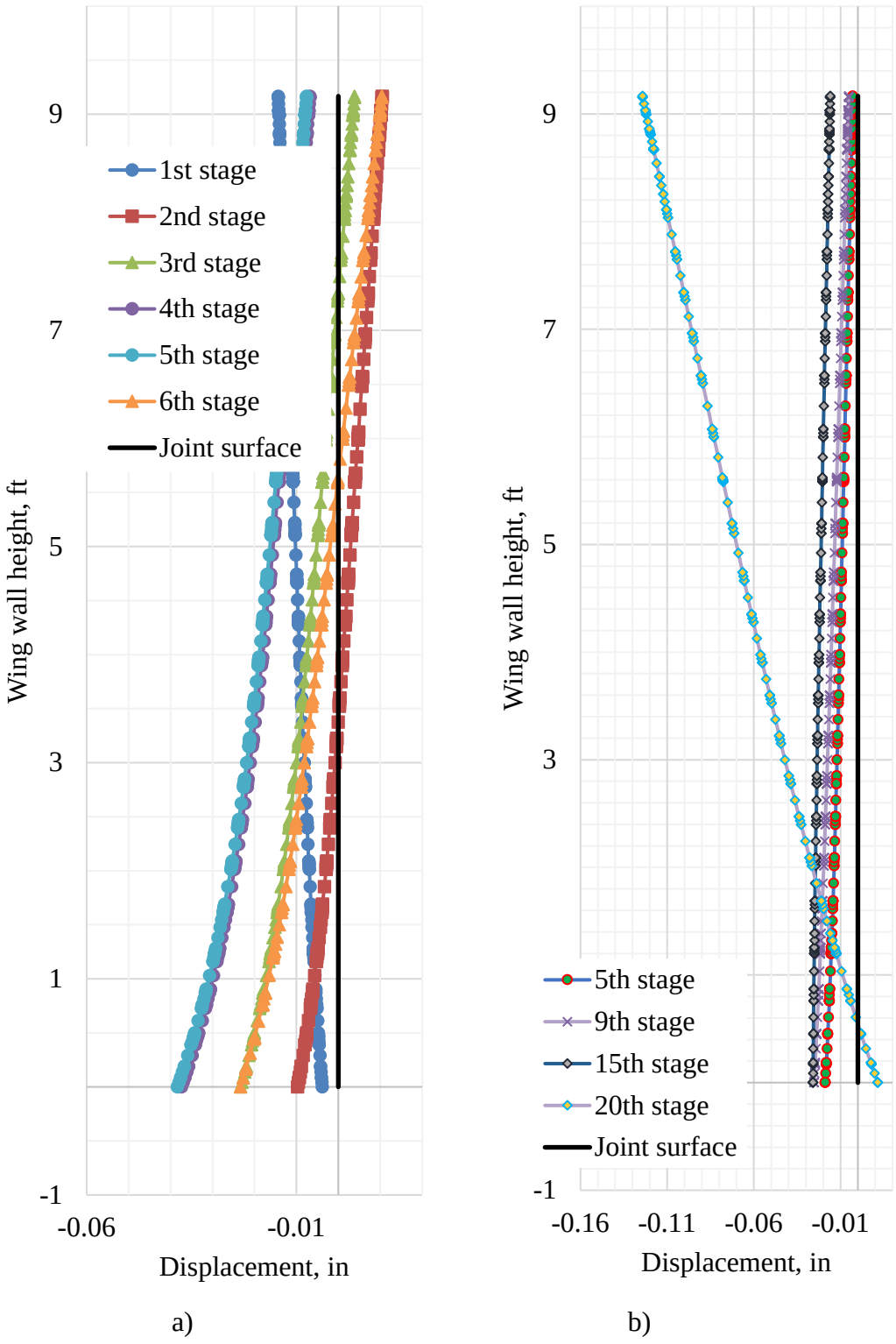

Figure 6-2. Summarized displacement of the wing wall along the tab extension a) under design loads and b) with scour development in Lee County culvert

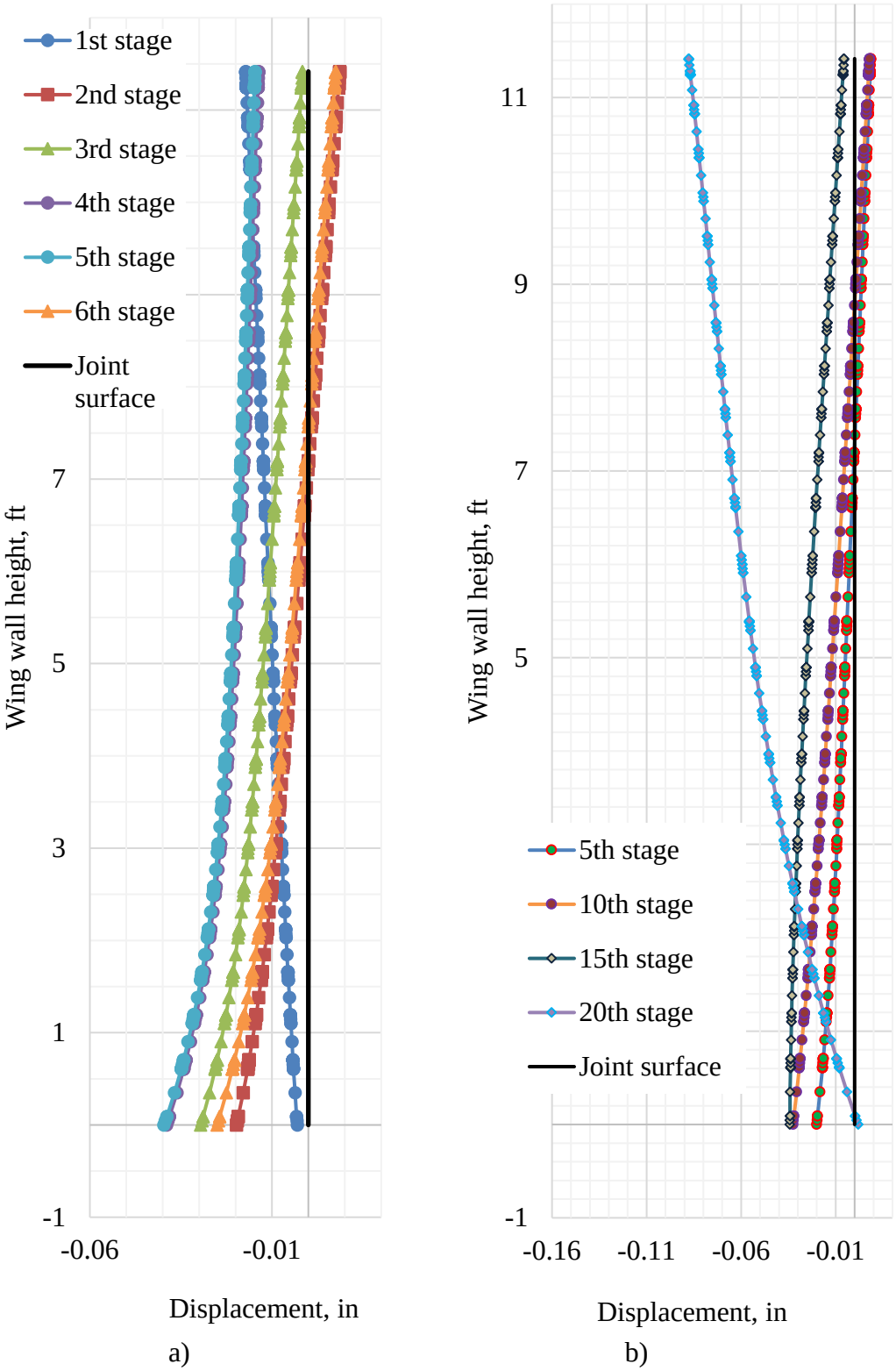

Figure 6-3. Summarized displacement of the wing wall along the tab extension a) under design loads and b)with scour development in Coosa County culvert

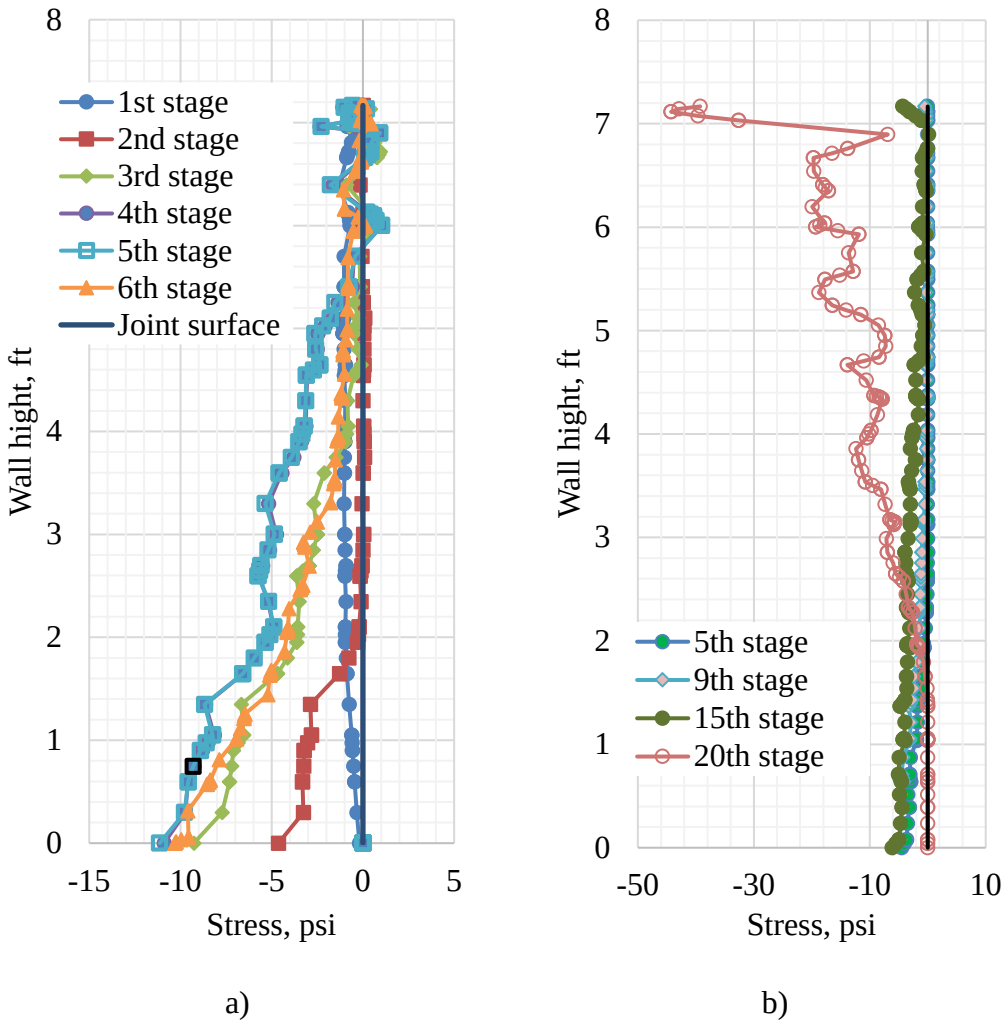

Figure 6-4. Development of stresses along the tab extension under a) design loads and b) with scour propagation for the Chambers County culvert.

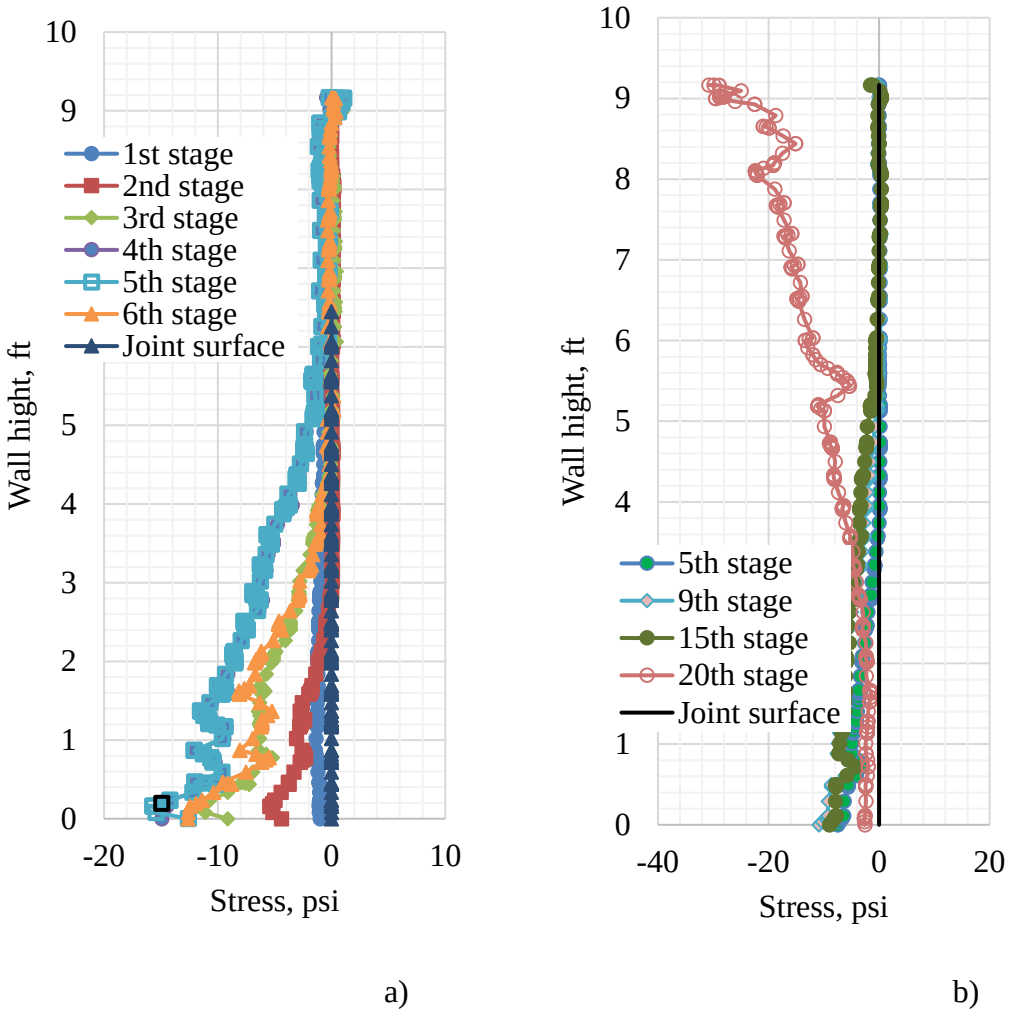

Figure 6-5. Development of stresses along the tab extension under a) design loads and b) with scour propagation for the Lee County culvert.

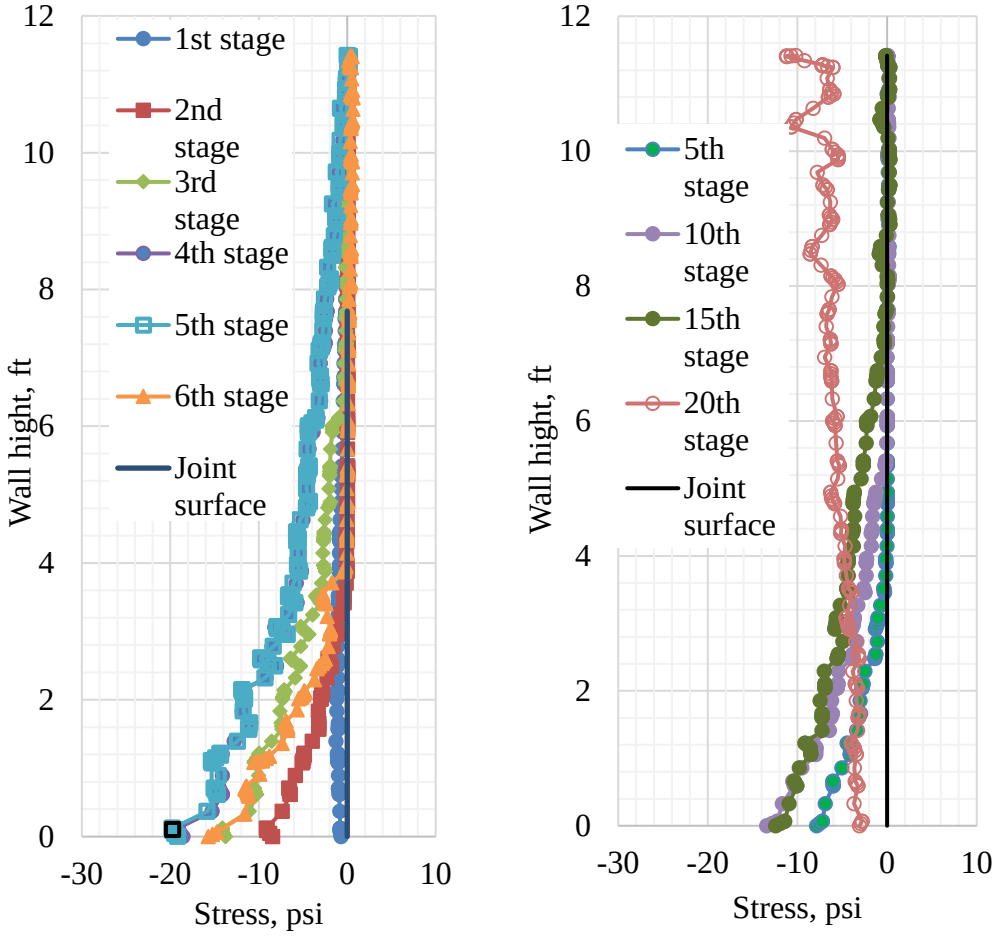

Figure 6-6. Development of stresses along the tab extension under a) design loads and b) with scour propagation for the Coosa County culvert.

6.4 Comparison of Numerical and Measured Results

The charts in this section present the comparison between stress distribution along the tab height obtained from numerical analysis and the stress distribution measured in the field. The stress distribution from numerical results was calculated for the design height of the backfill (Stage 2), which is in the level with culvert for all considered cases. The measured pressure distribution represents the maximum and average set of recorded data in constructed culvert from each cell within the tab.

The pressure distribution after placing the backfill showed a similar trend as the numerical solution for the Chambers County culvert. The maximum compression occurred at the bottom and decreased to the top of the wall (Figure 6-7a). The magnitude of maximum compression stresses was similar but it was more likely a coincidence than a trend. The field measurements were recorded in the uncontrollable environment, which involved a number of uncertainties. As it was mentioned in Chapter 5, after placing the backfill, the maximum recorded pressure gradually reduced to an average value of 2-psi in all three cells along the height.

The bottom pressure cells in the Lee County culvert experienced the greatest pressure among the constructed culverts. Unlike the previous case, the trend of pressure distribution showed evidence of nonlinearity similar to the numerical results. Despite the lower magnitude, the shape of average pressure distribution follows the shape of maximum distribution. The magnitude of the recorded stresses was three times higher than the numerical results after placing the backfill (Figure 6-7b). This may be explained by the dynamic effect during compaction, which was not considered in the numerical analysis.

The pressure distribution along the tab in the Coosa County culvert shows evidence of uniform translation and rotation of the wall away from the backfill. This resulted in maximum compression stresses at the top of the tab (Figure 6-7c). This behavior was completely different from predicted by the numerical model when the maximum pressure was located at the bottom of the wall. Also, unforeseen type of behavior was observed for most of the readings where the maximum pressure was greater at the central cell and smaller or near zero in other two locations.

Overall, different types of movement were recorded. Most of the tabs, where the maximum pressure at the bottom, exhibited evidence of wing wall rotation so that the top of the wall moved towards the backfill and the bottom away from it. This type of behavior corresponded with that predicted by numerical modeling. The rest of the tabs experienced comparatively small pressures due to sliding or bending of the wall.

Despite the difference in magnitude of compression stresses, the total behavior of the wing wall had the same trend as obtained in the numerical simulation with maximum compression at the bottom. These results were important and were used to develop the procedure of estimating the magnitude of the maximum force acting on the tab surface for the design, which will be explained in the following chapter.

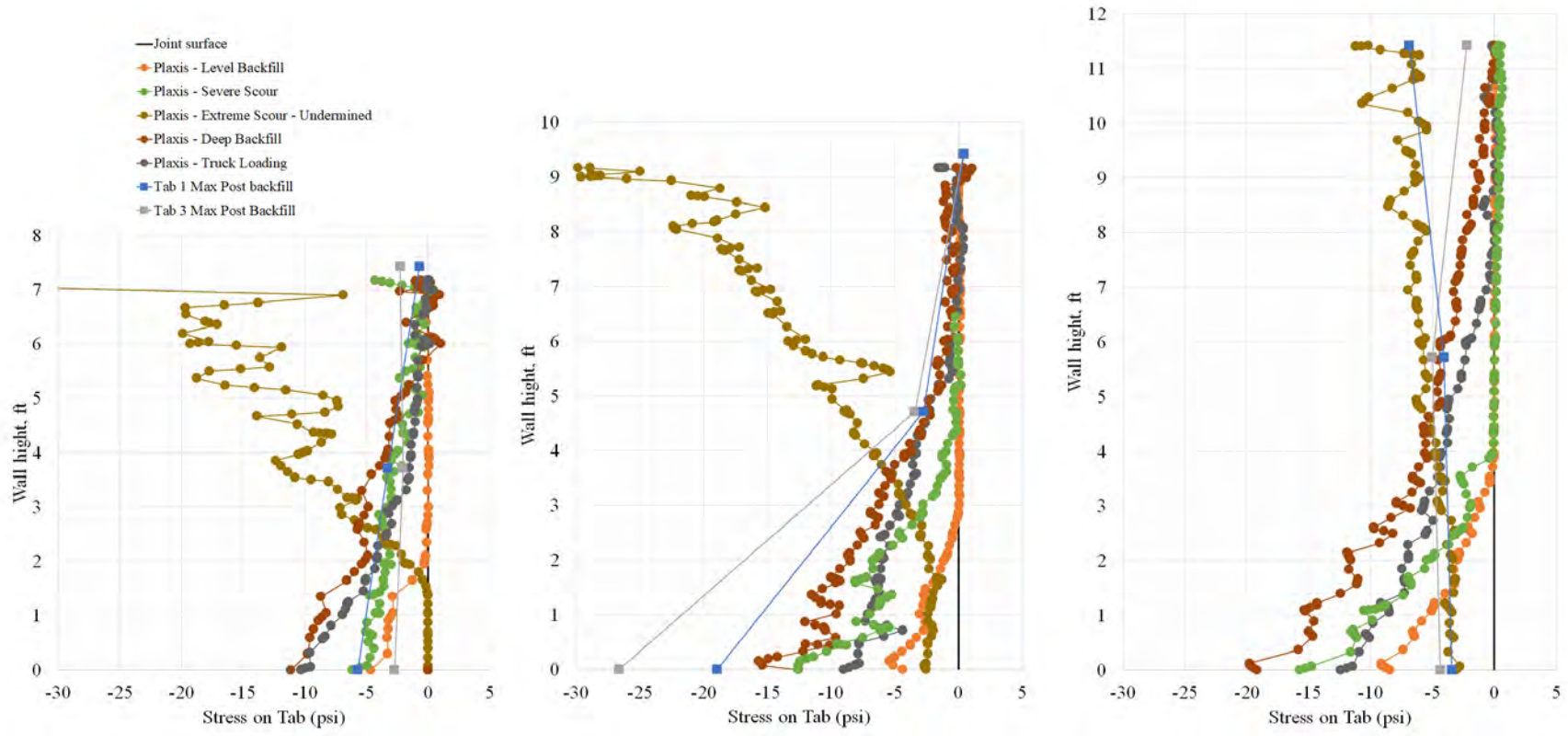

Figure 6-7. Pressure comparison for a) Chambers County b) Lee County and c) Coosa County Culverts

Chapter 7. Development of Proposed Tab Design

7.1 Estimation of Tab Design Forces

To estimate the forces acting upon the tab, it was necessary to first estimate the resultant forces caused by the lateral earth pressure acting upon the wing wall. These were determined using the following procedure, referencing the free-body diagram given in Figure 7-1, which incorporates the wall, the foundation, and the column of soil directly above the footing heel:

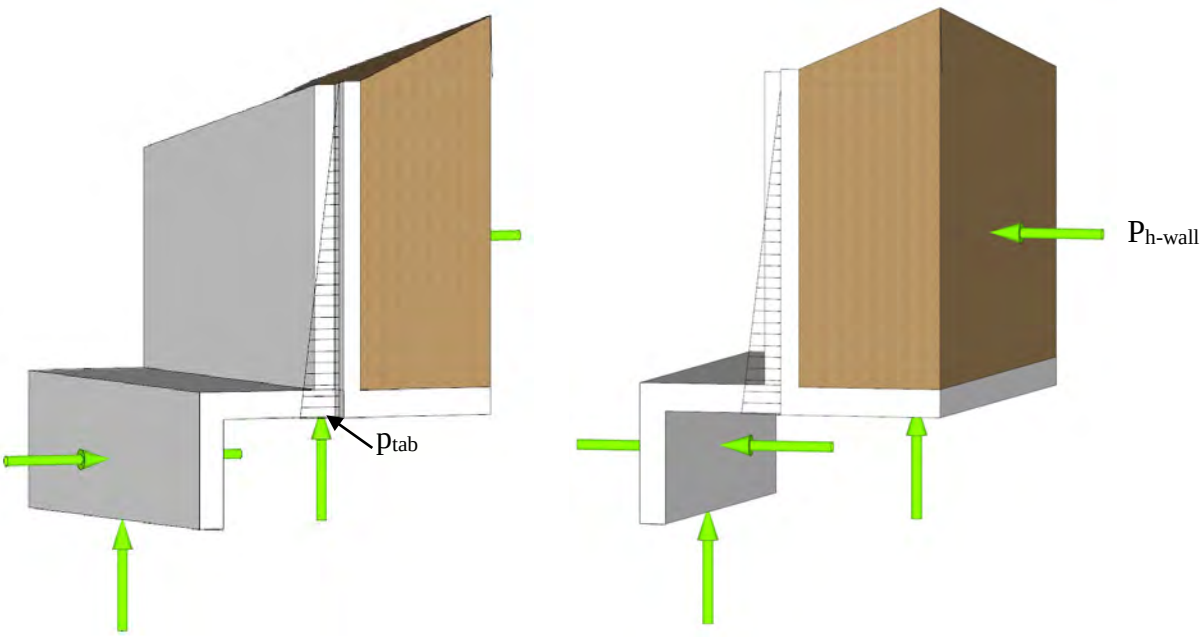

(a)

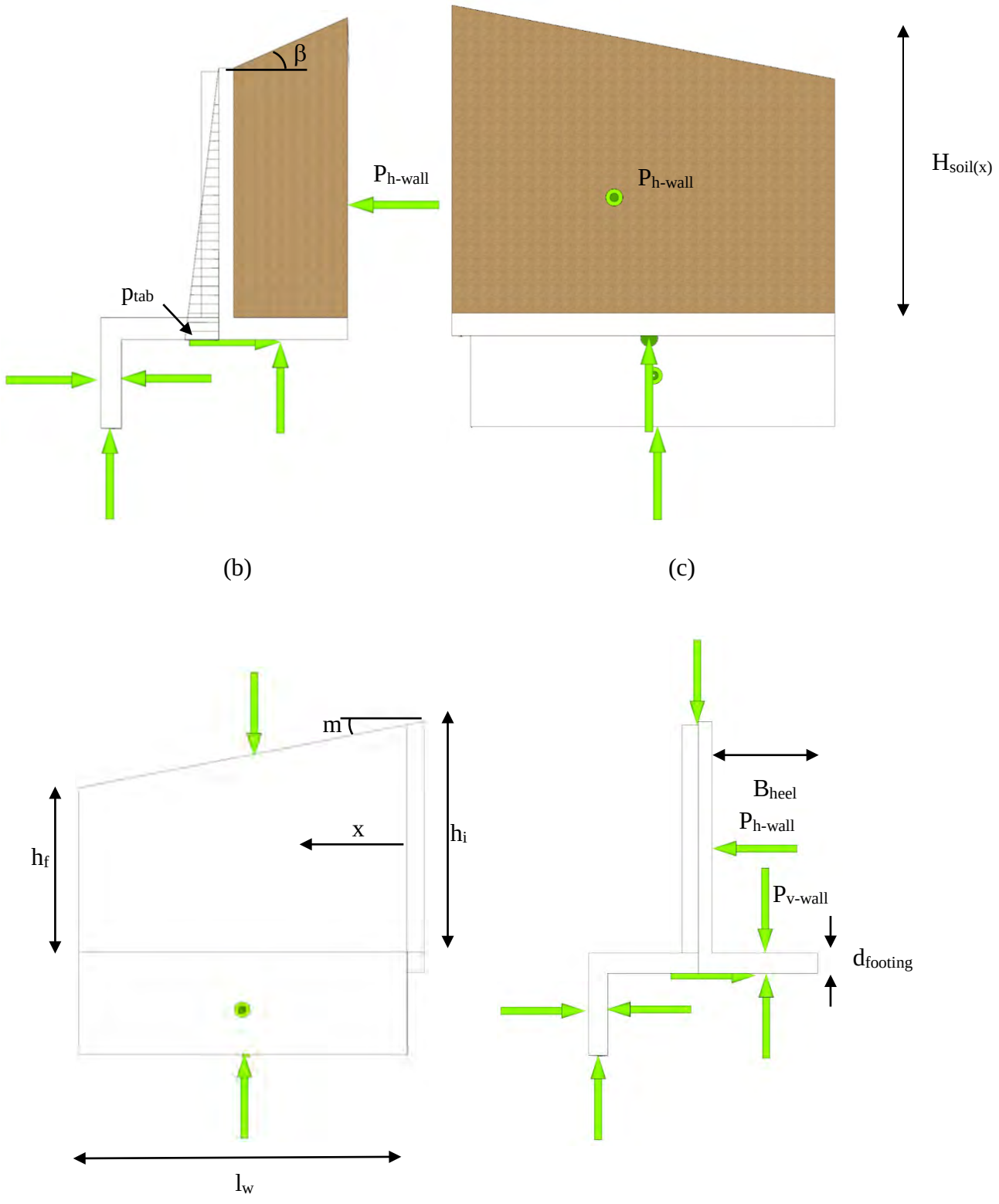

Figure 7-1. Wing Wall Free-Body Diagram

1. Height of wing wall, h, was expressed as function of its length, as shown in (7-1):

$$h(x) = h_i + m_{wall}x \tag{7-1}$$

Where

m_{wall} = slope of wing wall height, $\frac{(h_f - h_i)}{l_w}$, negative (downward)

h_i = height of wing wall taken at culvert support, ft

h_f = height of wing wall at furthest point from culvert, ft

l_w = length of wing wall, ft

x = distance along wing wall taken from culvert, ft

2. Height of soil exerting pressure, H_{soil}, was expressed as a function of the height of the wing wall and assumed backfill slope, as shown in (7-2):

$$H_{soil}(x) = d_{footing} + h(x) + B_{heel}\tan\beta \tag{7-2}$$

Where

$d_{footing}$ = depth of the footing, ft

B_{heel} = width of wing wall heel, ft

3. The resultant force of the lateral earth pressure, P(x), expressed as a force per unit length of the wing wall, was determined as a function of the height of the soil and estimated soil properties using (7-3):

$$P(x) = 0.5K_h\gamma[H_{soil}(x)]^2 \tag{7-3}$$

Where

K_h = coefficient of lateral earth pressure (K_0, at rest, $K_{0\beta}$, at rest with sloping backfill or K_A active) based on (2-2) through (2-9).

4. The horizontal resultant force of the total lateral earth pressure acting on the wing wall, $P_{h\text{-}wall}$, was determined by integrating the P(x) over the length of the wing wall, as shown in (7-4):

$$P_{h-wall} = \int_0^{l_w} P(x)\cos(\beta)\,dx \tag{7-4}$$

5. The vertical resultant force of all earth pressure, $P_{v\text{-}wall}$, was determined by integrating the vertical component of the lateral earth pressure and the weight of the soil over the length of the wing wall, using assumed soil properties, as shown in (7-5):

$$P_{v-wall} = \int_0^{l_w} [P(x)\sin(\beta) + H_{soil}(x)\gamma B_{heel}]\,dx \tag{7-5}$$

7.2 Critical Loading Conditions

7.2.1 Out-of-Plane Translation of Wall

The first critical loading condition considered was that of out-of-plane translation of the wing wall. In this case, the tab forces and the toe wall soil pressure must equilibrate the full horizontal force acting on the wall, $P_{h\text{-}wall}$. Considering rotational equilibrium about a vertical axis, the tab can be subjected to no more than one half of this total horizontal force before there is a loss of overall rotational stability of the wall. Therefore, it is conservatively assumed that *half* of the total lateral soil force, $P_{h\text{-}wall}$, on the wall is transmitted to the culvert tab. If this scenario (loss of rotational stability) were to occur, the wing wall would likely require rehabilitation; however, damage to the culvert tab and the body of the culvert itself would be mitigated, unlike with integrally constructed wing walls.

To determine the maximum tab loading corresponding to this wall movement, the horizontal resultant force of lateral earth pressure, $P_{h\text{-}wall}$, was converted to an equivalent linear distribution along the height of the tab, similar to the distribution shown in Figure 7-2. The magnitude of the base of this distribution was then used as the design force for each horizontal design strip of the tab. This magnitude, p_{tab}, in force per unit (1 ft) height of tab was calculated using (7-6):

$$p_{tab} = \frac{1}{2}\left(\frac{2P_{h-wall}}{h_i}\right) = \frac{P_{h-wall}}{h_i} = \frac{1}{h_i}\int_0^{l_w} P(x)\cos(\beta)\,dx \qquad (7\text{-}6)$$

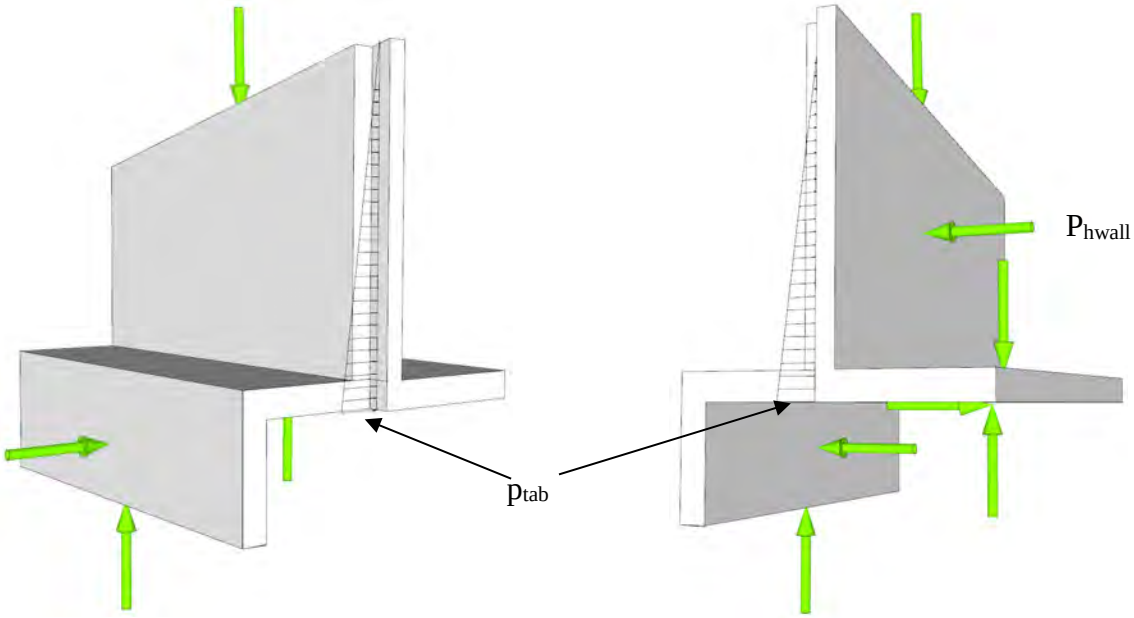

Figure 7-2. Wing Wall Translation Tab Loading

Table 7-1 below compares the unfactored "analytical" p_{tab} results of this analysis to the maximum forces observed in the field for each of the three monitored culverts. Field observations were measured as a pressure (psf); however, considering the area of the pressure cell was less than 1 ft^2, these values were conservatively assumed to be

uniform over an entire 1 ft tall horizontal design strip of the tab, and thus were converted to force per unit height (kips/ft).

Table 7-1. Tab Forces

	p_{tab} (lb/ft)		
Case	Chambers	Lee	Coosa
Analytical active, K_A	1851	1469	2012
Analytical at rest, K_0	**3289**	**2609**	**3575**
Field Tab 1	932	1727	1329
Field Tab 2 or 3	654	2389	1197
FEM Level Backfill	209	177	333
FEM Deep Backfill	1197	1245	1601
FEM Truck	880	676	453
FEM Severe Scour	728	802	936
FEM Extreme Scour Undermining	2369	2631	1595

Of note, only the culvert constructed in Lee County was observed during the process of backfill, and this was when the maximum "field tab" pressure was recorded. A fully loaded dump truck, weighing approximately 40 tons, was located as near to each tab as possible at the time of these measurements.

For comparison, p_{tab} was determined numerically for each of the three case studies in this project. The results of the FE models, expressed as stress on the wing tab, were converted to p_{tab} for comparison to the analytical estimates by integrating the stress on the tab face, presented in Figure 6-7, using a Simpson's Rule approach. These FEM forces are also reported in Table 7-1.

Based on these analyses and results, it is proposed that the analytical p_{tab} computed in accordance with (7-6) be used to provide an estimate of the unfactored force on the tab for design purposes. When p_{tab} is determined using at-rest earth pressure (K_0), this force safely envelops all the loading cases that were considered.

7.2.2 Rotation of Wall about Toe

The second scenario considered was rotation of the wing wall about the toe, which would result in contact between the culvert tab and wing wall at the top of the tab. Static analysis was performed referencing the free-body diagram shown in

Figure 7-3. For this scenario, the horizontal resultant force of the lateral earth pressure was placed at the vertical coordinate of the centroid of the soil load. The toe wall was taken as the fulcrum of rotation, but the soil loads upon the toe wall were neglected as was the base friction since the wall was assumed to be tipping. The vertical coordinate of the centroid of the soil load, $\bar{y}$, was calculated using (7-7):

$$\bar{y} = \frac{1}{3}\frac{\int_0^{l_w} h(x)^3 dx}{\int_0^{l_w} h(x)^2 dx} \tag{7-7}$$

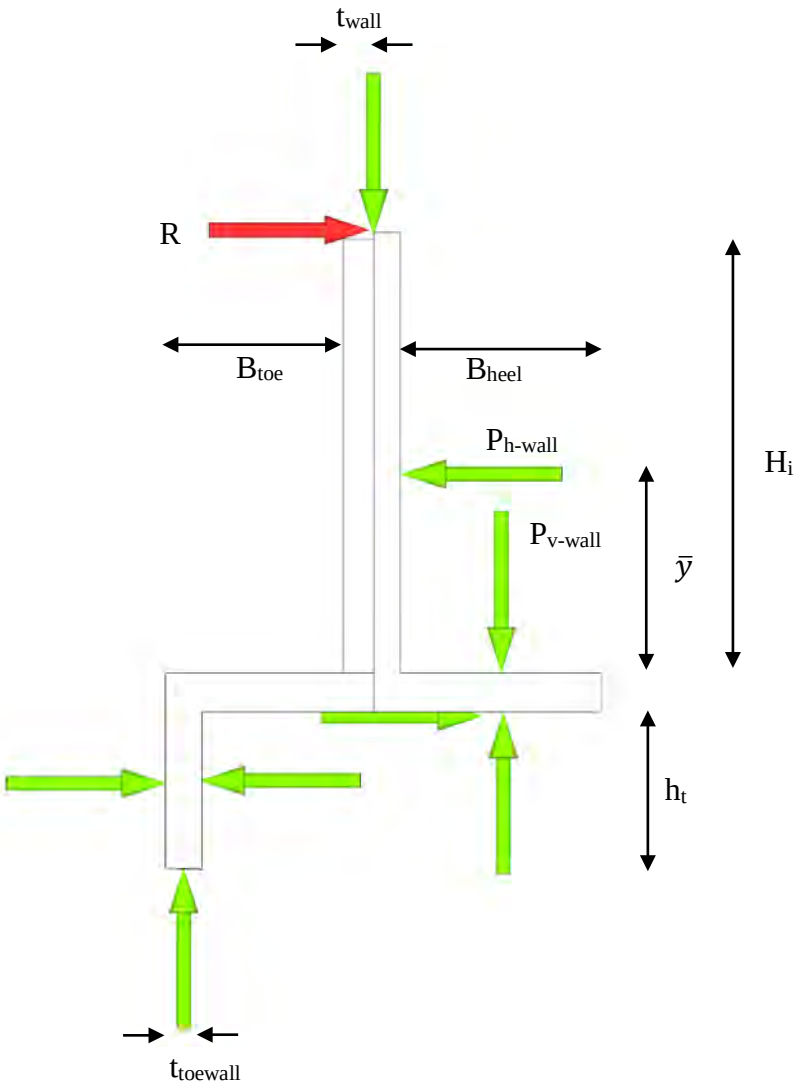

Figure 7-3. Wing Wall Free-Body Diagram

The variables shown in Figure 7-3 are defined as follows:

R = the force transmitted from the wall to the tab

t_{wall} = thickness of the wing wall

$t_{toewall}$ = thickness of toe wall

B_{toe} = width of toe

B_{heel} = width of heel

H_i = maximum height of wing wall

h_t = height of toe wall

$P_{v\text{-}wall}$ = vertical earth pressure force

$P_{h\text{-}wall}$ = horizontal earth pressure force

The magnitude of R was calculated using (7-8):

$$R = \frac{P_{h-wall}(h_t + y_{bar}) - P_{v-wall}(0.5B_{heel} + t_{wall} + B_{toe} - 0.5t_{toewall})}{h_t + H_i} \quad (7\text{-}8)$$

Carrying through this equilibrium analysis, no practical situation results in a compressive force on the tab. The tab rotates away from the wing wall for all equilibrium solutions. This is attributable to the large width of the heel, which bears a significant amount of soil weight to counteract the overturning. The field measurements are consistent with this behavior. The pressure measured near the top of each tab was never the greatest pressure, which indicates that the translation mode is dominant.

The FEM results presented in Chapter 6 (e.g., Figure 6-1 through Figure 6-3) indicate that rotation dominates only after a scour event that is severe enough to completely undermine the entire toe wall, which would require wall rehabilitation. Nonetheless, even the maximum tab forces generated in the numerical models of these extreme events (refer to the "FEM Extreme Scour Undermining" cases in Table 7-1) are well bounded by the translational force, p_{tab}, computed in accordance with (7-6). Therefore, the use of (7-6) is recommended to determine the unfactored force for tab design purposes.

7.3 Recommended Tab Design Procedure

The tab extension, shown in Figure 7-4, from the culvert barrel to the wing wall is a short cantilever reinforced concrete element employed to transfer the horizontal earth

pressure acting on the wing wall to the culvert barrel. The relatively short length of the extension is comparable to its thickness; therefore, the potential failure modes of the tab extension are like those of a beam ledge as discussed in Section 2.2.3. Thus, Article 5.8.4.3 of AASHTO LRFD (2020) for beam ledge design can be applied to the tab design.

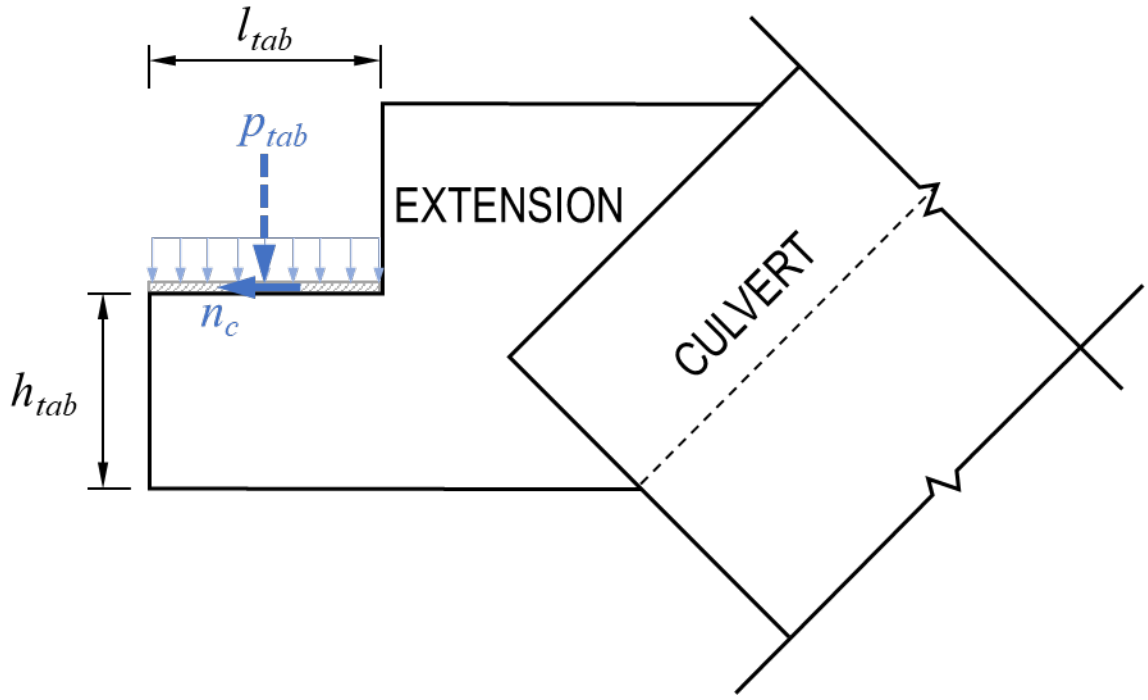

Figure 7-4. Plan View of Culvert Tab Extension with Loads

7.3.1 Design Strategy and Loads

One of the primary motivations for implementing this alternative wing wall to culvert connection is to avoid the concrete cracking that typically occurs in rigid wall-to-culvert connections. Therefore, the primary strategy for the design of the reinforced concrete components is to minimize cracking within the elements themselves. Thus, the concrete elements should be sized to provide adequate strength based only on the

minimum practical amount of reinforcement. It would be counterproductive to attempt to decrease the wall or tab thickness by increasing the amount of reinforcement; this would increase the likelihood of load-induced cracking. For these types of elements, the standard minimum practical reinforcement consists of No. 4 bars at 12 in. (maximum) spacing in each orthogonal direction in each face. If flexural or shear strength computations show that this minimum reinforcement is inadequate, the designer should consider increasing the thickness of the concrete element rather than increasing the reinforcement amount. If increased element size results in an increase in the minimum reinforcement required for crack control, the reinforcement spacing should be decreased (rather than increasing the size of the bars). The design procedure discussed here is focused on determining the extra reinforcement needed solely due to the special configuration and loading of the tab.

The design loads on the tab are depicted in Figure 7-4. The loading that results directly from the earth pressure on the wall is shown as p_{tab}. A conservative procedure for determining p_{tab} is described in Section 7.2.1. Note that p_{tab} is the force per unit height (lb/ft) of the tab. It is assumed to be distributed evenly along the length of the tab, with the resultant force located at the center of l_{tab}. Because p_{tab} is based on at-rest horizontal earth pressure, the design forces resulting from p_{tab} shall be conservatively computed by using a load factor ($\gamma_{p,EH}$) of 1.35 in accordance with Table 3.4.1-2 of AASHTO LRFD (2020).

The other design load depicted in Figure 7-4 is n_c, a load applied parallel to the face of the tab itself. This force, also given in force per unit height (lb/ft) of the tab, represents a friction force between the matching tabs that might develop due to relative

movement or restrained concrete shrinkage. Given the bituminous filler between the two tabs, the minimum value of $0.2p_{tab}$ prescribed in Articles 5.8.4.3.3 and 5.8.4.2.1 should be a safe value for n_c in this scenario. The corbel provisions (Article 5.8.4.2.1) prescribe that this value be treated as a live load. Accordingly, a load factor of 1.75 shall be applied to n_c.

Article 5.8.4.3 allows beam ledges to be designed in accordance with the strut-and-tie method or in accordance with the specific beam ledge provisions in Article 5.8.4.3 itself. For simplicity, and due to the relatively light loads experienced by these tabs, the latter approach is selected here for the culvert wing tab.

7.3.2 Behavior and Failure Modes

The most likely failure mode for a beam ledge or dapped beam follows the diagonal tension crack shown in Figure 7-5a, which reflects the biaxial state of tension resulting from shear and flexure. In the beam ledge provisions of Article 5.8.4.3, this type of failure is prevented by simultaneously preventing the simplified failures shown in Figure 7-5b (combined flexure and shear-friction) and Figure 7-5c (tension failure extending from tab face).

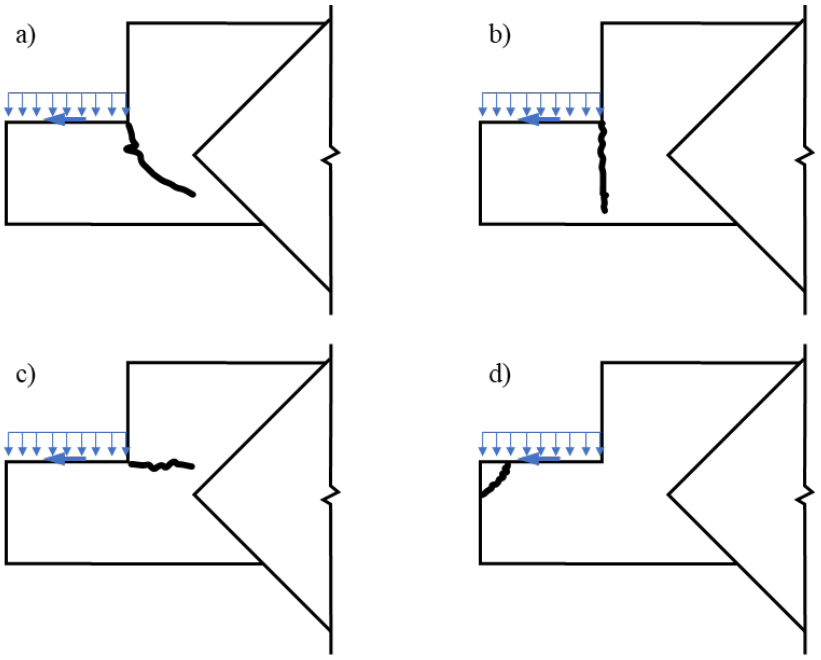

Figure 7-5. Failure types: a) diagonal tension, b) combined flexure and shear-friction, c) tension, and d) spalling

Two potential failure modes for beam ledges—punching shear and crushing due to bearing stresses—are not possible in these tabs given the magnitude and distributed nature of the pressure on the tab. However, a significant force parallel to the tab surface could cause a portion of the tab to spall as shown in Figure 7-5d if reinforcement is not extended to the end of the tab and anchored adequately.

7.3.3 Design Procedure

Figure 7-6 depicts a practical tab reinforcement configuration that provides the strength necessary to preclude the beam ledge failure modes noted previously. The three tab reinforcing bars—A, B, and C—in the figure are referred to in the following discussion of design procedure. All the horizontal reinforcement shown in this figure is spaced at regular vertical intervals—typically at a maximum spacing of 12 inches.

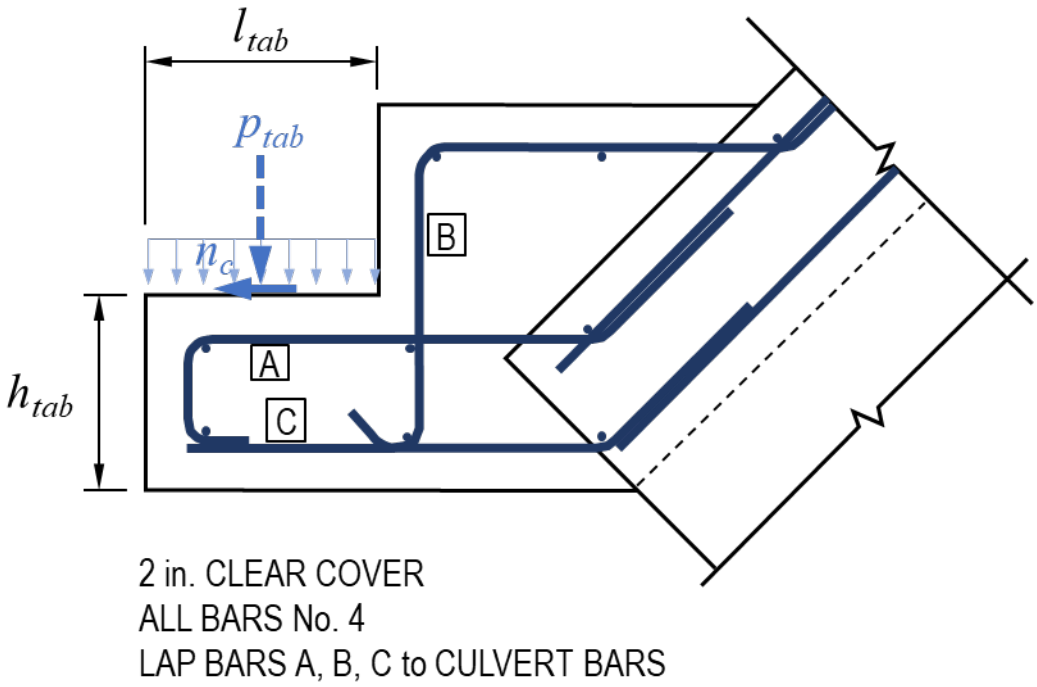

Figure 7-6. Practical tab reinforcement configuration

All design tasks are accomplished by considering the configuration shown in Figure 7-6 as a representative 1 ft tall average design strip of the tab. This is similar to a one-way slab or wall design concept; however, in this case, the design is replicated vertically up the tab. Thus, any “per ft” dimensions in the design calculations refer to vertical ft up the wall tab.

As discussed in Section 7.2, the critical design loading is expected to occur at the bottom of the tab. Therefore, the tab design will start at the bottom. Because minimum reinforcement will control for most, if not all, cases, it is safe and practical to simply extend the design of the bottom 1 ft strip upwards along the full height of the tab.

7.3.3.1 Critical Design Considerations

Figure 7-7 depicts the two critical sections for design of the tab in accordance with AASHTO LRFD Article 5.8.4.3 for beam ledges. Adequate flexural, shear, and axial strength must be provided at Section 1-1. Furthermore, Bars A and C must be adequately developed on each side of this section in accordance with 5.10.8.

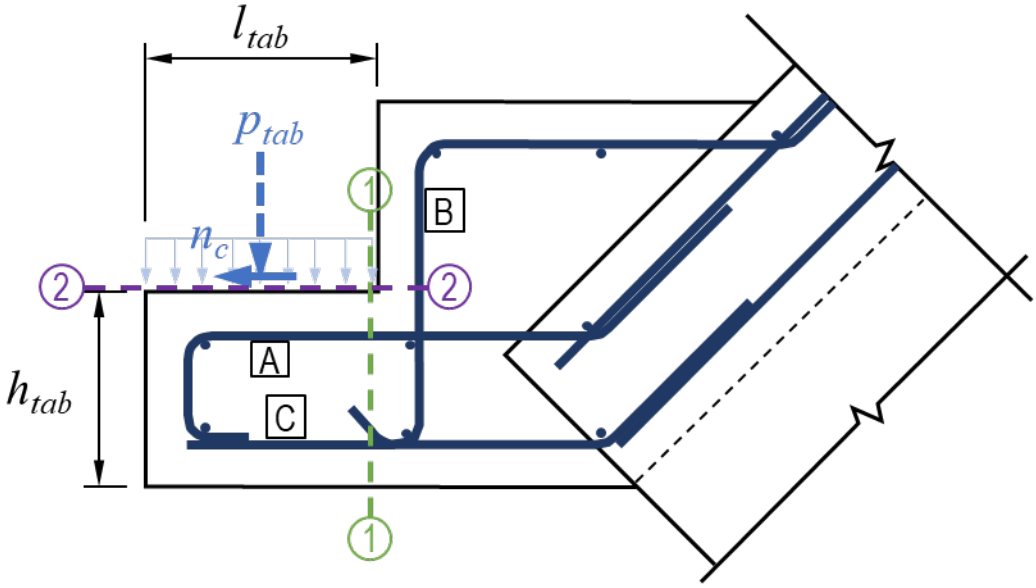

Figure 7-7. Critical Sections 1-1 and 2-2 for tab design

Bar B is referred to as the "hanger" reinforcement in a beam ledge because it hangs the applied vertical load back up into the full beam depth. In the same manner, Bar B must provide the tensile strength necessary across Section 2-2 to resist p_{tab}. Bar B needs to be fully developed on each side of Section 2-2; therefore, it is hooked around a vertical bar on each side and continues as the flexural reinforcement in the thicker segment of the culvert extension. Providing the necessary development is an important consideration when selecting the thickness of the tab (h_{tab}) and the culvert extension.

7.3.3.2 Design Forces on Tab

The first major tab design step is the computation of the forces on the tab, p_{tab} and n_c. The derivation and validation of the method for computing p_{tab} are provided in Section 7.2, resulting in Equation (7-6), which is repeated here.

$$p_{tab} = \frac{1}{h_i}\int_0^{l_w} P(x)\cos(\beta)\,dx$$

n_c is simply taken as $0.2p_{tab}$.

An example application of this method follows.

Consider the distribution of stress on a retaining structure in two dimensions at first:

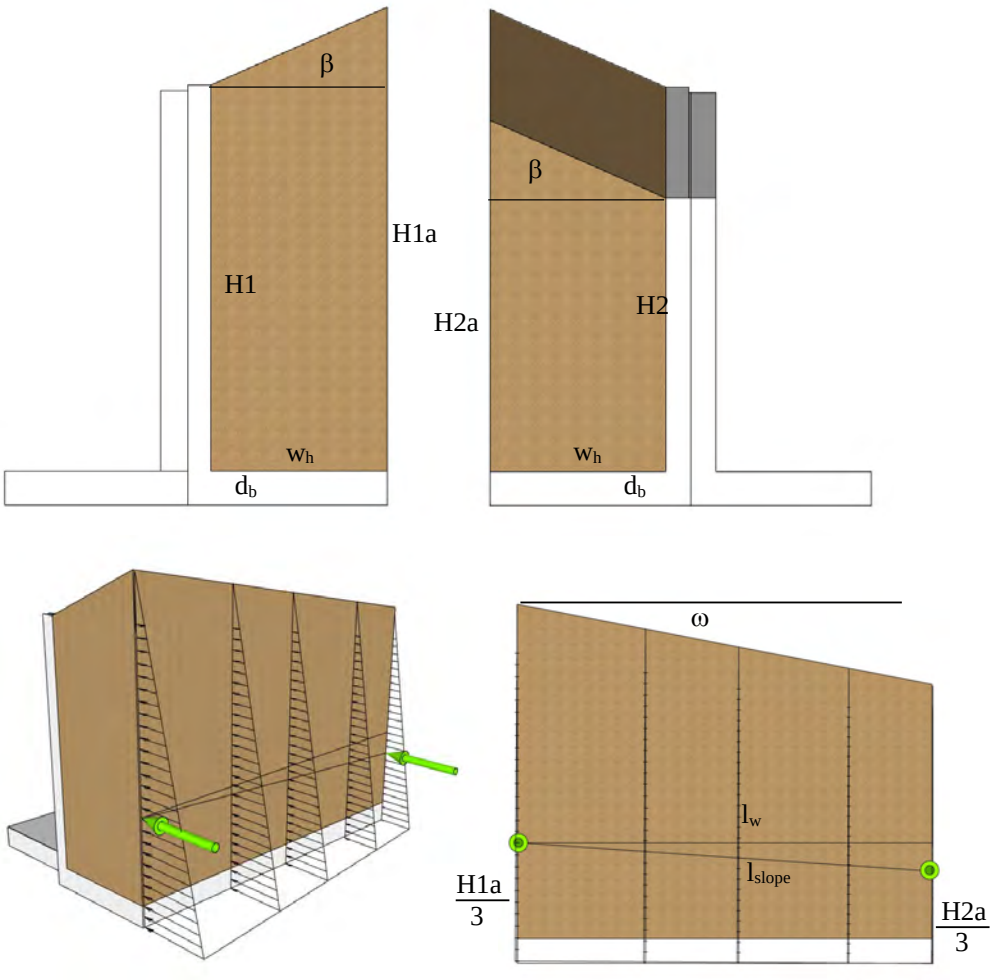

P_{hwall} is calculated using Rankine or Coulomb earth pressure. For simplicity, use at rest conditions with a sloping backfill based on Kezdi (1972):

$$K_0 = (1 - sin\phi)(1 + sin\beta)$$

Wall Parameters and Coefficients
$\phi = 35^o$
$\gamma = 110pcf$
$\beta = 10^o$
At rest earth pressure coefficient:

$$K_0 = (1 - sin\phi)(1 + sin\beta) = \big(1 - sin(35^o)\big)\big(1 + sin(10^o)\big) = 0.50$$

w_h = Heel width: 6.25 ft
d_b = Base thickness = 1 ft
l_w = Length of wing wall = 10.96 ft
H1 = Height of wing wall at tab = 11.42 ft
H2 = Height of wing wall at end = 5.71 ft

Determine dimensions on plane where forces are calculated:

H1a = Height of backfill at tab over heel = H1 + w_h tanβ + d_b = 11.42ft + 6.25ft tan(10^o) + 1ft = 13.52 ft
H2a = Height of backfill at end over heel = H2 + w_h tanβ + d_b = 5.71 ft + 6.25ft tan(10^o) + 1ft = 7.81 ft

At rest earth pressure at **t**ab side of backfill:

At rest pressure at base: $\sigma_0 = K_0\,\gamma H1a = (0.5)(110pcf)(13.52ft) = 744$ psf
At rest force: P(x) = P(t) = ½σ_0H1a = ½(743.6psf)(13.52ft) = 5030 lb/ft
Horizontal component of P(t) cosβ = 5026 lb/ft (cos 10^o) = 4950 lb/ft

At rest earth pressure at **e**nd side of backfill

At rest pressure at base: $\sigma_0 = K_0\,\gamma H2a = (0.5)(110pcf)(7.81ft) = 430$ psf
At rest force: P(x) = P(e) = ½σ_0H2a = ½(429.6psf)(7.81ft) = 1680 lb/ft
Horizontal component of P(e) cosβ = 1677.4 lb/ft (cos 10^o) = 1650 lb/ft

Perpendicular slope of backfill:

$$\omega = \arctan\left(\frac{H1a - H2a}{l_w}\right) = \arctan\left(\frac{13.52\,ft - 7.81\,ft}{10.96\,ft}\right) = 27.5^o$$

Estimated sloping distance between end resultant forces at tab and end of wall:

$$l_{slope} = (l_w)\sec(\omega) = (10.96\text{ft})(\sec(27.52^o)) = 12.36\text{ ft}$$

Total resultant force of the horizontal pressure on the wing wall:

$$P_{h-wall} = \int_0^{l_w} P(x)\cos(\beta)\,dx$$

For a simple, safe estimate of the integral:

$$P_{h-wall} = (Average\ of\ P_0 cos\beta)(l_{slope})$$

$$P_{h-wall} = \left(\frac{4950\frac{lb}{ft} + 1650\frac{lb}{ft}}{2}\right)(12.36\ ft) = 41{,}000\ lb$$

As discussed in the derivation of Equation (7-6), the force acting on the tab (per ft of height) at the bottom of the tab is therefore:

$$p_{tab} = \frac{P_{h-wall}}{h_i} = \frac{41{,}000\ lb}{11.42\ ft} = 3600\ lb/ft$$

The force parallel to the tab face, n_c, is taken as

$$n_c = 0.2p_{tab} = 0.2(3600\ lb/ft) = 720\ lb/ft$$

The *factored* design forces, $p_{u,tab}$ and n_{uc}, are

$$p_{u,tab} = 1.35p_{tab} = 1.35(3600\ lb/ft) = 4900\ lb/ft$$

$$n_{uc} = 1.75n_c = 1.75(720\ lb/ft) = 1260\ lb/ft$$

7.3.3.3 Tab Length

Once the design forces have been established, the next major step is to establish the length of the tab, l_{tab}. Ease of construction is a key consideration. Enough tab overlap length should be provided to allow for some anticipated movement of the wall. The bearing capacity of the concrete tab surface is not a concern for any reasonable

magnitude of design tab force. The primary driving factor related to strength is the need to adequately develop the reinforcement at Section 1-1, as shown in Figure 7-7. Assuming Grade 60 reinforcement and standard 4000 psi concrete with standard 2 in. clear cover, the hooked No. 4 Bar A would be adequately developed if l_{tab} is 10 in. (or greater). Development of larger bar sizes would require l_{tab} of at least 12 in. However, as noted in the previous discussion of design strategy, better performance in this type of component will result from decreasing bar spacing than from increasing bar size.

Selecting a tab length longer than justified by these considerations is not recommended. A longer tab will increase the flexural demand on Section 1-1. Therefore, this example proceeds assuming l_{tab} is 10 in., as depicted in Figure 7-8.

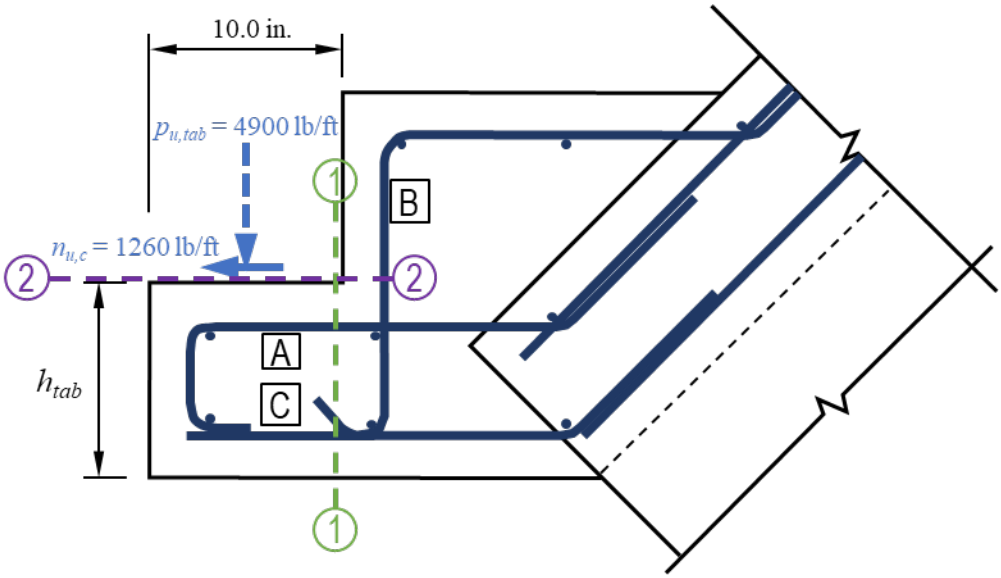

Figure 7-8. Tab length selected

Bar C will not experience large tension; this is discussed in Section 7.3.3.5. The development length check for hooked Bar A proceeds as follows (Article 5.10.8.2.4):

$$l_{hb} = \frac{38.0 d_b}{60.0}\left(\frac{f_y}{\sqrt{f'_c}}\right) = \frac{38.0(0.5\ in)}{60.0}\left(\frac{60\ ksi}{\sqrt{4\ ksi}}\right) = 19.0(0.5\ in) = 9.5\ in \quad (7\text{-}9)$$

$$l_{dh} = l_{hb} \times \left(\frac{\lambda_{rc}\lambda_{cw}\lambda_{er}}{\lambda}\right) = 9.5\ in \times \frac{(0.8)(1.0)(1.0)}{1.0} = 7.6\ in \quad (7\text{-}10)$$

The reinforcement confinement factor (λ_{rc}) was taken as 0.8 in this calculation because of the abundant side and tail cover for the hooked bar. The provided hook embedment length is computed as l_{tab} minus the clear cover: 10.0 in. – 2.0 in. = 8.0 in. Because the provided embedment length of 8.0 in. exceeds the required development length, l_{dh}, of 7.6 in., Bar A is adequately developed within the tab length.

7.3.3.4 Tab Thickness

The tab thickness is also be driven by practical construction issues. The default choice for the tab thickness is to select the same thickness as the wing wall. The two structural performance factors that are most likely to affect the tab thickness selection are the shear strength of Section 1-1 and the need to provide adequate length to fully develop Bar B on each side of Section 2-2. Selecting a tab thickness of 10 inches or greater will ensure adequate shear strength in almost all cases. A 10 in. tab thickness will also provide adequate development length for Bar B if it is a No. 4 bar and hooked as shown in Figure 7-8. The development length calculation is the same as shown in the previous section for Bar A. Use of larger bars would require a thicker tab and thicker culvert extension to adequately develop Bar B. The wall tab will likely have the same thickness as the culvert tab because they are subjected to the same demands. Therefore, the nominal thickness of the culvert extension is twice the thickness of the tab, and Bar B will be adequately developed on each side of Section 2-2 if hooked around a vertical bar at each end. This example proceeds assuming a tab thickness of 10 in. as shown in Figure 7-9.

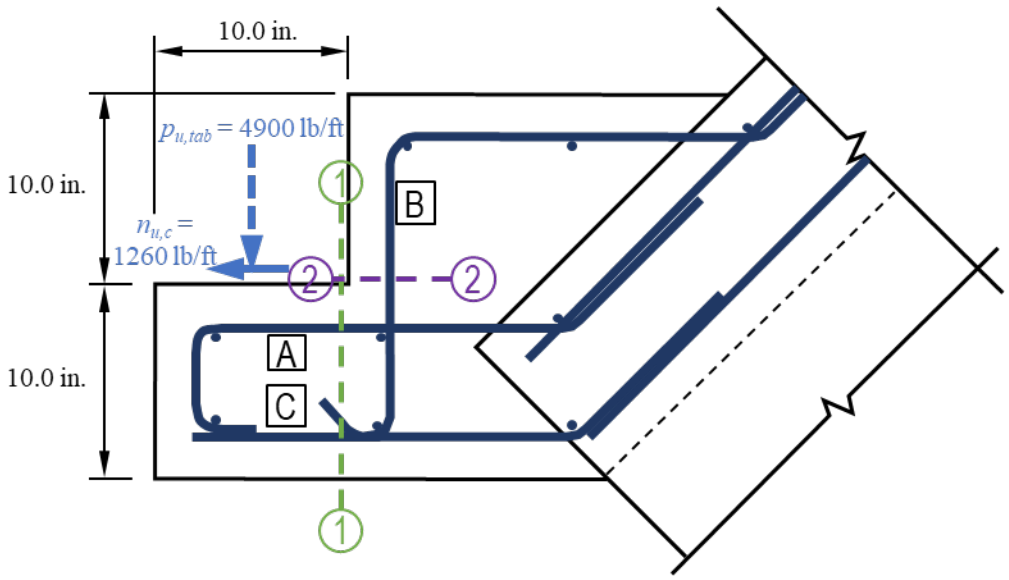

Figure 7-9. Tab thickness selected

The strength checks of Section 1-1 remain. These should be done in concert with checking the longitudinal reinforcement for shear, flexural, and axial strength in the next step.

7.3.3.5 Longitudinal Reinforcement

The longitudinal reinforcement of the tab (Bar A and Bar C) must be sufficient to provide adequate shear, flexural, and axial strength on Section 1-1. Figure 7-10 depicts the factored internal forces that must be resisted on this critical section.

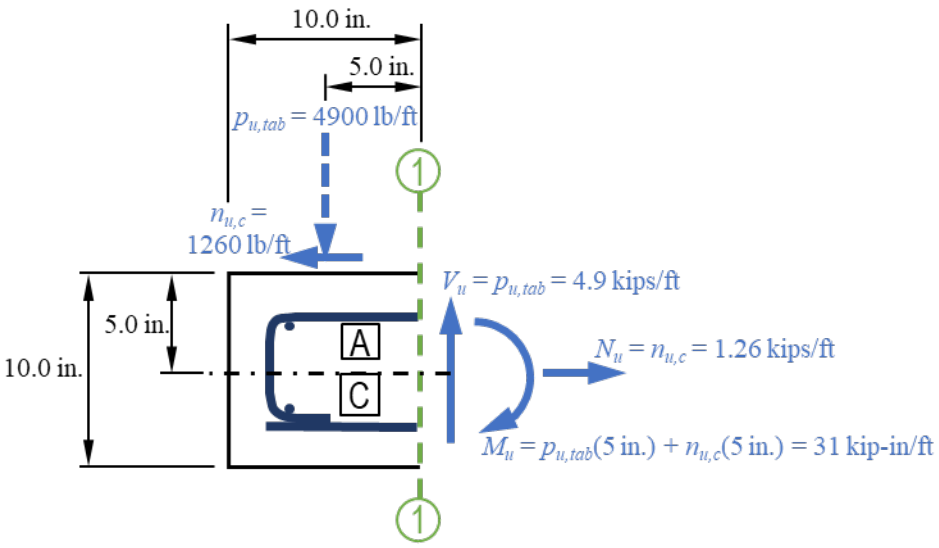

Figure 7-10. Design internal forces (V_u, M_u, and N_u) to be resisted on Section 1-1

Article 5.8.4.3.2 specifies that the design of Section 1-1 for shear strength shall be based on the shear friction requirements of Article 5.7.4 with some additional resistance limits that are specific to applied concentrated loads; these additional limits do not apply because of the distributed loading on the tab. The shear friction requirements begin with a requirement (5.7.4.2) for a minimum amount of shear friction reinforcement, A_{vf}, crossing the sectional area, A_{cv}, resisting the shear force on Section 1-1:

$$A_{vf} \geq \frac{0.05A_{cv}}{f_y} = \frac{0.05\left[(10.0\ in)\left(12.0\frac{in}{ft}\right)\right]}{60} = \frac{0.05\left[120\frac{in^2}{ft}\right]}{60} = 0.10\ in^2/ft \quad (7\text{-}11)$$

Therefore, Bar A and Bar C must together provide at least 0.10 in^2 of reinforcement per 1.0 ft vertical spacing. The suggested No. 4 bars at 12 in. spacing for Bar A and Bar C together provide four times this amount of reinforcement.

The nominal interface shear resistance, V_{ni}, of the plane of Section 1-1 is given by (5.7.4.3-3) as

$$V_{ni} = cA_{cv} + \mu\left(A_{vf}f_y + P_c\right) \tag{7-12}$$

where

c = cohesion factor specified as 0.40 ksi in Article 5.7.4.4 for normal weight concrete placed monolithically,

μ = friction factor specified as 1.4 in Article 5.7.4.4 for normal weight concrete placed monolithically, and

P_c = permanent net compressive force normal to the shear plane, taken as 0 if the force is tensile, as is the case with Section 1-1.

Therefore, the interface shear resistance that corresponds to the *minimum* required A_{vf} for this tab (0.10 in^2/ft) is

$$V_{ni} = 0.4\ ksi\ \left(120\frac{in^2}{ft}\right) + 1.4\left[\left(0.10\frac{in^2}{ft}\right)(60\ ksi) + 0\right]$$

$$V_{ni} = 48\frac{kips}{ft} + 8.4\frac{kips}{ft} = 56\frac{kips}{ft}$$

For normal weight concrete placed monolithically, V_{ni} is not permitted to exceed either of

$$V_{ni} \le 0.25f'_cA_{cv} = 0.25(4\ ksi)\left(120\frac{in^2}{ft}\right) = 120\frac{kips}{ft}$$

$$V_{ni} \le (1.0\ ksi)A_{cv} = (1.0\ ksi)\left(120\frac{in^2}{ft}\right) = 120\frac{kips}{ft}$$

Neither of these upper limits will control the strength in this lightly reinforced tab. Therefore, the design interface shear resistance, ϕV_{ni}, (per ft of height) for this section when only the minimum reinforcement is supplied is

$$\phi V_{ni} = 0.90\left(56\frac{kips}{ft}\right) = 50\frac{kips}{ft}$$

This design shear resistance far exceeds the factored shear force on Section 1-1, V_u = 4.9 kips/ft. Therefore, the shear strength of the tab is more than adequate. However, because the net axial force on Section 1-1 is tensile, Article 5.7.4.5 requires additional reinforcement beyond the minimum A_{vf} determined above. The additional reinforcement, A_{vpc}, must satisfy (5.7.4.5-3):

$$A_{vpc} = \frac{P_c}{\phi f_y} = \frac{1.26\ kips/ft}{0.90(60\ ksi)} = 0.023\ in^2/ft \tag{7-13}$$

Combining A_{vf} and A_{vpc} gives the total amount of interface reinforcement required as 0.12 in^2/ft. When spaced vertically at the recommended 12 inches, Bars A and C together provide 0.40 in^2 per ft of reinforcement across Section 1-1. Therefore, all requirements related to the shear strength of the tab are satisfied.

Section 1-1 must also provide adequate strength for the combined flexure and axial force acting on the section. For this purpose, it is instructive to decompose the bending moment and axial force into the forces shown in Figure 7-11.

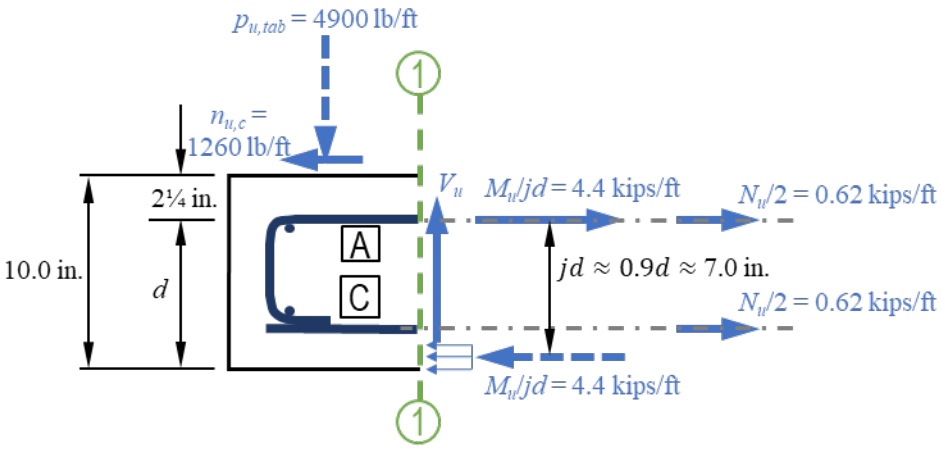

Figure 7-11. Longitudinal force components of M_u and N_u to be resisted on Section 1-1

Therefore, Bar A reinforcement must resist a total factored tension force, T_u, of

$$T_u = \frac{M_u}{jd} + \frac{N_u}{2} = 4.4\frac{kips}{ft} + 0.62\frac{kips}{ft} = 5.0\frac{kips}{ft} \tag{7-14}$$

The design tension capacity, ϕT_n, provided by the recommended No. 4 Bar A at 12 in. vertical spacing (0.20 in^2/ft) is

$$\phi T_n = \phi A_s f_y = 0.9\left(0.20\frac{in^2}{ft}\right)60\ ksi = 0.9\left(12.0\frac{kips}{ft}\right) = 10.8\ \frac{kips}{ft} \tag{7-15}$$

Therefore, Bar A provides approximately twice the flexure plus axial force capacity required—as long as these bars are adequately developed. The net compression force on the opposite side of the tab (the Bar C side) is easily resisted by the concrete. Article 5.8.4.3.3 requires that this reinforcement also satisfy the check for minimum primary tension reinforcement, A_s, from the corbel design provisions (5.8.4.2.2-5):

$$A_s \geq \frac{2A_{vf}}{3} + A_n \tag{7-16}$$

In this expression from the corbel design provisions (5.8.4.2.2), A_n is defined as the area of reinforcement dedicated to resisting N_{uc}. This area of reinforcement is functionally equivalent to A_{vpc} from the shear-friction provisions (5.7.4.5-3), which was computed using Equation (7-13) for this example as A_{vpc} = 0.023 in^2/ft. Accordingly,

$$A_s \geq \frac{2A_{vf}}{3} + A_{vpc} \tag{7-17}$$

$$A_s \geq \frac{2\left(0.10\ \frac{in^2}{ft}\right)}{3} + 0.023\frac{in^2}{ft}$$

$$A_s \geq 0.090\frac{in^2}{ft}$$

Therefore, this minimum A_s check is satisfied by the recommended use of No. 4 bars at 12 in. spacing (0.20 in^2/ft) for Bar A.

All the checks related to shear, flexural, and axial strength of Section 1-1 and the size and spacing of Bar A have been described here. Recall that the development of Bar A in the tab was checked as part of the process described in Section 7.3.3.3 for establishing an adequate tab length. In addition to being adequately developed in the tab, Bar A must extend in the opposite direction and be lapped with the culvert wall reinforcement. This is necessary to fully anchor this tension reinforcement as assumed for developing the tension resistance computed above. This concludes all the design checks and considerations for Section 1-1 of the tab.

7.3.3.6 Hanger Reinforcement

Bar B is needed to bring the tab force into the larger culvert extension and resist the cracking and failure shown in Figure 7-5c. Therefore, it has the same function as "hanger" reinforcement in a beam ledge. In accordance with 5.8.4.3.5, the design loads and critical location for Bar B are depicted in Figure 7-12.

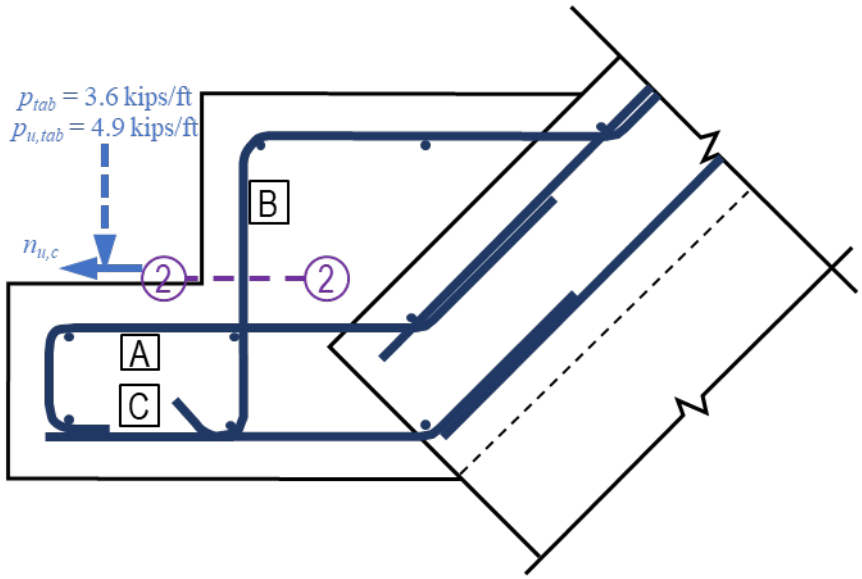

Figure 7-12. Design forces and critical location for Bar B "hanger" reinforcement

Both the unfactored and factored p_{tab} forces are shown because service and strength limit state checks are required. The service and strength limit state checks prescribed in Article 5.8.4.3.5 are based on concentrated loads applied by girders bearing on a beam ledge. For the purposes of this procedure, they are simplified here to apply to the distributed tab loading. The strength limit state check of 5.8.4.3.5-2 gives the following equivalent requirement for A_{hr}, the area of hanger reinforcement (per ft of tab height) Bar B crossing Section 2-2:

$$A_{hr} \geq \frac{p_{u,tab}}{\phi f_y} \tag{7-18}$$

$$A_{hr} \geq \frac{4.9 \frac{kips}{ft}}{0.90(60\ ksi)}$$

$$A_{hr} \geq 0.09 \frac{in^2}{ft}$$

The service limit state check (5.8.4.3.5-1) is similar, but it appears as if formulated to limit the stress in the reinforcement to approximately one-half of the yield stress under (unfactored) service loads. Thus, the purpose of this expression is to control the width of cracks crossing Bar B.

$$A_{hr} \geq \frac{p_{tab}}{0.5 f_y} \tag{7-19}$$

$$A_{hr} \geq \frac{3.6 \frac{kips}{ft}}{0.5(60\ ksi)}$$

$$A_{hr} \geq 0.12 \frac{in^2}{ft}$$

Because this service-level requirement is focused on crack control rather than strength, it is recommended that a reinforcement stress limit (e.g., 30 ksi) be used in the denominator

rather than $0.5f_y$. This will prevent the unforeseen allowance of larger than desirable cracks if higher strength reinforcement is used. This results in the following recommended requirement for limiting crack widths, coupled with a bar spacing no greater than 12 in.:

$$A_{hr} \geq \frac{p_{tab}}{30\ ksi} \tag{7-20}$$

$$A_{hr} \geq 0.12 \frac{in^2}{ft}$$

The recommended Bar B configuration of Grade 60, No. 4 bars at 12 in. spacing (0.20 in^2/ft) satisfies the requirements for the hanger reinforcement if these bars are adequately developed. If any of the reinforcement checks indicate that a 12 in. spacing of No. 4 bars is not adequate, first consider decreasing the reinforcement spacing or increasing the tab dimension(s) before increasing the bar size. Increasing the bar size is likely to require larger bar bend diameters and larger tab dimensions for adequate reinforcement development.

As noted in Section 7.3.3.4, the development of Bar B should be checked when first selecting the tab thickness. Bar B should be anchored at each end by a hook around a vertical bar as depicted in Figure 7-12. It is recommended that Bar B continue from the reinforcement on the soil face of the culvert extension as shown in the figure. If this is not possible, both Bar B and the culvert extension reinforcement should terminate with hooks around the vertical corner bar.

7.3.3.7 Vertical Reinforcement

The vertical reinforcing bars in the tab and extension should establish the corners of the horizontal reinforcement layout. Standard minimum reinforcement rules for

retaining walls should be satisfied, and the vertical bar spacing should be no greater than used in the wing wall. No. 4 bars shall be spaced at no more than 12 in. in each face. Vertical bars shall be located inside all hooks of horizontal reinforcement to promote adequate anchorage.

The example culvert wing tab design resulting from this procedure is shown in Figure 7-13.

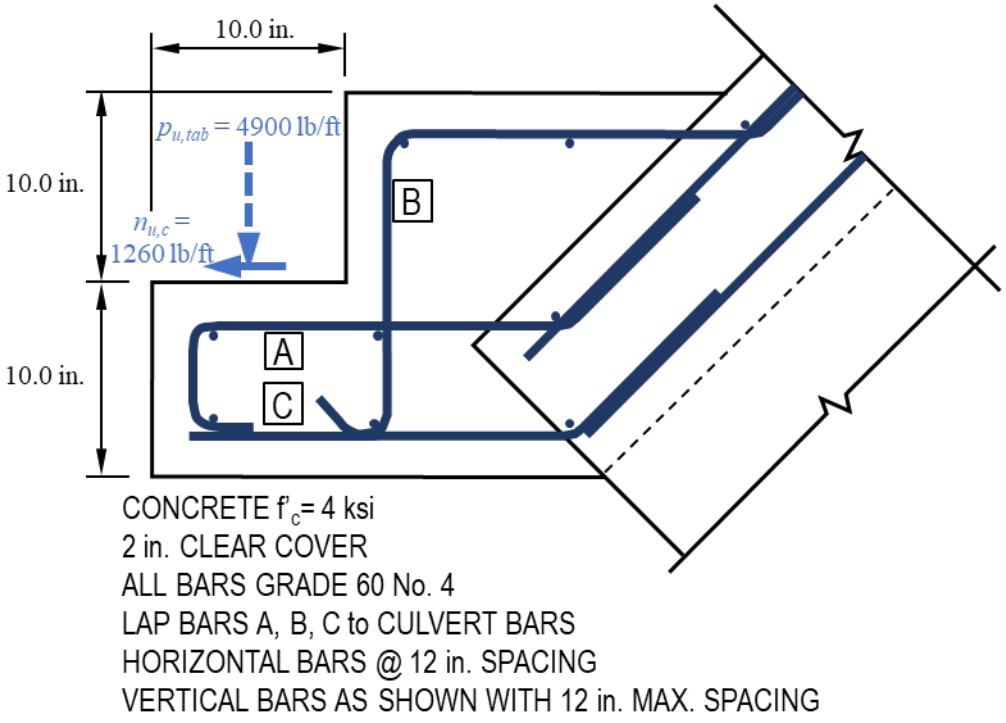

Figure 7-13. Culvert wing tab design for example case

7.3.3.8 Wall Tab Design—Strut-and-Tie Method

Figure 7-14 shows a potential wing wall tab geometry and reinforcement configuration that pairs with the example culvert wing tab design. Bars A, B, and C in the figure have similar roles to Bars A, B, and C, respectively, in the culvert tab example.

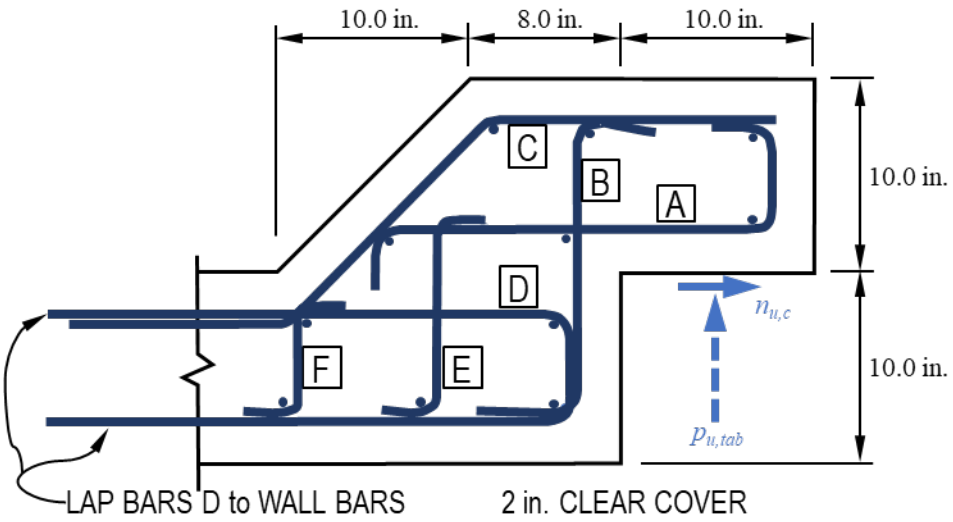

Figure 7-14. Potential wall tab geometry and reinforcement configuration

There are some key differences from the culvert wing tab design. One difference is that a distributed earth pressure is acting on the wall face simultaneous with the applied transverse tab reaction force, $p_{u,tab}$. A major difference is that $p_{u,tab}$ and $n_{u,c}$ must flow through the tab geometry into an offset thin element (the wing wall) rather than the relatively thick culvert tab. Therefore, the Article 5.8.4.3 beam ledge method is not directly applicable here. There are multiple possible critical locations, and the force in the hanger reinforcement (Bar B) is greater than in same reinforcement in the culvert tab.

The strut-and-tie method (STM) of Article 5.8.2 is useful to visualize the flow of forces in the D-region and to position and proportion the reinforcement. Figure 7-15 depicts the strut-and-tie model used in concert with the reinforcement configuration shown in Figure 7-14.

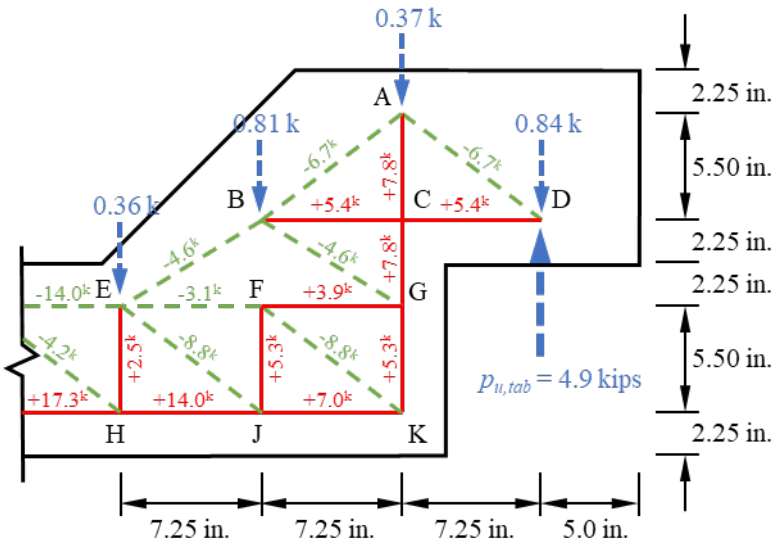

Figure 7-15. Strut-and-tie model for a wing wall tab resisting earth pressure

This strut-and-tie model shows resultant forces for a potential distribution of stress fields resulting solely from the earth pressure and tab force in a representative 1 ft thick strip of the wing wall tab. The model consists of (tension) ties, in red, and (compression) struts, in green, connected by nodal zones. The distributed external loads are concentrated into resultant forces at the nearest node locations. These are indicated by the dashed blue lines. The $n_{u,c}$ force is not applied in this model because it is not always present. The internal effects of $n_{u,c}$ are investigated separately. The axes of the ties (and struts) were selected to correspond to the most practical reinforcement locations while also accommodating a reasonable flow of stresses through the model. The strut and tie forces necessary for equilibrium of the resulting statically determinate model are shown. Recall that this model, loads, and forces all represent a single, 1 ft thick slice of the tab.

Several behavioral observations can be made based on the visualization of flow of forces made possible by using the model. First, it can be seen why the specified 8.0 in.

dimension of Figure 7-14 is shorter than the corresponding dimension (10 in.) in the Coosa County wall tab tested in this project. In fact, based on the flow of forces from (nodes) A to B to E in Figure 7-15, it appears that the dimension could be shortened further in concert with using a reduced slope of the taper. However, the accompanying reduction in concrete may not be worth the complexity of using a slope other than 1:1.

Note that the force that must be resisted by Bar B is somewhat greater than what was required in the culvert tab design based on the beam ledge provisions. Here the maximum force to be resisted by Bar B is 7.8 kips (between Nodes A and G), while it was only 4.9 kips in the culvert tab. Note also that the transfer of forces from the tab to the wall element results in tension demands in the region reinforced by the U-shaped bar labeled Bar D in Figure 7-14. These are the forces on the exposed face of the wing wall and between Nodes F and G in Figure 7-15. Finally, there are small transverse tension forces that appear in the wall portion (between Nodes H and E, J and F, etc.). These forces can be thought of as representing the shear forces in the extension of the wing wall. Depending on their magnitude, they may be resisted by the concrete alone (in shear) or they may require the reinforcement depicted as Bar E and Bar F in Figure 7-14.

The forces resulting solely from $n_{u,c}$ in the strut-and-tie model are shown in Figure 7-16.

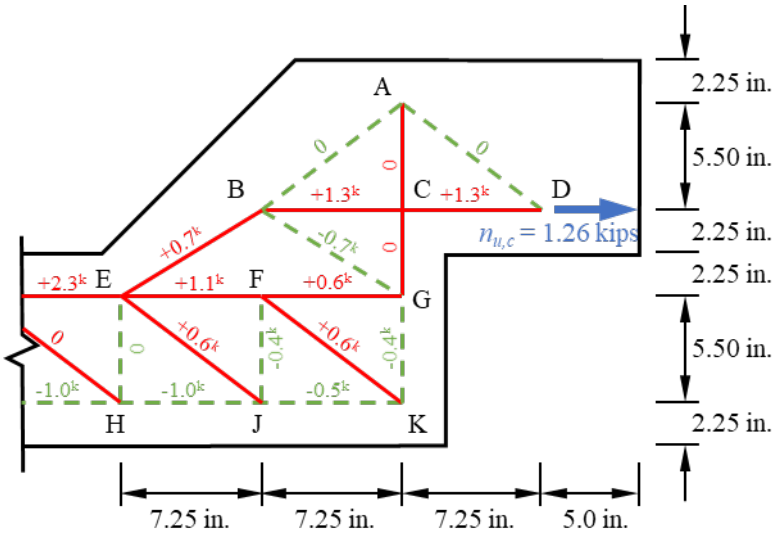

Figure 7-16. Strut-and-tie forces caused by $n_{u,c}$

Inspecting the tie forces, this load increases the demand on Bar A (Tie BCD) and Bar D (Tie FG). There is a small increase in the compression in Strut BG, but the compressive stresses are quite small in this model. In other locations, the $n_{u,c}$ loading tends to reduce the demand of the primary transverse tab reaction force ($p_{u,tab}$).

Once a realistic strut-and-tie model has been conceived and configured to satisfy the geometric constraints, the strut-and-tie forces are determined for each loading. The strut demands in this model are quite low, which is ideal, so the design proceeds with the checking of reinforcement amounts and detailing to provide adequate strength in the ties. The greatest strut stresses in the wall tab zone are found in Struts EJ and FK, which each have a worst-case factored strut compression force of 8.8 kips. The thickness of this representative 1 ft strip of the tab is 12 inches, and the available width of these diagonal struts and their node faces is at least 4 inches—resulting in a node face effective cross-sectional area, A_{cn}, of at least 48 in^2. Based on Article 5.8.2.5, the most conservative (worst-case) limiting stress at a node face, f_{cu}, is

$$f_{cu} = mvf'_c \tag{7-21}$$

$$f_{cu} = (1.0)(0.45)(4\ ksi) = 2.25\ ksi$$

And the resulting strut design strength is

$$\phi P_n = \phi f_{cu} A_{cn} \tag{7-22}$$

$$\phi P_n = (0.70)(2.25\ ksi)(48 in^2) = 76\ kips$$

This design strut strength is more than eight times the factored strut demand (8.8 kips), which illustrates that compressive stresses are not critical in this model (aside from in the wing wall itself).

When it comes to tie strength, it is informative to consider the strength of a tie represented by the standard minimum amount of reinforcement provided: a Grade 60 No. 4 bar spaced at 12 inches. In accordance with Article 5.8.2.4, the design resistance of a No. 4 tie is

$$\phi P_n = \phi f_y A_{st} \tag{7-23}$$

$$\phi P_n = (0.90)(60.0\ ksi)(0.20 in^2) = 10.8\ kips$$

Therefore, inspection of the forces in Figure 7-15 and Figure 7-16 reveals that a single No. 4 bar in each 12 in. vertical width will satisfy the tension force demands in all ties except those running along the exposed face of the wall (Bar D on either side of Node H).

The struts and ties that run along the face of the wall as it leaves the tab region (beyond Nodes E and H) warrant further discussion. According to the strut-and-tie model, these forces continue to increase with distance away from the tab. However, the actual wall is designed as a one-way cantilever structure in which all forces are carried in flexure by vertical strips. The simplified strut-and-tie model used here conservatively

ignores this action—assuming that all resistance is one-way in the perpendicular direction (spanning horizontally). This conservative assumption works well for safe design of the tab region, but breaks down outside of the tab. Therefore, it is recommended to compute the tie reinforcement required at the boundary of the tab region (Node H), and then extend that reinforcement over the first 30 percent of the wall length (measured from the tab).

For this example, this recommendation indicates that 14.0 kips of factored tension resistance per ft of wall height is required at the tab boundary (Node H). The area of Grade 60 reinforcement required to satisfy this requirement is

$$A_{st,required} = \frac{P_{n,required}}{f_y} = \frac{P_u}{\phi f_y} \tag{7-24}$$

$$A_{st,required} = \frac{14.0\ kips/ft}{(0.90)(60.0\ ksi)} = 0.26\ kips/ft$$

The simplest way to provide this reinforcement is to provide supplementary No. 4 bars midway between the standard horizontal No. 4 bars on the exterior face of the wall for the first 30 percent of the wall length. In the case of the example wall, these supplemental bars should extend 3 ft from the tab end of the wall.

The ties represented by Bars E and F could readily be reinforced by a single No. 4. Alternatively, for this example, a judgment could be made to drop these bars based on the shear strength of the concrete alone in this region. These tie (EH and FJ) forces can be thought of as the shear force acting on the extension of the wall into the tab. If the force in the corresponding tie is significantly less than the one-way shear strength of the wing

wall itself without shear reinforcement, Bar E or Bar F could potentially be deleted. (This would be the case with the magnitude of the forces in this example.)

Proper anchorage of ties is crucial to adequate performance. Each bar that serves as tie reinforcement should have a standard hook around a perpendicular bar. A hook around a vertical bar is ideal. As with the culvert tab, minimum vertical reinforcement rules for wall reinforcement should be satisfied. At a minimum, vertical bars shall be placed in the corners of all horizontal reinforcement and at a maximum spacing of 12 inches.

A summary of the potential wing wall tab design for the example design scenario is depicted in Figure 7-17.

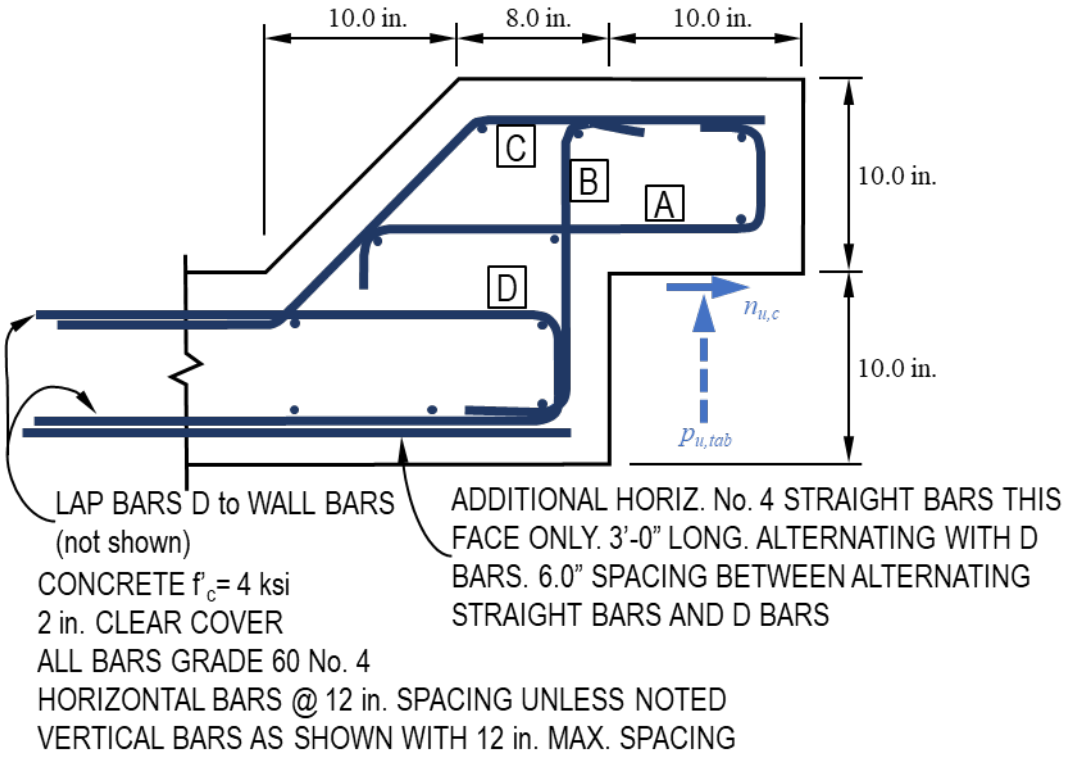

Figure 7-17. Wing wall tab design for example case

Chapter 8. Summary and Conclusions

8.1 Summary

The objectives of this project were to determine force on the culvert wing tab using field measurements and numerical simulations and develop an LRFD design procedure for the culvert wing tab to determine dimensions and reinforcing steel details. The scope of work included a literature search, the instrumentation of prototype culverts, and FE simulations of model culverts under various service and extreme event scenarios. The results of these three tasks were used to develop both a function to calculate the tab force and the LRFD design procedure.

This study examined the ALDOT proposed design of new tabbed wing wall-to culvert connection, that disconnects the wing wall from the culvert barrel thereby allowing the wing wall to deflect separately from the barrel. This causes the wing wall to behave similarly to a cantilever retaining wall with a pin support along one side. To evaluate the behavior of the proposed design, three culverts of varying heights were constructed in Alabama. The four tabs in each culvert were equipped with three pressure sensors equidistantly installed along tab height. Since it was not possible to simulate the behavior of the structure under all possible load conditions. Finite element simulations were conducted using Plaxis 3D to investigate deep fill and extreme event loading. The combined results of numerical analyses and field measurements were used to develop an analytical approach of estimating the force on the tab surface.

A design procedure consistent with AASHTO LRFD (2020) design provisions was developed for the culvert tab. The design procedure and a detailed example are discussed in Section 7.3. The recommended procedure begins with the computation of the

design forces acting on the tab. Equations (7-1) through (7-6) provide a reasonably straightforward and conservative procedure to estimate the tab force. An example calculation of the force, p_{tab}, (acting on a representative 1 ft height of the tab) is given in Section 7.3.3.2. The structural concrete design procedure is based primarily on adapting AASHTO LRFD (2020) beam ledge design philosophy and provisions to the loads and geometry of the tab. The structural concrete design steps proceed sequentially as described in Section 7.3.3, beginning with determination of tab length and thickness, followed by verification of adequate size, spacing, and configuration of reinforcing steel. Section 7.3.3 contains a full example design of a culvert wing tab.

8.2 Conclusions

The testing, analysis, and design performed for this study support the following conclusions:

1. The stress distribution on the culvert wing tab surface is generally approximated by a distributed triangular loading with maximum magnitude located at the bottom of the tab and reducing toward the top. This is verified by the field instrumentation and finite element models. In the case of extreme undermining scour the rotation of the wing wall imposes a concentrated force at the top of the wall.
2. The force on the tab is best approximated using an at rest, K_0, earth pressure distribution along the wing wall. This distribution is integrated along the height and width of the wall to determine the total horizontal force on the wall. Based on the resistive forces due to base sliding and the existence of a toe wall, no more than one-half of the total wing wall horizontal force can be transferred to the culvert tab prior to the loss of overall wall stability.

3. Use of the culvert tab design procedure presented in Section 7.3 is recommended. The procedure is consistent with AASHTO LRFD (2020) provisions for earth pressure loading and the design of structural concrete.

8.3 Recommendations

Construction of the wing walls was perceived to be more complicated than conventional integral construction. It would be beneficial to consider the cost comparison between a culvert of this type and a conventional bridge.

The design loads provided were based on scenarios, it would be beneficial to compile field data (maintenance inspection records) on the performance of culverts with integral wing walls alongside the culverts from this study in the long term. Qualitative and quantitative information will prove useful to designers as this standard is implemented.

References

AASHTO (2014). LRFD Bridge Design Specifications, 7th Edition. Washington, D.C. American Association of State Highway and Transportation Officials.

AASHTO (2020). LRFD Bridge Design Specifications, 9th Edition. Washington, D.C. American Association of State Highway and Transportation Officials.

ABAQUS (2018). Dassault Systèmes, Providence, RI, USA.

Abuhajar, O., Newson, T., and Naggar, H. E. (2017). "The Effect of Soil Depth and Box Culvert Geometry on the Static Soil-Culvert Interaction." Geotechnical Frontiers, Proceedings.

ACPA. (1983). BOXCAR. Box Culvert Analysis and Reinforcing Design. American Concrete Pipe Association, Irving, TX.

Ahmed, B., Amanat, K.M., Saflullah, A.M.M., and Choudhury, J. R. (2003). "Causes of cracking of culverts on filled soil and their performance after repair." Journal of Civil Engineering, CE 30(1).

ALDOT. (2012a). "Bureau of Research & Development Research Need Problem Statement: Culvert Wing Tab Design Loads." Alabama Department of Transportation.

ALDOT. (2008). "Roadway Plans Preparation Manual: Plans Preparation and Assembly." Alabama Department of Transportation.

Alkhrdaji, T., and Nanni, A. (2001). "Design, Construction, and Field-Testing of an RC Box Culvert Bridge Reinforced with GFRP Bars." Non-Metallic Reinforcement for Concrete Structrures, FRPRCS-5, 1055–1064.

Ashari, S. (2014). "Ultimate Strength Design Method of Reinforced Concrete Structures."

ASTM C31/C31M-15ae1 Standard Practice for Making and Curing Concrete Test Specimens in the Field. (2015). ASTM International, West Conshohocken, PA.

ASTM C39 / C39M-17a, Standard Test Method for Compressive Strength of Cylindrical Concrete Specimens. (2017). ASTM International, West Conshohocken, PA.

ASTM D1557-12e1, Standard Test Methods for Laboratory Compaction Characteristics of Soil Using Modified Effort (56,000 ft-lbf/ft3 (2,700 kN-m/m3)). (2012). ASTM International, West Conshohocken, PA.

Bentler, J. G., and Labuz, J. F. (2006). "Performance of a Cantilever Retaining Wall." Journal of Geotechnical and Geoenvironmental Engineering, 132(8), 1062–1070.

Bowles, J. E. (1988). Foundation Analysis and Design, 4lh ed. McGraw Hill.

Bruner, R. F., Coyle, H. M., and Bartoskewitz, R. E. (1983). “Cantilever retaining wall design.” Texas A&M University.

BS 5400-2. (1978). “British standard BS 5400-2: Steel, concrete and composite bridges — Part 2:Specification for loads.” Board of BSI.

Casagrande, L. (1973). “Comments on Conventional Dessign of Retaining Structures (Discussion).” Journal of Soil Mechanics & Foundations Div, 99(sm8).

Chugh, A. K., Guney, O. C., and Labuz, J. F. (2016). “Soil Structure Interactions of Retaining Walls.” Geotechnical and Structural Engineering Congress 2016, Proceedings.

Clough, G. W., and Duncan, J. M. (1971). “Finite Element Analyses of Retaining Wall Behavior.” Journal of the Soil Mechanics and Foundations Division, 97(12), 1657–1673.

Coghlan, B. K. (1916). “Highway bridges and culverts.” Agricultural and Mechanical College of Texas.

ConnDOT. (2000). Drainage Manual. Connecticut Department of Transportation (ConnDOT).

Coulomb, C. A. (1776a). Essai sur une application des règles de maximis & minimis à quelques problèmes de statique, relatifs à l’architecture. De l’Imprimerie Royale, Paris.

Coulomb, C. A. (1776b). Essai sur une application des règles de maximis & minimis à quelques problèmes de statique, relatifs à l’architecture. De l’Imprimerie Royale, Paris.

CYBER 180-840A. (1986). Control Data, Saint Paul, MN.

Dasgupta, A., and Sengupta, B. (1991). “Large-Scale Model Test on Square Box Culvert Backfilled with Sand.” Journal of Geotechnical Engineering, 117(1).

Dunavant, D. A. (1985). “High degree efficient symmetrical Gaussian quadrature rules for the triangle.” International Journal for Numerical Methods in Engineering, 21(6), 1129–1148.

Duncan, J. M., and Chang, C.-Y. (1970). “Nonlinear Analysis of Stress and Strain in Soils.” Journal of the Soil Mechanics and Foundations Division, 96(5), 1629–1653.

ETCulvert. (2017). Eriksson Technologies, Lakewood, CO.

FDOT. (1993). Reinforced Concrete Box Culvert and Wingwall Design and Analysis User's Manual. Version 2.3, Structures Design Office Florida Department of Transportation.

FDOT. (2011). Plans Preparation Manual. Florida Department of Transportation (FDOT).

FHWA. (1983). Structural Design Manual for Improved Inlets & Culverts. U.S. Department of Transportation.

Garg, A. K., and Abolmaali, A. (2009). "Finite-Element Modeling and Analysis of Reinforced Concrete Box Culverts." Journal of Transportation Engineering, ASCE.

Geokon, Inc. (2011). Models 4800, 4810, 4815, 4820 and 4830 VW Earth Pressure Cells. Lebanon, NH: Geokon, Inc.

Goh, G. A. T. (1993). "Behavior of Cantilever Retaining Walls." Journal of Geotechnical Engineering, 119(11), 1751–1770.

"Google Maps." (2017a). 4300 County Road 258. La Fayette, Alabama.

"Google Maps." (2017b). 722 Lee Rd 156. Opelika, Alabama.

"Google Maps." (2017c). County Road 68. Sylacuaga, Alabama.

Huntington, W. C. (1957). Earth pressures and retaining walls. Wiley, New York.

Hurd, J. O. (1991). "Field Performance of Precast Reinforced Concrete Box Culverts." In Transportation Research Record, Transportation Research Board, (№1315), 53–57.

IES. (2017). VisualAnalysis. IES, Bozeman, MT.

IODOT. (2013). Culvert Calc, Technical Manual, Automated RCB culvert analysis and design in accordance with the AASHTO LRFD Bridge Design Specifications, 5th Edition. Iowa Department of Transportation.

Itasca. (2017). FLACK. Itasca, Minneapolis, MN.

Jaky, J. (1948). "Pressure in silos." Vol. 1, 103–107.

Katona, M. G. (2017). CANDE. Culvert Analysis and Design. CANDE, Gig Harbor, WA.

Kezdi, A. (1972). "Stability of Rigid Structures." Proceedings, 5th European Conference on Soil Mechanics and Foundation Engineering, Volume 2, 105-130.

Koiter, W. T. (1960). General Theorems for Elastic-plastic Solids. North-Holland.

Kondner, R. L. (1963). A hyperbolic stress-strain formulation for sands. Northwestern University.

Kulhawy, F. H. (1992). “On the Evaluation of Static Soil Properties.” ASCE, 95–115.

Kulhawy, F. H., Callanan, J. F., and Cornell University. (1985). Evaluation of procedures for predicting foundation uplift movements. Electric Power Research Institute, Palo Alto, Calif.

KYTC. (2011). Drainage Manual. Kentucky Transportation Cabinet (KYTC).

Lee, H. L. (2017). “Design of Lateral Support for Non-Integral Wing Walls of Culverts.” Master’s Thesis, Auburn University.

Mattock, A. H. (1976). “Design proposals for reinforced concrete corbels.” Precast/Prestressed Concrete Institute. Journal, 21(3).

Mayne, P. W., and Kulhawy, F. H. (1982). “K0-OCR relationships in soil.” Vol. 108 (GT6), 851–872.

McGrath, T. J., Selig, E. T., and Beach, T. J. (1996). “Structural Behavior of Three-Sided Arch Span Bridge.” In Transportation Research Record: Journal of the Transportation Research Board, (№1541), 112–119.

Meyerhof, G. G. (1956). “Penetration Tests and Bearing Capacity of Cohesionless Soils.” Journal of the Soil Mechanics and Foundations Division, 82(1), 1–19.

Musser, S. C. (1995). “A Synthesis of the Application and Performance of Three-Sided Precast Box Culverts.” In Transportation Research Record: Journal of the Transportation Research Board, (№951091).

Nisha, S., Shivashankar, R., and Ravi Shankar, A. U. (2011). “Role of Shear Keys in Cantilever Retaining Wall.” Scribd, (Geotechnical Engineering, Chemical Product Engineering).

NYSDOT. (2012). Geotechnical Design Manual. NYSDOT.

PLAXIS 3D AE.02. (2017). PLAXIS, Delft, Netherlands.

Plaxis bv. (2010). Plaxis Version 8. Validation manual. Plaxis.

Plaxis bv. (2015a). Plaxis 3D AE - Scientific Manual. Plaxis.

Plaxis bv. (2015b). Plaxis 3D AE - Reference Manual. Plaxis.

Plaxis bv. (2015c). Plaxis 3D AE - Material Models Manual. Plaxis.

Powell, R. E., and Foster, S. J. (1996). Experimental Investigation on Rectangular Corbels Cast in High Strength Concrete. University of New South Wales.

Ranganathan, R. (1999). “Structural reliability and design.”

Rankine, W. (1857). On the Stability of Loose Earth. Royal Society of London.

Rankine, W. J. M. (1858). A Manual Of Applied Mechanics. Hoar Press.

Reinforced concrete box culvert and wing wall design and analysis computer program user’s manual. (1993). Florida Department of Transportation (FDOT).

Scanlon, R. F. (2012). “Detailed visual culvert inspection guidelines.” Main Roads Western Australia.

Schanz, T. (1998). Zur Modellierung des mechanischen Verhaltens von Reibungsmaterialien. Universitat Stuttgart., Mitteilung 45 des Instituts fur GeotechnikUniversit ¨ ¨at Stuttgart.

Senthil, K., Iqbal, M. A., and Kumar, A. (2014). “Behavior of cantilever and counterfort retaining walls subjected to lateral earth pressure.” International Journal of Geotechnical Engineering, 8(2), 167–181.

Skempton, A. W. (1986). “Standart penetration test procedures and the effects in sands of overburden pressure, relative density, particle size, ageing and overconsolidation.” Geotechnique, 36(3).

Spangler, M. G. (1960). “Marston theory for soil pressure on conduits.” International Text Book Co.

Smith, I. M., and Griffiths, D. V. (2004). *Programming the finite element method*. Wiley,

Hoboken, NJ.

Terzaghi, K. (1934). “Large Retaining Wall Tests. I. Pressure of Dry Sand.” Engineering News-Record, 102(20).

Terzaghi, K. (1947). Theoretical Soil Mechanics. NY.

Terzaghi, K., Peck, R. B., Mesri, G., and Knovel (Firm). (1996). Soil mechanics in engineering practice. Wiley, New York.

Tschebotarioff, G. P. (1973). Foundations, Retaining and Earth Structures: The Art of Design and Construction and Its Scientific Basis in Soil Mechanics. Mcgraw-Hill, New York.

Van Langen, H., and Vermeer, P. A. (1990). “Automatic step size correction for non-associated plasticity problems.” International Journal for Numerical Methods in Engineering, 29(3), 579–598.

Van Langen, H., and Vermeer, P. A. (1991). “Interface elements for singular plasticity points.” International Journal for Numerical and Analytical Methods in Geomechanics, 15(5), 301–315.

Voitenko, P. (2018). Load Testing, Analysis, and Design of a New Box Culvert Wing Tab, Dissertation, Auburn University.

Appendix A Constructed Culvert Design Drawings

A.1 Chambers County Culvert

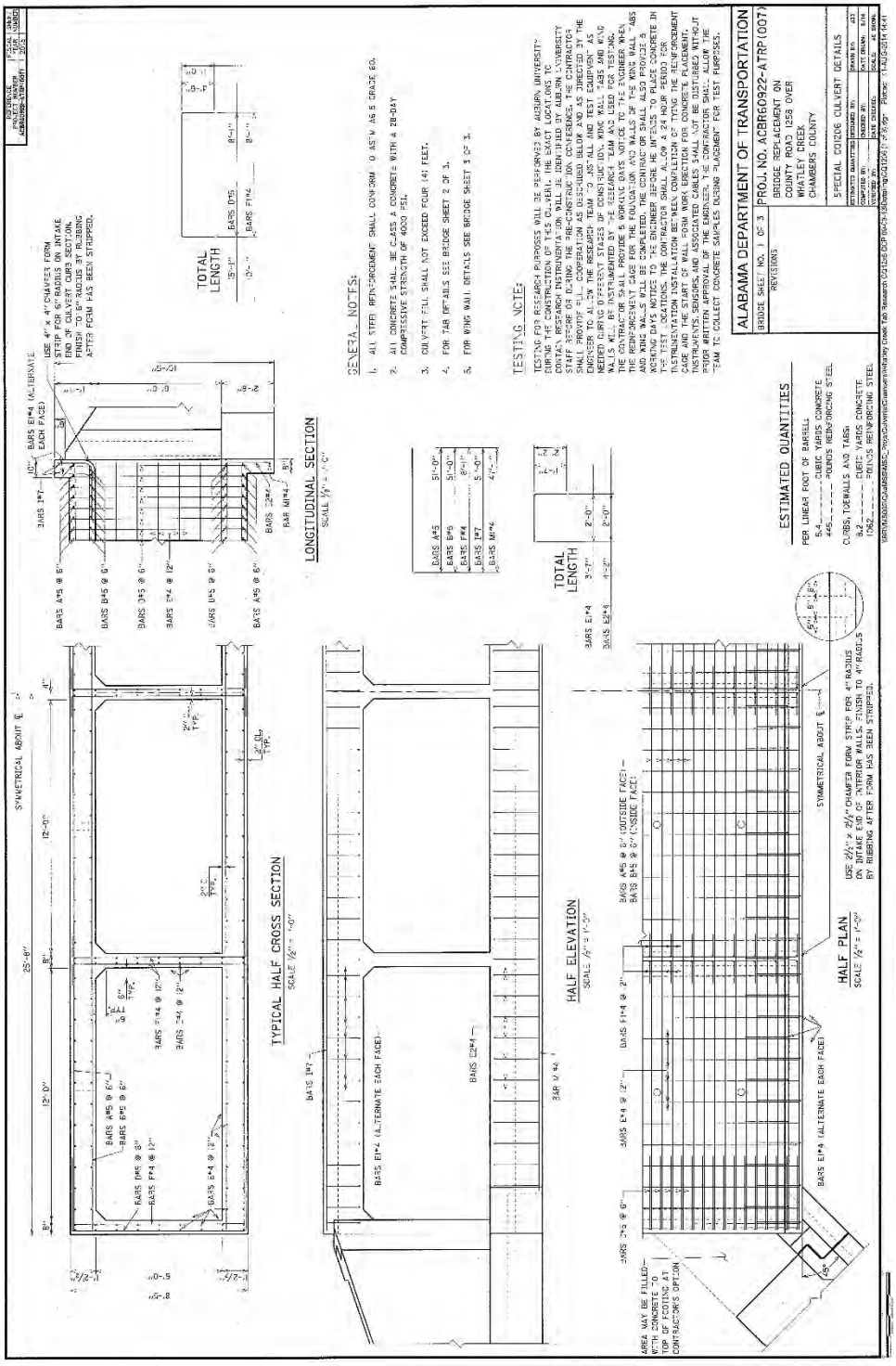

Figure A-1. Chambers County culver detail, sheet #1

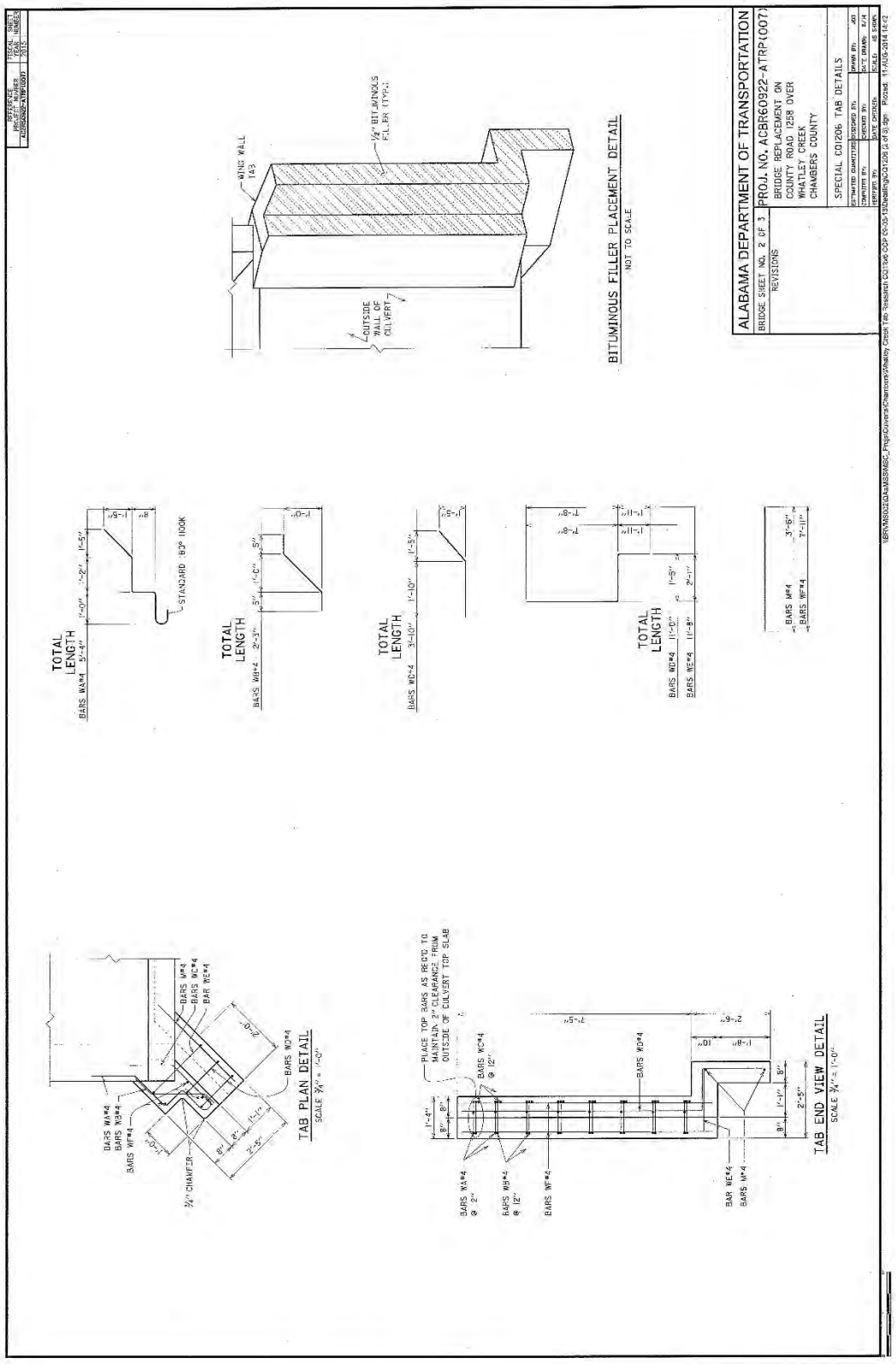

Figure A-2. Chambers County culver detail, sheet #2

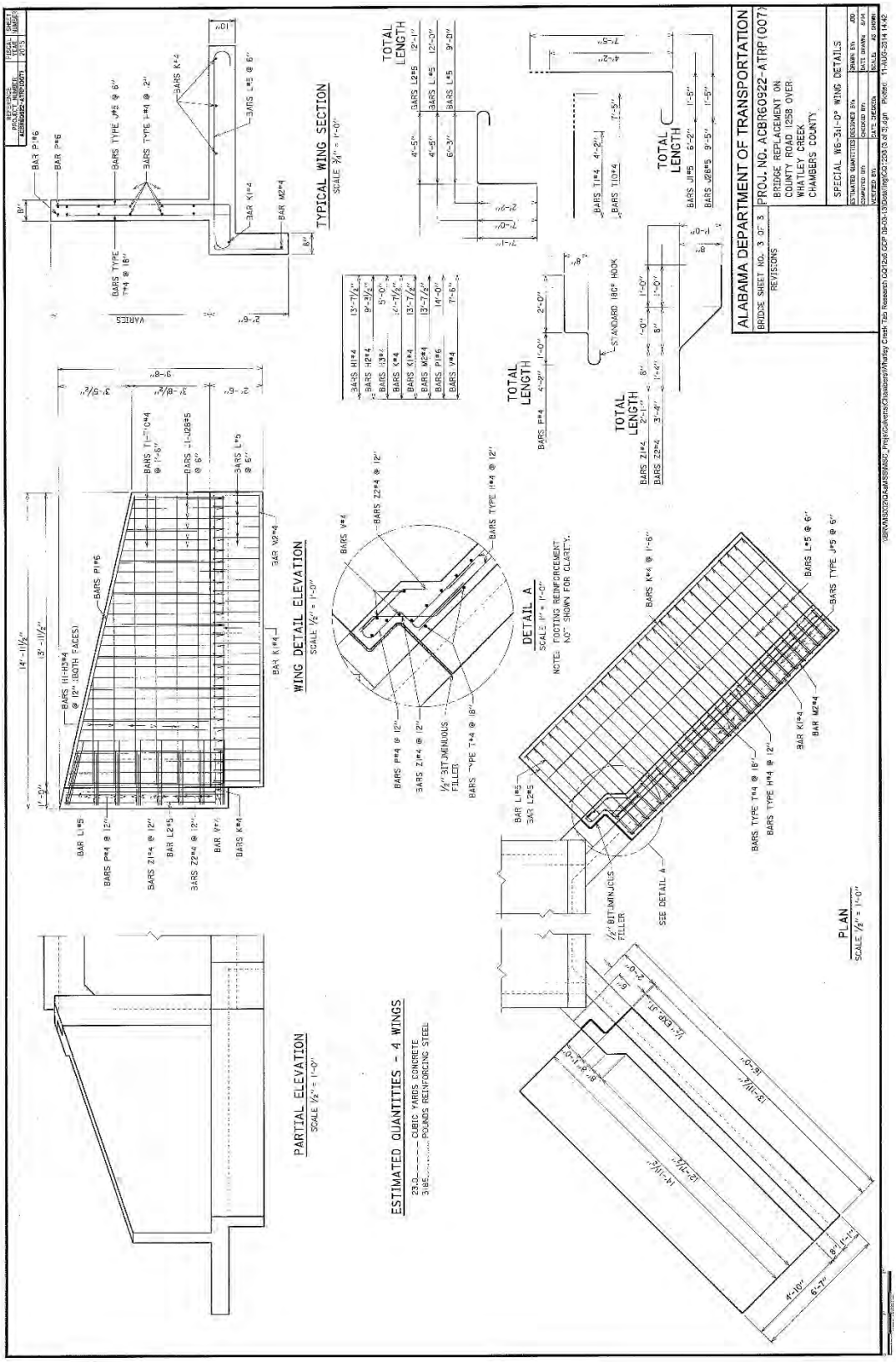

Figure A-3. Chambers County culver detail, sheet #3

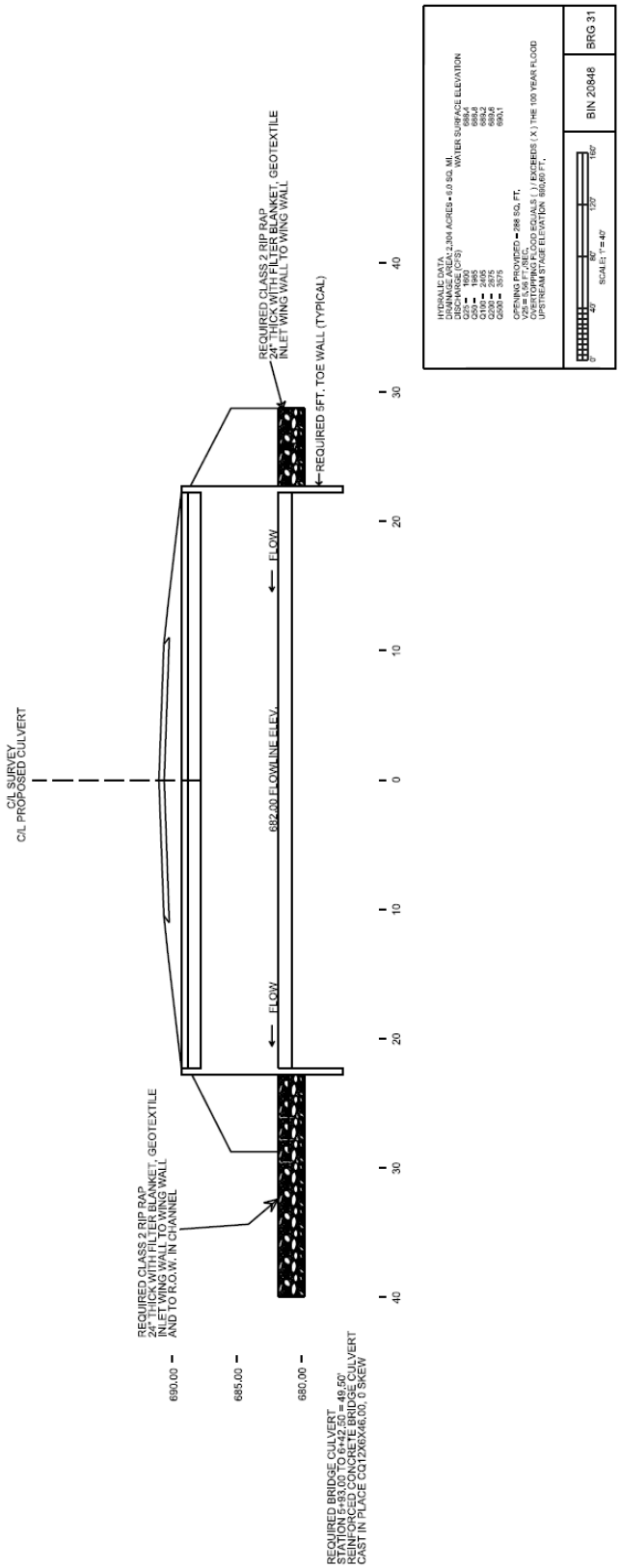

Figure A-4. Chambers County culver drainage section and profile

A.1 Lee County Culvert

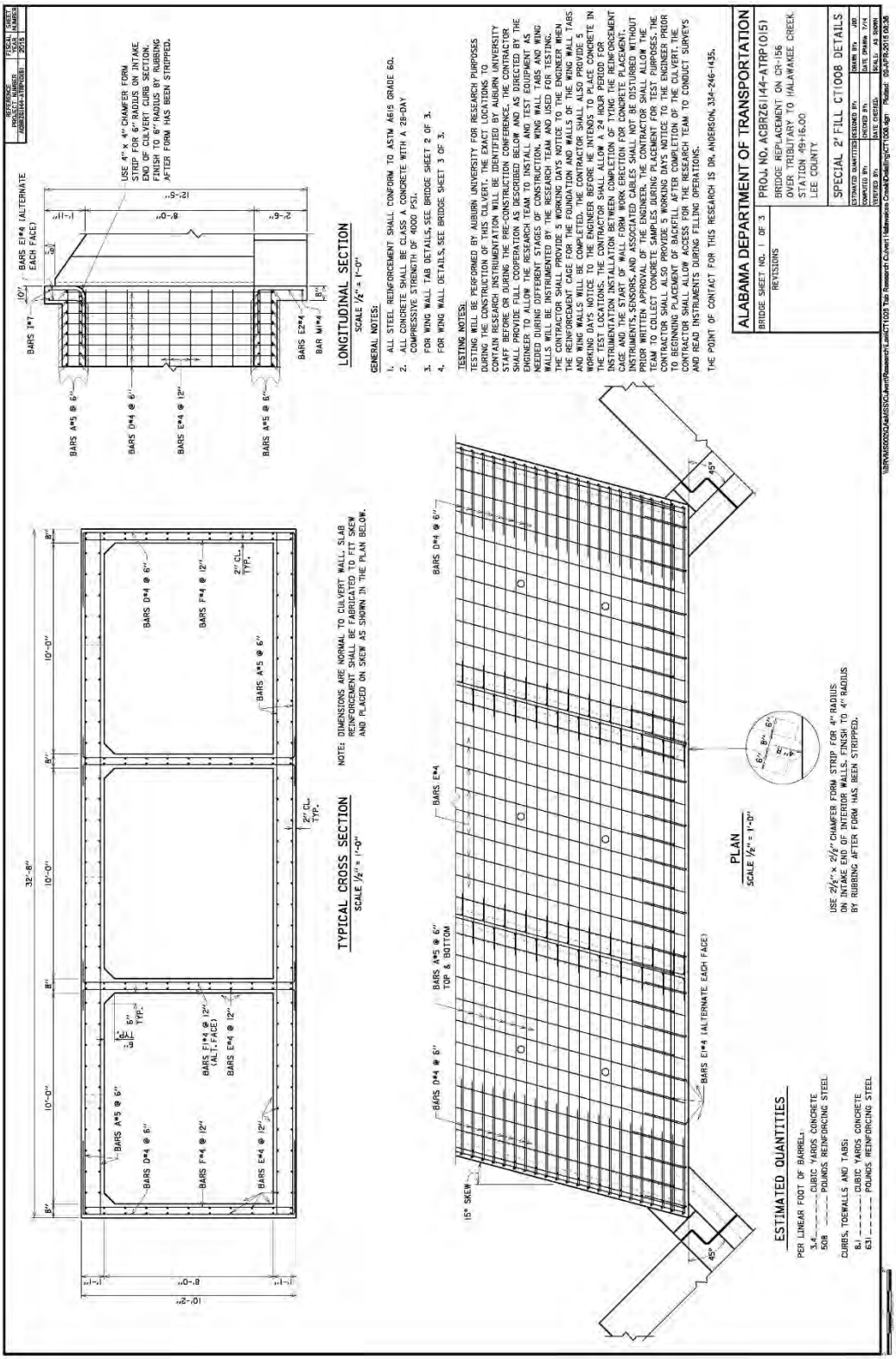

Figure A-5. Lee County culver detail, sheet #1

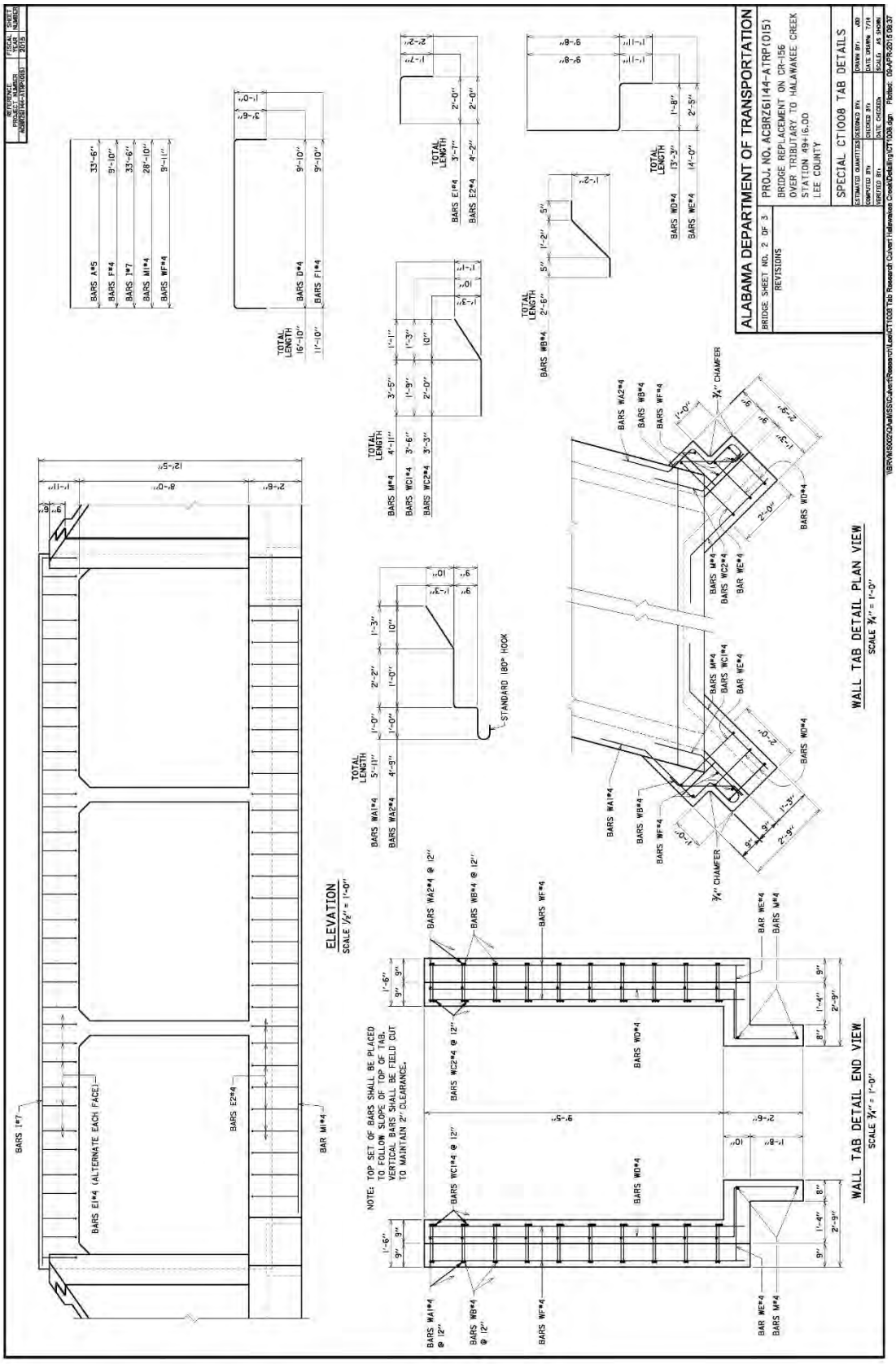

Figure A-6. Lee County culver detail, sheet #2

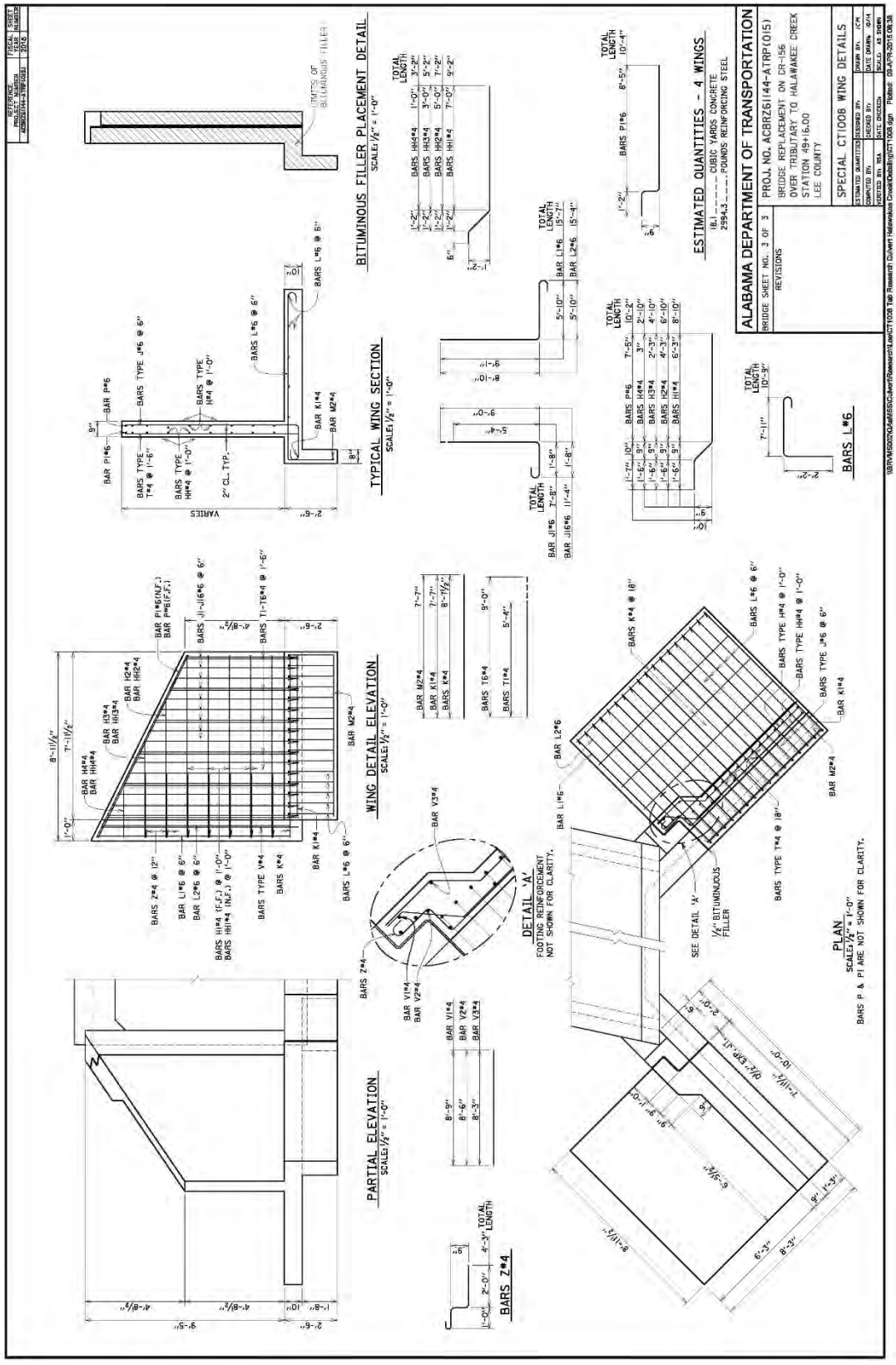

Figure A-7. Lee County culver detail, sheet #3

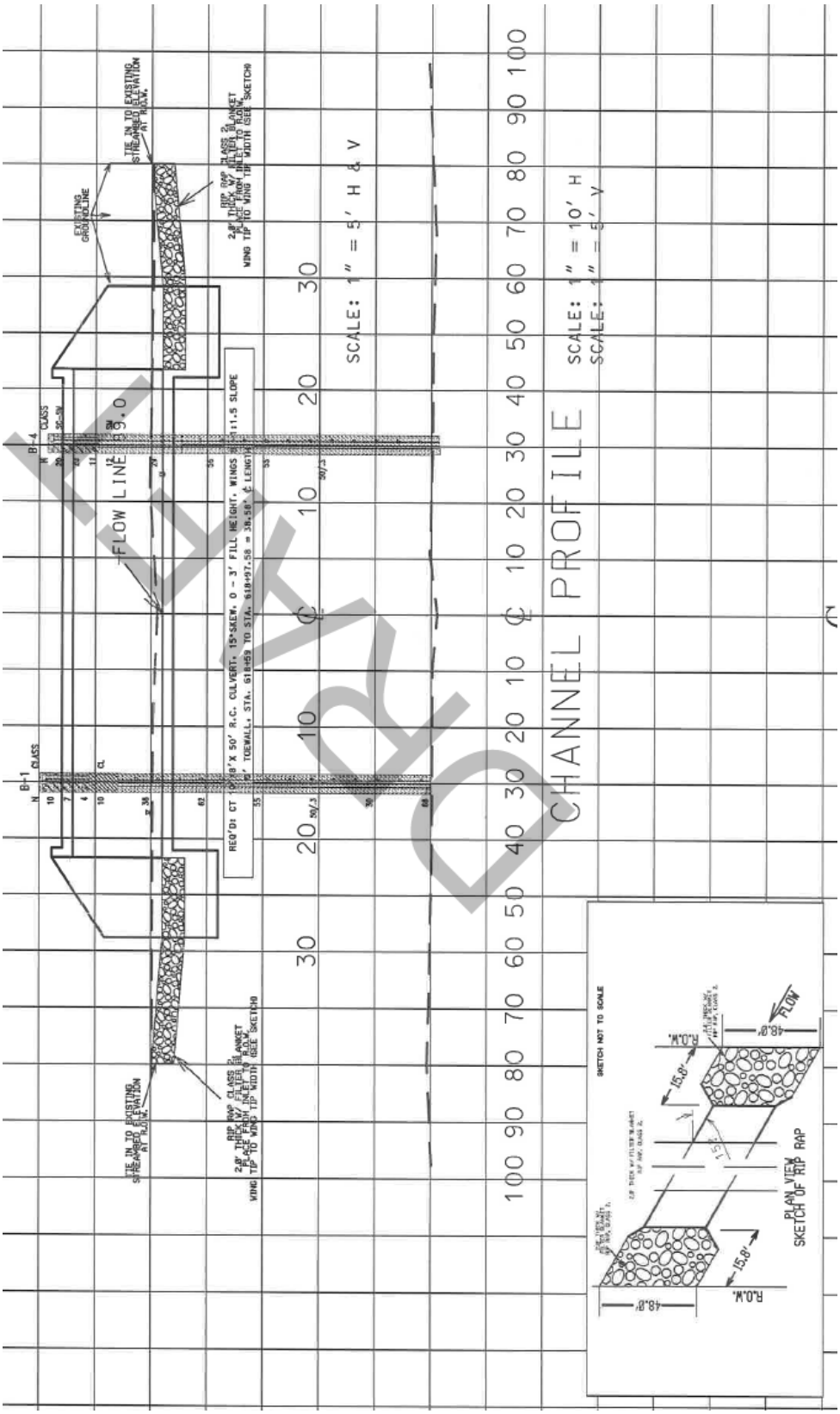

Figure A-8. Lee County culver drainage section and profile

A.1 Coosa County Culvert

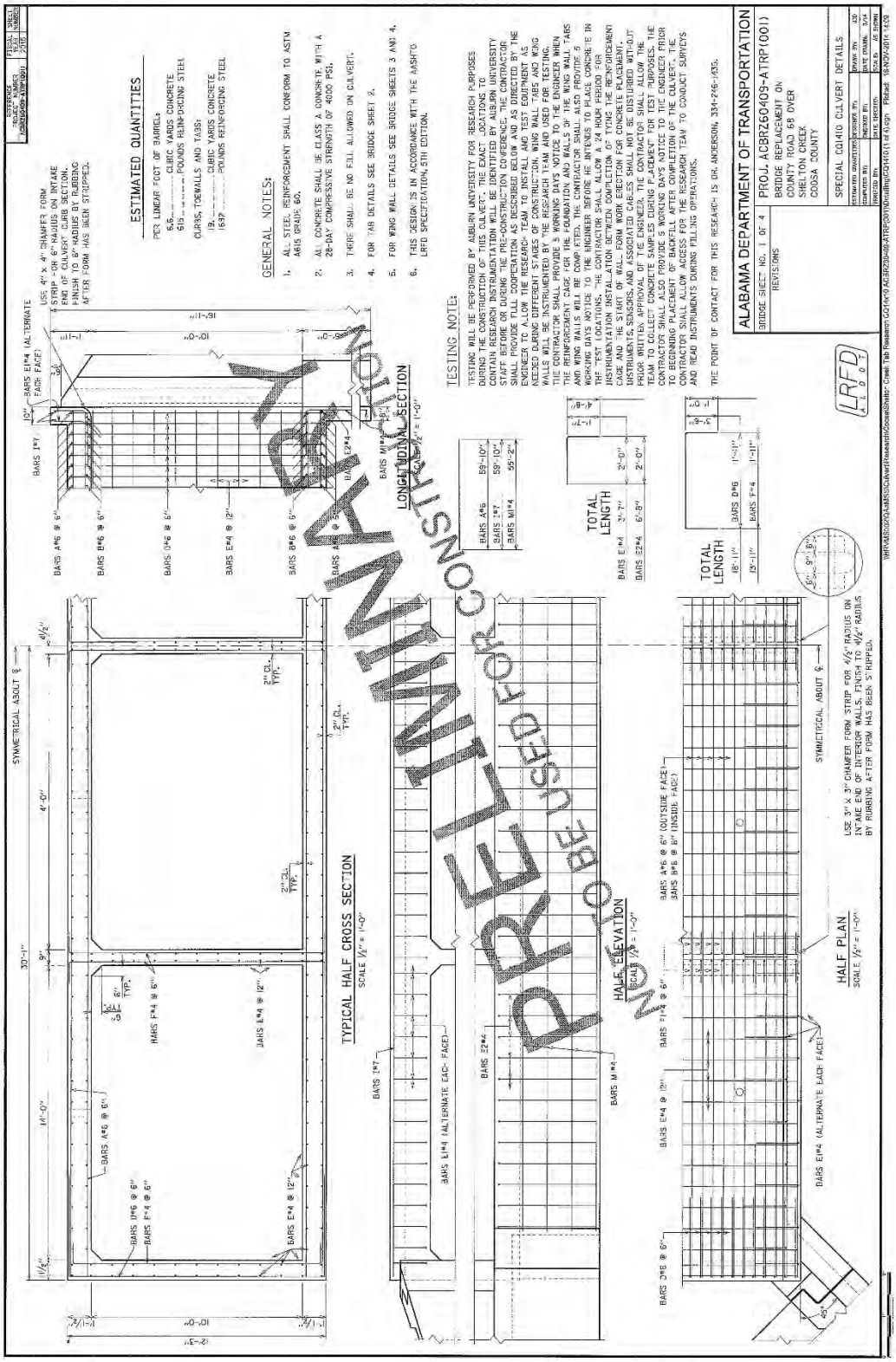

Figure A-9. Coosa County culver detail, sheet #1

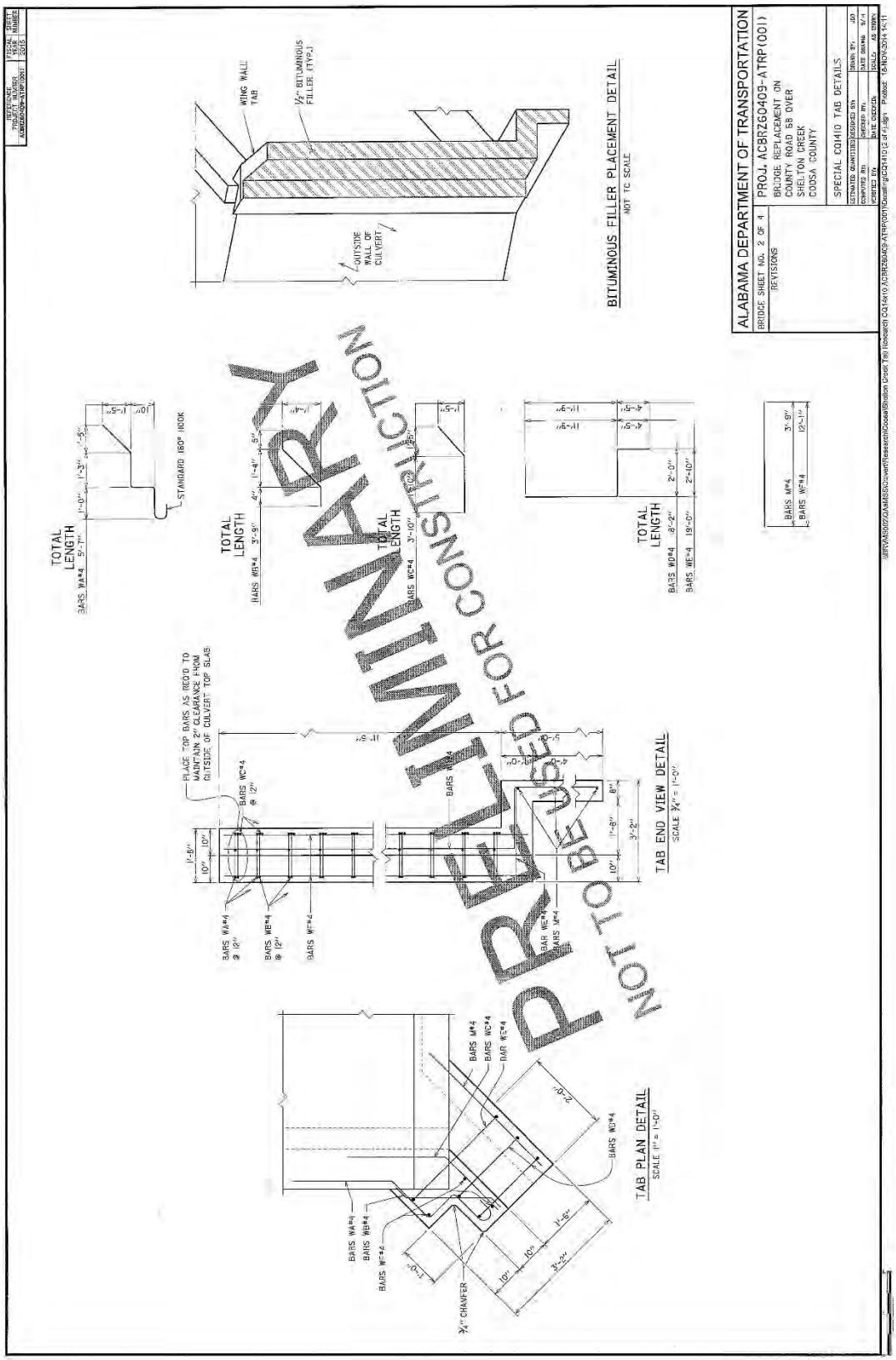

Figure A-10. Coosa County culver detail, sheet #2

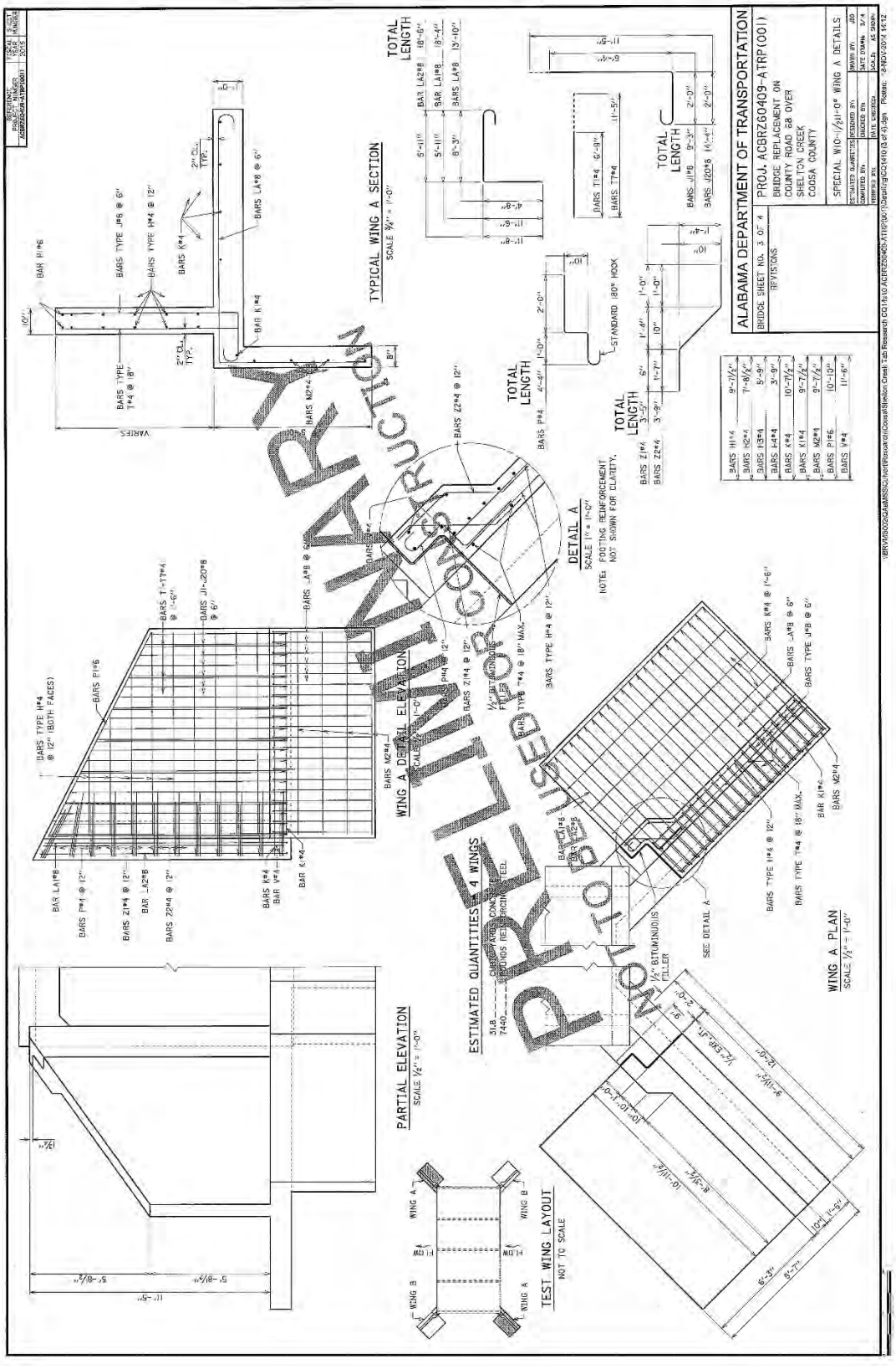

Figure A-11. Coosa County culver detail, sheet #3

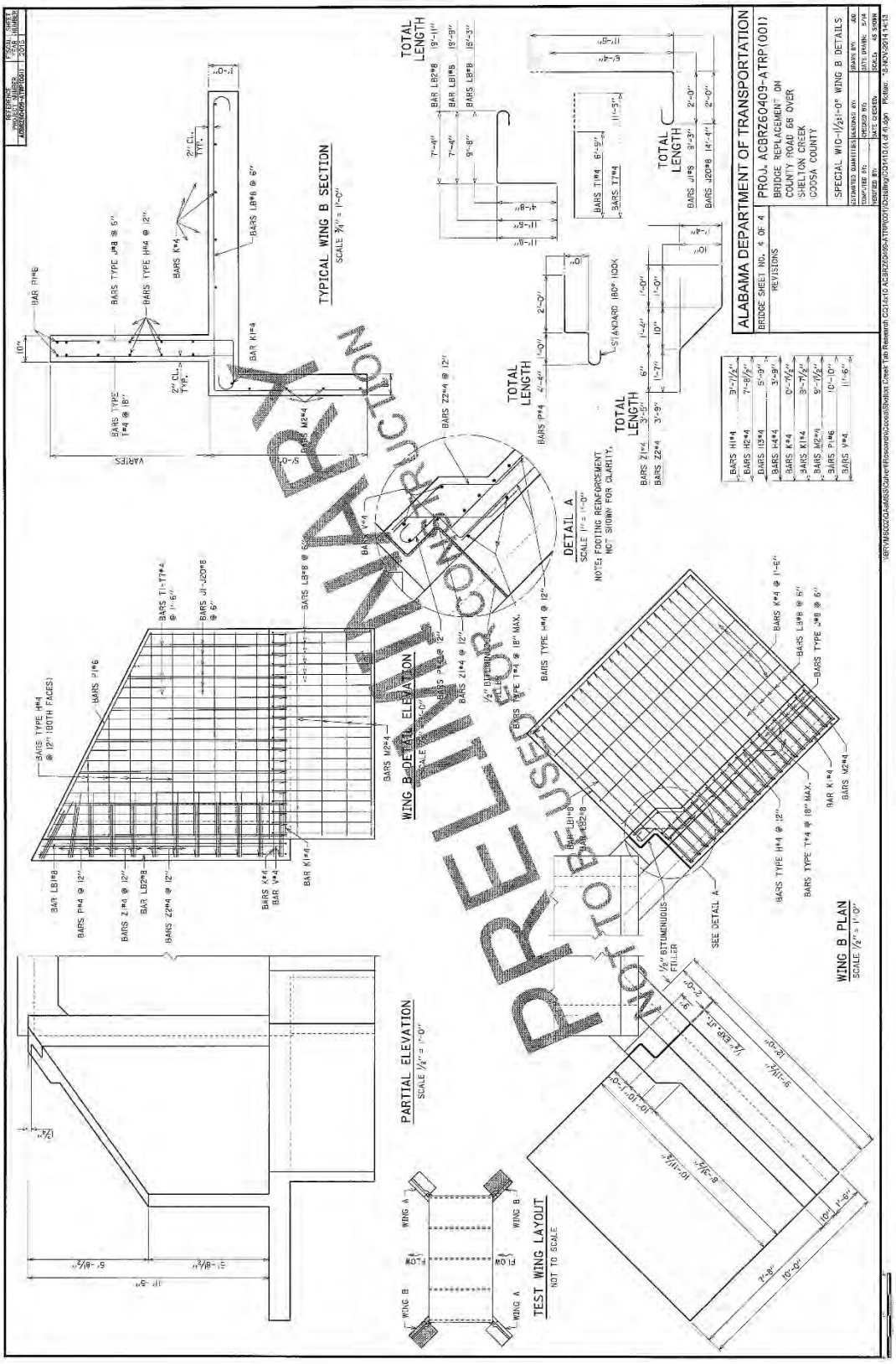

Figure A-12. Coosa County culver detail, sheet #4

Appendix B Boring Logs

B.1 Chambers County Borings

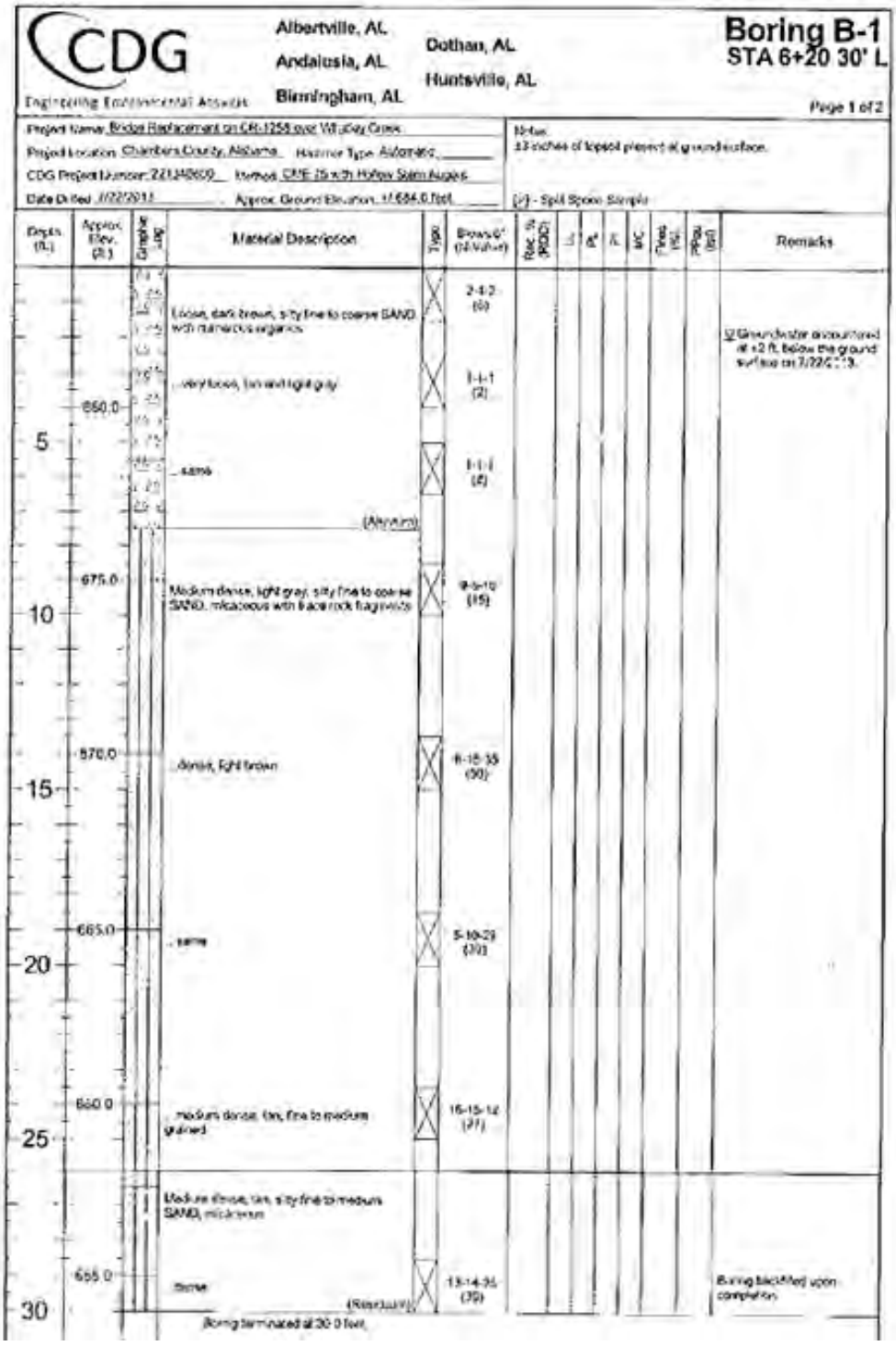

Figure B-1. Chambers County boring B-1

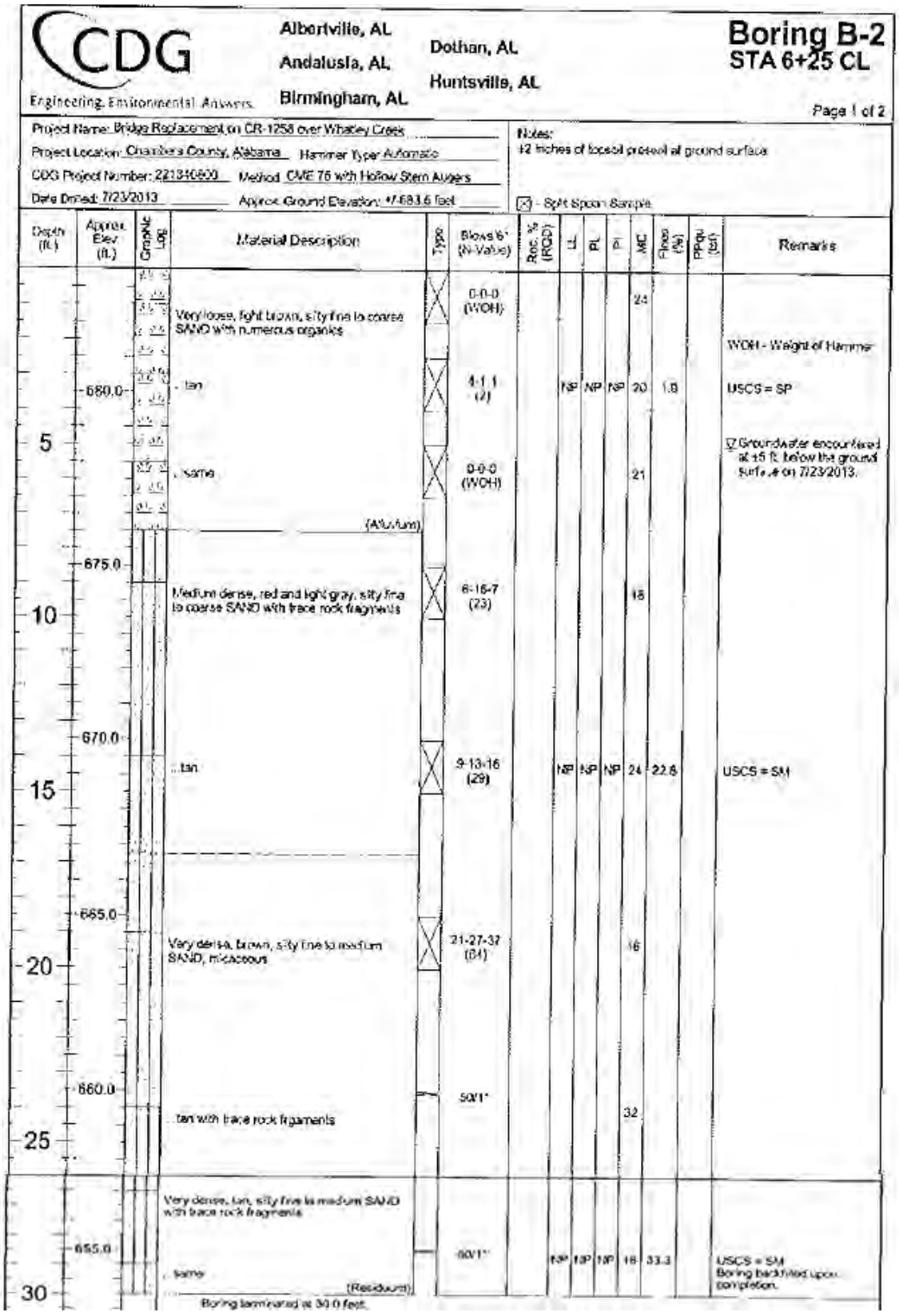

Figure B-2. Chambers County boring B-2

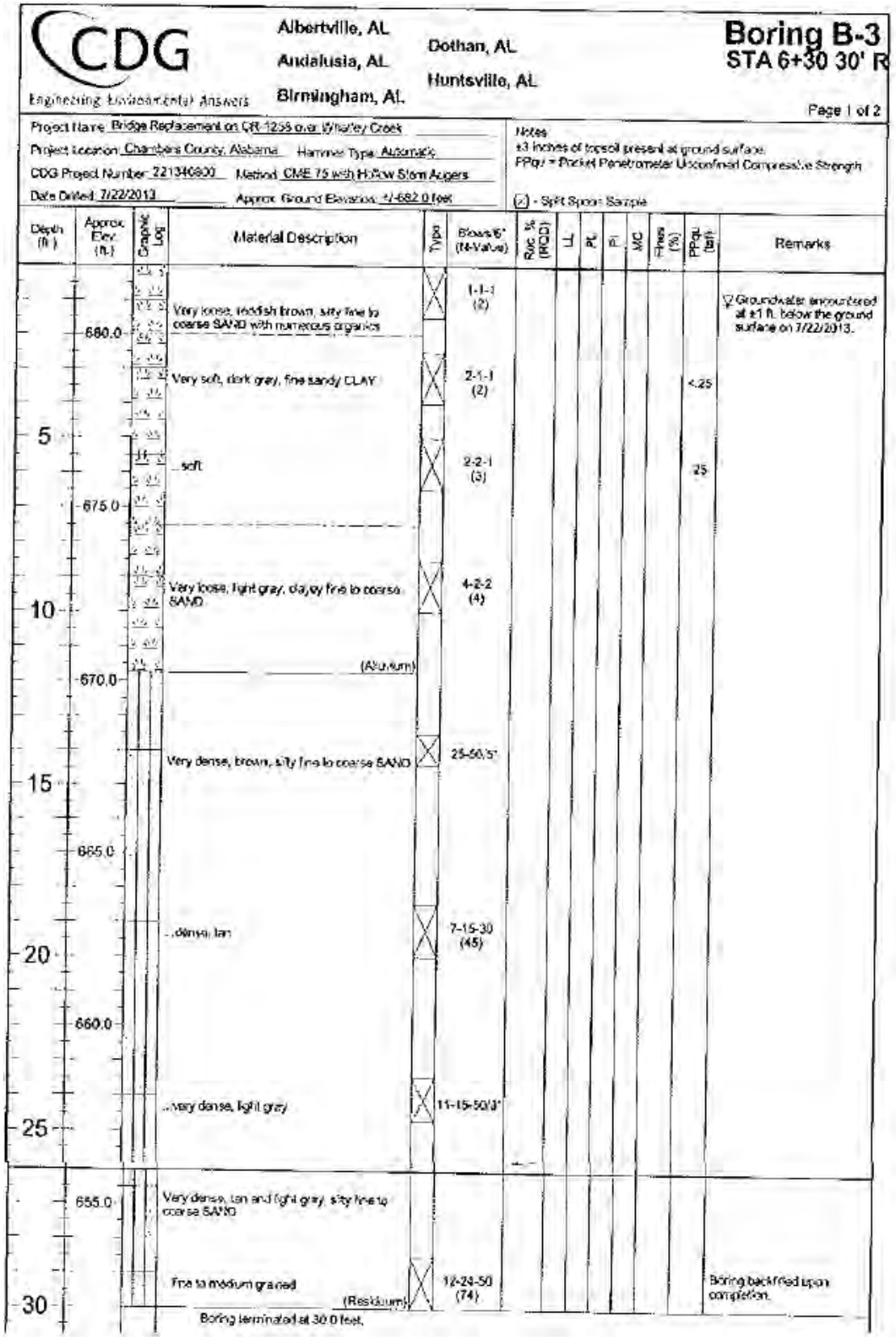

Figure B-3. Chambers County boring B-3

B.2 Lee County Borings

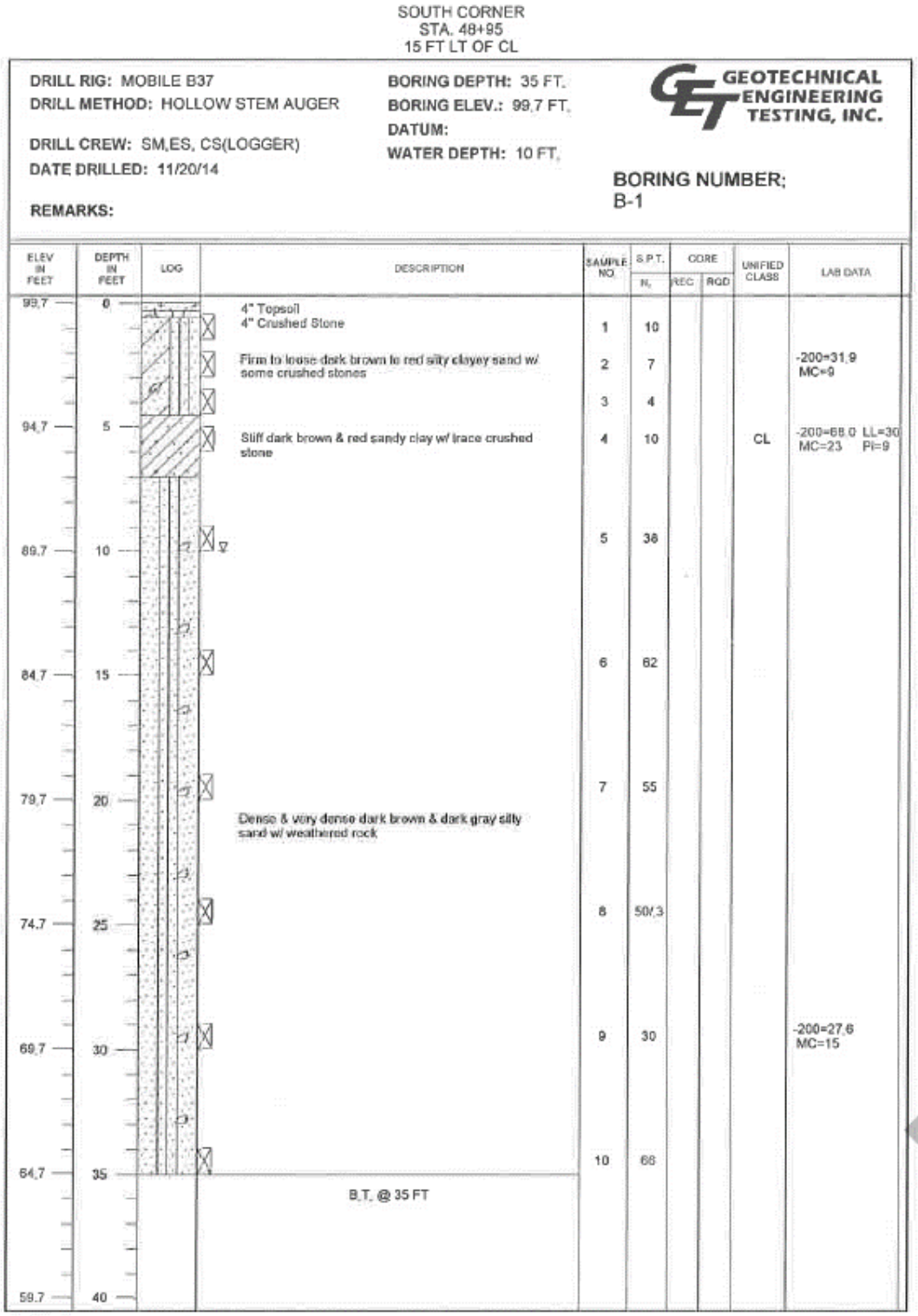

Figure B-4. Lee County boring B-1

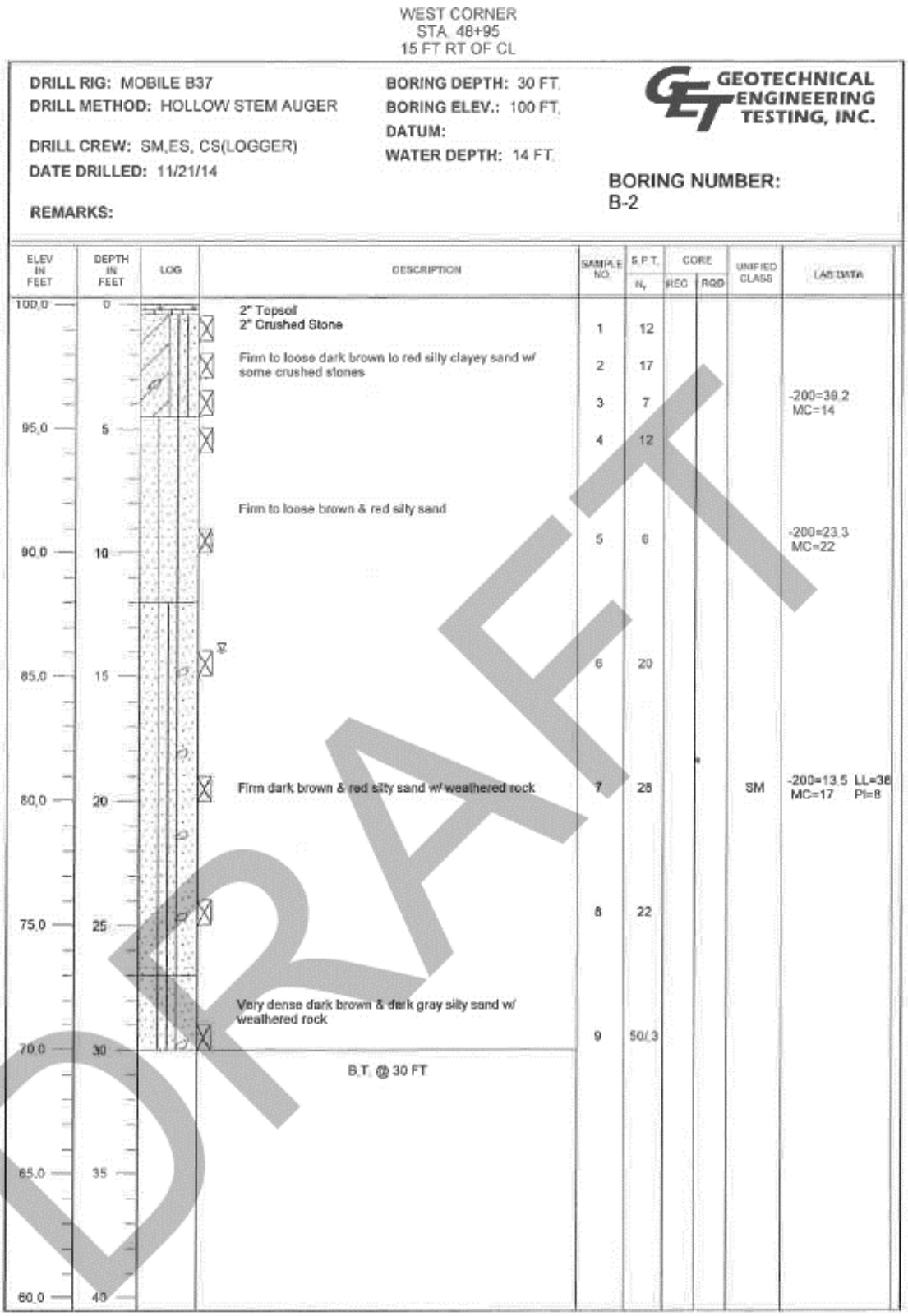

Figure B-5. Lee County boring B-2

EAST CORNER
STA. 49+76
15 FT RT OF CL

DRILL RIG: MOBILE B37
DRILL METHOD: HOLLOW STEM AUGER
DRILL CREW: SM,ES, CS(LOGGER)
DATE DRILLED: 11/20/14
REMARKS:

BORING DEPTH: 35 FT.
BORING ELEV.: 98.6 FT.
DATUM:
WATER DEPTH: 9.5 FT.

GEOTECHNICAL ENGINEERING TESTING, INC.

BORING NUMBER: B-3

ELEV IN FEET	DEPTH IN FEET	DESCRIPTION	SAMPLE NO.	S.P.T. N_c	CORE REC	CORE RQD	UNIFIED CLASS	LAB DATA
98.6	0	3" Topsoil 3" Crushed Stone	1	11				
		Firm & loose dark brown to red silty clayey sand w/ some crushed stone	2	9			SC-SM	-200=31.4 LL=25 MC=11 PI=6
			3	10				
93.6	5		4	6				
		Loose dark brown & dark gray coarse sand w/ trace crushed stone						
88.6	10		5	9				
		Firm dark brown silty sand w/ clay & some rock fragments	6	26				-200=28.3 MC=20
83.6	15							
78.6	20		7	50/.3				
73.6	25		8	50/.3				
		Dense & very dense dark brown silty sand w/ weathered rock						
68.6	30		9	60				
63.6	35		10	50/.3				
		B.T. @ 35 FT						
58.6	40							

Figure B-6. Lee County boring B-3

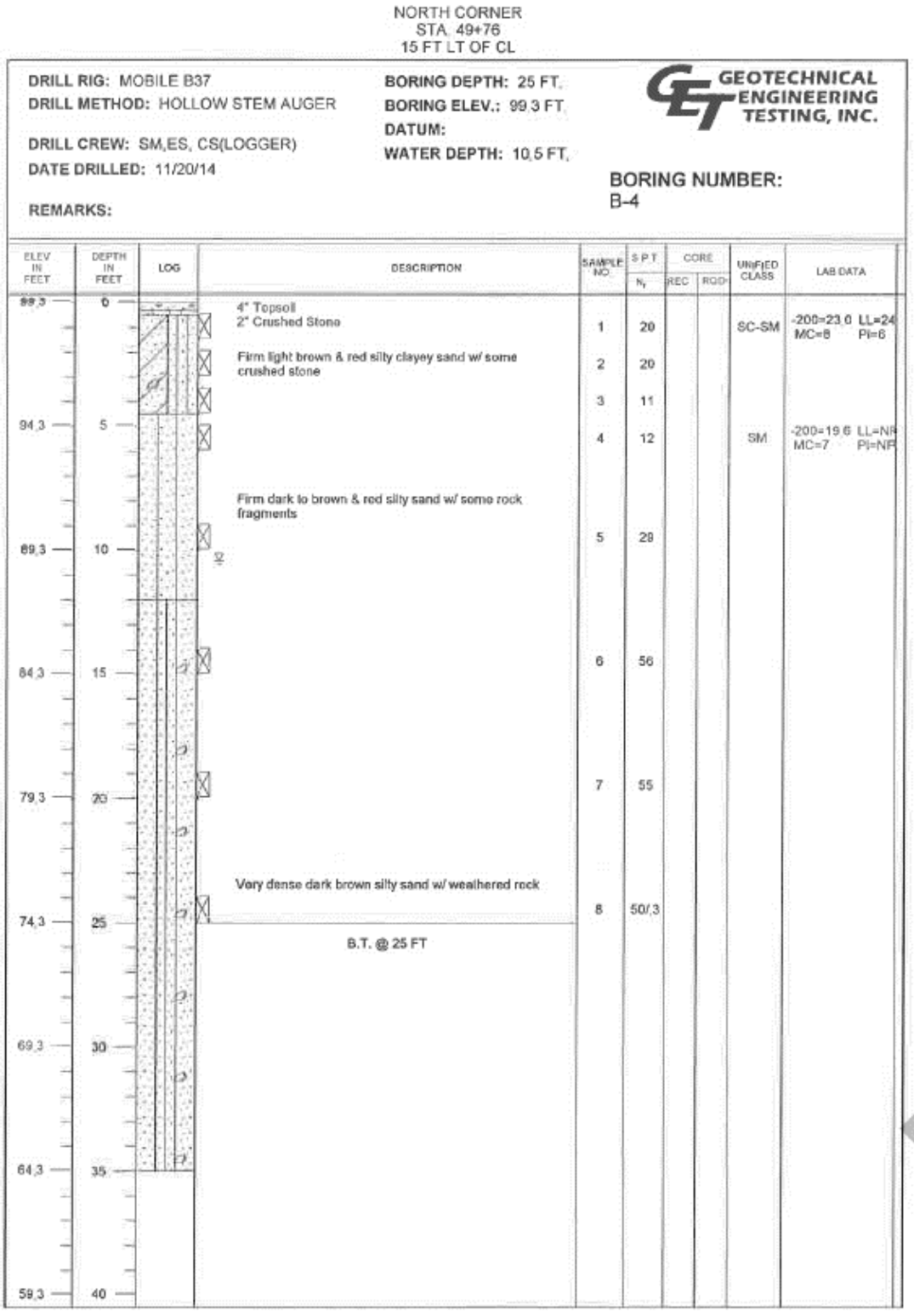

Figure B-7. Lee County boring B-7